DELPHI Collaboration

DELPHI 2001-085 CONF 513
25 June, 2001

Searches for supersymmetric particles in e^+e^- collisions up to 208 GeV, and interpretation of the results within the MSSM

J. Abdallah[1], **T. Alderweireld**[2], **R. Alemany**[3], **S. Amato**[4], **S. Ask**[5], **A. Brambilla**[6], **M. Berggren**[1], **M. Besancon**[7], **M. Espirito Santo**[3], **M. Gandelman**[4], **C. Garcia**[8], **N. Ghodbane**[15], **K. Hultqvist**[9], **P. Johansson**[9], **B. King**[10], **A. Lipniacka**[9], **J. H. Lopes**[4], **M. Margoni**[11], **F. Mazzucato**[12], **S. Paiano**[13], **A. Perrotta**[13], **P. Rebecchi**[3], **T. Rovelli**[13], **A. Savoy-Navarro**[1], **U. Schwickerath**[3], **J. Strauss**[14], **P. Verdier**[15], **A. Washbrook**[10]

Abstract

DELPHI data collected at centre-of-mass energies up to 208 GeV have been analysed in search of charginos, neutralinos and sfermions in the framework of the Minimal Supersymmetric Standard Model (MSSM) with R-parity conservation. No evidence for a signal was found in any of the channels. The results of each search were used to derive upper limits on production cross-sections and masses. In addition, the combined result of all searches excludes regions in the parameter space of the constrained MSSM, leading to limits on the mass of the Lightest Supersymmetric Particle and other supersymmetric particles. All limits are given at 95% confidence level, all results are preliminary.

Contributed Paper for EPS HEP 2001 (Budapest) and LP01 (Rome)

[1] LPNHE, Universités Paris VI et VII, F-75230 Paris Cedex 05, France
[2] Faculté des Sciences, Université de l'Etat Mons, Mons, Belgium
[3] CERN, CH-1211 Genève 23, Switzerland
[4] Univ. Federal do Rio de Janeiro, Rio de Janeiro, Brazil
[5] Department of Physics, University of Lund, Lund, Sweden
[6] Dipartimento di Fisica, Univ. di Milano-Bicocca and INFN-MILANO, IT-20126 Milan, Italy
[7] DAPNIA/Service de Physique des Particules, CEA-Saclay, FR-91191 Gif-sur-Yvette Cedex, France
[8] IFIC, Valencia-CSIC, and D.F.A.M.N., U. de Valencia, Valencia, Spain
[9] Fysikum, Stockholm University, Box 6730, S-113 85 Stockholm, Sweden
[10] Department of Physics, University of Liverpool, P.O. Box 147, Liverpool L69 3BX, UK
[11] Dipartimento di Fisica, Universita di Padova, Padova, Italy
[12] Currently at Dep. de Physique Nucleaire et Corpusculaire, University of Geneva, Switzerland
[13] Dipartimento di Fisica, Università di Bologna and INFN, Bologna, Italy
[14] Institut für Hochenergiephysik, Österr. Akad. d. Wissensch., Vienna, Austria
[15] Université Claude Bernard de Lyon, IPNL, IN2P3-CNRS, FR-69622 Villeurbanne Cedex, France

1 Introduction

Supersymmetry (SUSY) [1] is at present one of the most attractive possible extensions of the Standard Model (SM) and its signatures could be observed at LEP through a large variety of different channels. In this paper searches for pair-produced charginos, neutralinos, sleptons and squarks are presented. The searches were performed and interpreted in the most model-independent way possible in terms of production cross-sections and masses. The results are interpreted in the framework of SUSY models, with different search channels complementing each other in constraining the parameter space.

The data collected by the DELPHI experiment in e^+e^- collisions at centre-of-mass energies ($\sqrt{s}$) up to 208 GeV were used.

The paper is organized as follows. In section 2 the basic supersymmetric framework is described: some general phenomenological considerations are discussed in section 2.1, and implications of more constrained models used for interpreting the data are given in section 2.2. The DELPHI detector is very briefly described in section 3, and in section 4 the data sets and event generators are reviewed. In section 5 the general analysis framework is described, the analysis methods are briefly mentioned and the specific search strategies for chargino, neutralino, slepton and squark searches are discussed. The results of each search are separately presented and interpreted in section 6. In section 7 the results are combined and interpreted in the framework of constrained SUSY scenarios with supergravity-inspired (SUGRA) breaking of supersymmetry. A brief summary is given in section 8.

Previous results published by DELPHI can be found in references [2] to [11].

2 SUSY framework

The searches presented in this paper were performed in the framework of the Minimal Supersymmetric extension of the Standard Model (MSSM) [1]. R-parity conservation is assumed [1], implying that the Lightest Supersymmetric Particle (LSP) is stable and SUSY particles ("sparticles", defined as having $R = -1$) are pair-produced. In addition, they decay directly or indirectly into the LSP which is weakly interacting and escapes detection, giving a signature of missing energy and momentum. In the present paper the lightest neutralino ($\tilde{\chi}_1^0$) is assumed to be the LSP.

The searches for sparticle production were developed with minimal assumptions, and the selections employed depended primarily on the masses of the particles involved. In particular, the sensitivities of the searches depend on the visible energy released in the decay process. For direct decays into the LSP, this visible energy is largely determined by the mass difference (ΔM) between the decaying sparticle and the LSP. In case of indirect (cascade) decays, other mass differences can also be important.

The MSSM has a large number of free parameters in addition to the SM ones. The most model independent interpretation of the results is in terms of those masses or cross-sections which explicitly affect each production channel searched for. A common interpretation of the results from the various searches can also be performed in terms of the parameters of

[1] R-parity is a multiplicative quantum number defined as $R = (-1)^{3(B-L)+2S}$ where B, L and S are the baryon number, the lepton number and the spin of the particle, respectively. SM particles have R=+1 while their SUSY partners have $R = -1$

the model, but this requires a manageable number of free parameters. For this reason, assumptions must be made and specific scenarios defined for such an interpretation. Below the general phenomenology of the searches will be discussed in section 2.1, followed by a description of the implications of more specific scenarios in section 2.2.

2.1 General phenomenology

Squarks and Sleptons

The "sfermions", squarks and sleptons, are the scalar partners of the SM fermions. The left- and right-handed chiral states of each SM fermion, f_L and f_R, have as SUSY partners two scalars, usually labeled $\tilde{f}_L$ and $\tilde{f}_R$.

Sleptons and squarks could be pair-produced at LEP via e^+e^- annihilation into Z/γ, leading to $\tilde{f}_R\overline{\tilde{f}_R}$ or $\tilde{f}_L\overline{\tilde{f}_L}$ final states. Selectrons could also be produced through t-channel neutralino exchange. The selectron cross-section therefore depends critically on the neutralino mass, and destructive interference can make it very small. The t-channel contribution also introduces the possibility of $\tilde{e}_L\tilde{e}_R$ production.

If the unification of sfermion masses at a high mass scale typical of Grand Unified Theories (GUT) is assumed, lower masses and cross-sections are typically expected for the partners of right-handed fermions. Under this assumption, the kinematic accessibility of first and second family sfermions at LEP depends only on their assumed common mass at the unification scale. However, for sfermions of the third family the large Yukawa couplings lower the masses and large mixing between left and right states may occur. In this case, the lighter mass states of third family sleptons and squarks, $\tilde{\tau}_1$, $\tilde{b}_1$and $\tilde{t}_1$, are candidates for the lightest charged supersymmetric particle

In large regions of the SUSY parameter space the dominant decay of the sfermions is to the corresponding fermion and the lightest neutralino, $\tilde{f} \to f\tilde{\chi}^0_1$. In the case of the $\tilde{t}$, the decay $\tilde{t} \to t\tilde{\chi}^0_1$ is not kinematically allowed at LEP, and the dominant 2-body decay channel is expected to be $\tilde{t} \to c\tilde{\chi}^0_1$ ($\tilde{t} \to b\tilde{\chi}^\pm_1$ being disfavoured by existing limits on the chargino mass). If $m_{\tilde{\nu}} < M_{\tilde{t}_1}$, the three-body decay $\tilde{t}_1 \to b\ell\tilde{\nu}$ may compete with the $c\tilde{\chi}^0_1$ decay.

Thus, final state topologies with a pair of leptons or jets and missing energy are the relevant ones in the search for sleptons and squarks, respectively, and the total energy of the detectable final state particles (and, thus, the sensitivity of the search) depends primarily on the mass difference between the sfermion and the LSP.

Charginos and Neutralinos

In the MSSM there are four neutralinos, $\tilde{\chi}^0_i, i = 1, 4$ (numbered in order of increasing mass) and two charginos $\tilde{\chi}^\pm_i, i = 1, 2$ which are linear combinations of the SUSY partners of neutral and charged gauge and Higgs bosons (gauginos and higgsinos). The lightest states can be mainly gaugino or higgsino, or strongly mixed (for similar gaugino and higgsino mass parameters).

Neutralinos (charginos) could be pair-produced at LEP via s-channel Z (Z/γ) exchange or t-channel exchange of a selectron (sneutrino). The t-channel contribution can be important if the slepton is light. The interference with the s-channel diagram is constructive in the case of neutralinos but destructive in the case of charginos.

The decays of $\tilde{\chi}_i^0$ and $\tilde{\chi}_j^\pm$ are likely to be $\tilde{\chi}_i^0 \to \tilde{\chi}_1^0 \mathrm{f}\bar{\mathrm{f}}$ and $\tilde{\chi}_j^\pm \to \tilde{\chi}_1^0 \mathrm{f}\bar{\mathrm{f}}'$, respectively. If the sfermions are heavy, these decays proceed via Z or W emission. However, sfermion emission may also contribute if the sfermions are light, increasing the partial width for decays into the corresponding fermions, and two-body decays into $\bar{\mathrm{f}}\tilde{\mathrm{f}}$ can dominate if kinematically allowed. The one-loop decay $\tilde{\chi}_2^0 \to \tilde{\chi}_1^0\gamma$ can be important in specific regions of the parameter space when other decays are suppressed.

Thus the sfermion mass spectrum may significantly affect both the production cross-section and the decay modes of charginos and neutralinos, and many final state topologies are possible.

In the case of chargino pair production, the final state is expected to be four jets if both charginos decay hadronically, two jets and one lepton if one chargino decays into $\ell\nu\tilde{\chi}_1^0$, and leptons only if both charginos decay into leptons. The branching-ratio of $\tilde{\chi}_1^\pm \to \tilde{\chi}_2^0 \mathrm{f}\bar{\mathrm{f}}'$ can be sizeable, in particular in the regions of the parameter space where $\tilde{\chi}_2^0 \to \tilde{\chi}_1^0\gamma$ is important. In this case, the above topologies are accompanied by photons.

If the mass difference ΔM between the chargino and the LSP is very small the visible energy released in the decay is very small, making the signal hard to detect. The simultaneous production of a photon by initial state radiation was used to explore such regions, as this allows a very efficient background rejection at the expense of a low signal cross-section. Still lower mass differences imply a long lifetime of the chargino, which can then be identified as a heavy stable charged particle or one with a displaced decay vertex.

In the case of the detectable $\tilde{\chi}_1^0\tilde{\chi}_k^0$ neutralino production channels (*i.e.* excluding $\tilde{\chi}_1^0\tilde{\chi}_1^0$), the most important signatures are expected to be acoplanar pairs of jets or leptons with high missing energy and momentum. Although $\tilde{\chi}_1^0\tilde{\chi}_2^0$ and $\tilde{\chi}_1^0\tilde{\chi}_3^0$ are expected to dominate in most of the parameter space, for a complete coverage one must also consider channels like $\tilde{\chi}_2^0\tilde{\chi}_3^0$ and $\tilde{\chi}_2^0\tilde{\chi}_4^0$. These give rise to cascade decays with multiple jets or leptons in the final state, possibly accompanied by photons from $\tilde{\chi}_2^0 \to \tilde{\chi}_1^0\gamma$.

2.2 Constraining the parameter space

To make the model more predictive the unification of some parameters at a high mass scale typical of Grand Unified Theories (GUT) can be assumed. The MSSM parameters and the assumptions that can be relevant in the interpretation of the results are listed below:

- $\boldsymbol{\tan\beta}$, the ratio of the vacuum expectation values of the two Higgs doublets;
- $\boldsymbol{\mu}$, the Higgs mass parameter;
- $\boldsymbol{M_1, M_2, M_3}$, the $U(1) \times SU(2) \times SU(3)$ gaugino masses at the electroweak (EW) scale: when gaugino mass unification at the GUT scale is assumed, with a common gaugino mass of $\boldsymbol{m_{1/2}}$, the relation between M_1 and M_2 is $M_1 = \frac{5}{3}\tan^2\theta_W M_2 \sim 0.5 M_2$;
- $\boldsymbol{m_{\tilde{\mathrm{f}}}}$, the sfermion masses: under the assumption of sfermion mass unification, $\boldsymbol{m_0}$ is the common sfermion mass at GUT scale;
- the masses in the Higgs sector depend on one more parameter taken to be the pseudoscalar Higgs mass, $\boldsymbol{m_A}$: if scalar mass unification is assumed, m_A at the EW scale can be derived from m_0;

- the trilinear couplings $\boldsymbol{A_f}$ determining the mixing in the sfermion families: the third family trilinear couplings are the most relevant ones, $\boldsymbol{A_\tau, A_b, A_t}$, and under the assumption of universal parameters at high mass scale there is a common trilinear coupling $\boldsymbol{A}$.

Mass mixing terms at the EW scale given by $m_\tau(A_\tau - \mu\tan\beta)$, $m_b(A_b - \mu\tan\beta)$ and $m_t(A_t - \mu/\tan\beta)$ are considered for $\tilde{\tau}$, $\tilde{\mathrm{b}}$ and $\tilde{\mathrm{t}}$, respectively. The mass splitting grows with the mixing terms, and for large μ this can give light $\tilde{\tau}_1$ and $\tilde{\mathrm{b}}_1$ states if $\tan\beta$ is large, or a light $\tilde{\mathrm{t}}_1$ for small $\tan\beta$.

In the model referred to as the "Constrained MSSM" (CMSSM) in the following, sfermion and gaugino mass unification are assumed. The parameter set is then reduced to $M_2, m_0, \tan\beta, \mu, m_A$ and three A_f couplings. This is the model considered in section 7.

Alternatively, tightening the assumptions, the individual A_f couplings can be replaced by an universal coupling A and m_A can be related to the other parameters by assuming scalar (including Higgses) mass unification. Requiring in addition the correct reproduction of the EW symmetry scale, which fixes the absolute value of μ, defines the minimal supergravity-broken MSSM (MSUGRA).

The direct results of the searches are first derived and presented in the most model-independent way possible. Under the assumptions described above, the results are then used to constrain the SUSY parameters. Presently the strongest constraints on SUSY models come from the Higgs searches [12].

Chargino production is the most important direct SUSY detection channel for large regions of the parameter space. However, if sfermions are light (corresponding to a low m_0 scenario), or if the parameters take particular values, the cross-section can be greatly suppressed or undetectable final states can dominate (in particular for small mass splittings). The most relevant of these cases are the following:

High m_0

For high m_0, the sfermions are heavy and have little influence on the observable phenomenology. The chargino pair-production cross-section is large and the chargino is excluded nearly up to the kinematic limit. The standard search for charginos has been applied down to $\Delta\mathrm{M} = M_{\tilde{\chi}_1^\pm} - M_{\tilde{\chi}_1^0} = 3$ GeV/c^2. Smaller values of ΔM may occur in scenarios without gaugino mass unification [13]. Even if mass unification is assumed, they are expected for very high values of M_2 ($M_2 > 1400$ GeV/c^2). The region $\Delta\mathrm{M} < 3$ GeV/c^2 is covered by the search requiring an ISR photon and by the searches for long-lived charginos.

At low $\tan\beta$ ($\tan\beta < 1.2$), neutralino searches can extend the coverage beyond the kinematic limit for chargino production. This concerns the region of (low) negative μ and $M_2 > 60$ GeV/c^2. In particular, searches for neutralino cascade decays are crucial for investigating $M_2 < 120$ GeV/c^2 where the $\tilde{\chi}_1^0\tilde{\chi}_2^0$ cross-section is small.

Low m_0

If m_0 is low, light sfermions affect the chargino and neutralino production cross-sections. In particular, the decrease of m_0 causes the chargino production cross-section to drop in the region where the gaugino components dominate (low M_2 and high $|\mu|$). Down to $m_0 \simeq 200$ GeV/c^2 it remains high enough to allow chargino exclusion nearly up to the kinematic limit. For lower m_0 the neutralino production cross-section is very much

enhanced, and neutralino searches become sensitive instead.

If m_0 is very low ($m_0 \simeq 100\text{GeV}/c^2$), sleptons can be sufficiently light to affect drastically the decay patterns of charginos and neutralinos, and nearly invisible final states can become dominant in some cases. However, for such low m_0 and low M_2 (below 200 GeV/c^2) sleptons can also be searched for in direct pair production.

If $M_{\tilde{\chi}_1^\pm} > m_{\tilde{\nu}}$ and the mass difference $M_{\tilde{\chi}_1^\pm} - m_{\tilde{\nu}}$ is small, the chargino decay chain $\tilde{\chi}_1^\pm \to \tilde{\nu}\ell \to \nu\tilde{\chi}_1^0\ell$ is dominant, and leads to an experimentally undetectable final state (the only visible final state lepton has very low momentum). However, in this case the search for selectrons can be used to constrain the sneutrino mass, under the assumption of unification, and thus the chargino mass.

It can also happen, in scenarios with important mixing among sfermions and high $\tan\beta$ and M_2, that 'blind spots' occur in the chargino detection sensitivity due to $\tilde{\chi}_1^\pm \to \tilde{\tau}\nu \to \tau\tilde{\chi}_1^0\nu$ with a small mass difference $M_{\tilde{\tau}} - M_{\tilde{\chi}_1^0}$. In this case $\tilde{\chi}_1^0\tilde{\chi}_2^0$ or $\tilde{\chi}_2^0\tilde{\chi}_2^0$ production with $\tilde{\chi}_2^0 \to \tilde{\tau}\tau$ are the only detectable channels. A specific search was designed for this case.

3 Detector description

The DELPHI detector is described in detail in [14]. The central tracking system consists of a Time Projection Chamber (TPC), supplemented by a system of silicon tracking detectors and drift chambers. It is situated inside a solenoidal magnetic field of 1.2 T, parallel to the beam axis. The average momentum resolution for charged particles in hadronic final states is in the range $\Delta p/p^2 \simeq 0.001 - 0.01$ (GeV/c)$^{-1}$.

The electromagnetic (EM) calorimeters are symmetric around the plane perpendicular to the beam ($\theta = 90^\circ$) [2], with the High density Projection Chamber (HPC) extending from 88.7° to 43.1° (barrel region), the Forward Electromagnetic Calorimeter (FEMC) from 36° down to 9°, overlapping with the Small angle Tile Calorimeter (STIC), which covers the range $1.7^\circ \leq \theta \leq 10.6^\circ$. The region of poor electromagnetic calorimetry at a polar angle close to 40° is instrumented by scintillators (hermeticity taggers) [15] which serve to reject events with unmeasured photons.

The Hadron Calorimeter (HCAL) covers 98% of the solid angle. Muons with momenta above 2 GeV/c penetrate the HCAL and are recorded in sets of Muon drift chambers in the barrel (MUB) and forward (MUF) regions of the detector.

4 Data samples and event generators

During 2000 DELPHI collected data in the centre-of-mass energy range from 201.5 to 208.8 GeV. The average centre-of-mass energy was $< \sqrt{s} >= 206$ GeV and the total integrated luminosity amounted to about 224 pb^{-1}. In 1999 (1998) the DELPHI detector collected about 227 pb^{-1} (158 pb^{-1}) at centre-of-mass energies around 192, 196, 200 and 202 GeV (189 GeV).

[2] In DELPHI, a right-handed cartesian coordinate system is used with the z direction defined by the direction of the electron beam, and the x-axis pointing towards the centre of the LEP ring. The origin is at the centre of the detector. The polar and azimuthal angles θ and ϕ are defined with respect to the z axis and ϕ=0 corresponds to the x-direction.

For all searches, the analysis of the data collected in the year 2000 is presented in section 5. Details on the combination with data taken in previous years are given for each channel in section 6.

On September 1st 2000, sector 6 of the TPC (corresponding to 1/12 of the TPC acceptance) failed beyond repair. This required modifications of the pattern recognition, and affected the quality of charged track reconstruction. Thus special care had to be taken for each search when analysing the data collected without sector 6, and these data were not used for all searches, as detailed below. The accumulated integrated luminosities with and without a working sector 6 are 164 pb^{-1} and 60 pb^{-1}at average centre-of-mass energies of 205.9 GeVand 206.5 GeV, respectively.

In order to increase the sensitivity for a discovery, the data collected in 2000 were divided into 4 regions of centre-of-mass energy as given in table 1 [3].

$\sqrt{s}$ region of analysis			$\mathcal{L}$ (pb^{-1})	$<\sqrt{s}>$ (GeV)
1	Sector 6 On	$\sqrt{s}\leq$ 205.75 GeV	78.3	204.9
2	Sector 6 On	205.75 $<\sqrt{s}\leq$ 207.5 GeV	78.8	206.7
3	Sector 6 On	207.5 GeV$<\sqrt{s}$	7.2	208.2
4	Sector 6 Off	all $\sqrt{s}$	60.0	206.5

Table 1: Definition of the $\sqrt{s}$ regions used to analyse the data collected in 2000.

To evaluate the signal efficiencies and background contaminations, simulated events were generated using several different programs.

The background process $\mathrm{e^+e^-} \to \mathrm{q\bar{q}}(n\gamma)$ was generated with `PYTHIA 6.125` [16]. For $\mu^+\mu^-(\gamma)$ and $\tau^+\tau^-(\gamma)$, `DYMU3` [17] and `KORALZ 4.2` [18] were used, respectively, while the `BHWIDE` generator [19] was used for Bhabha events. Simulation of four-fermion final states was performed using `EXCALIBUR` [20] and `grc4f` [21].

Two-photon interactions giving hadronic final states were generated using `TWOGAM` [22], `PHOJET` [23] and `PYTHIA 6.143` [16], while leptonic final states were generated using the generator of reference [24], including radiative corrections for the $\mathrm{e^+e^-}\,\mu^+\mu^-$ and $\mathrm{e^+e^-}\,\tau^+\tau^-$ final states.

`SUSYGEN 2.2004` [25] was used to generate chargino, neutralino, slepton, and sbottom signal events and to calculate cross-sections and branching ratios for these channels. For the nearly mass-degenerate case, the chargino decays were modelled with the results of the computations of reference [13]. Stop events were generated according to the expected differential cross-sections using the `BASES` and `SPRING` program packages and taking special care in the modelling of the stop hadronisation [26].

In all cases except for stop generation, `JETSET` 7.4 [16], tuned to LEP 1 data [27], was used for quark fragmentation.

The generated signal and background events were passed through the detailed simulation of the DELPHI detector and then processed with the same reconstruction and analysis programs as the real data. The numbers of simulated events from different background processes were several times the numbers in the real data.

[3]The three energy bins shown in the table for the period in which the detector was fully operational will be referred to in the text by their approximate average centre-of-mass energies: 205, 207 and 208 GeV.

5 Descriptions of the analyses

The analyses described below can be divided into two stages. The first stage was very similar for all searches and consisted of the selection of charged and neutral particles followed by an event preselection. In the subsequent stage, analyses differed according to the characteristics of the various signals. Each analysis has a set of additional preselection cuts complementing the ones described in section 5.1.2 and then specific higher selection levels.

As discussed above, the sensitivities of the searches depend on the mass difference (ΔM) between the produced sparticles and the LSP, which determines the visible energy released in the process. The coverage of all the relevant ΔM regions often requires the combination of different searches or the optimization of the selection criteria separately in each ΔM interval. Sparticle searches for very low values of ΔM are particularly challenging and required different criteria also in the preselection. In most searches several different topologies were considered, accounting for the different possible final states; in particular, high and low multiplicity topologies had to be treated separately.

Different analysis techniques were chosen for the various searches: some analyses were based on simple requirements on individual event variables ("sequential cut analyses"), others used multidimensional techniques based on likelihood ratios or neural networks. The preselection and the details of each analysis are described in the following parts of this section.

5.1 Basic selections and techniques

5.1.1 Particle selection

The following quality requirements were applied to the charged and neutral particles observed in the detector.

Charged particles were required to have momentum p above 100 MeV/c and below $1.5\sqrt{s}/2$ and to extrapolate back to within 5 cm of the main vertex in the transverse plane and 10 cm/$\sin\theta$ in the longitudinal direction. Similar but more stringent criteria were applied to tracks inside the acceptance of the TPC which gave no signal in this detector.

In the nearly degenerate chargino search (see section 5.2.2) there was no lower bound on the momentum for tracks at polar angle above 25°, while $p > 150$ MeV/c was required otherwise. In addition, the impact parameter requirements were less stringent.

Energy clusters in the calorimeters were taken as neutral particles if not associated to a charged particle and if above an energy threshold ranging from 300 to 500 MeV for deposits in the electromagnetic calorimeters (depending on the region of the detector) to 900 MeV for deposits in the hadron calorimeters.

5.1.2 Event preselection

In the preselection, events were kept if there were at least two charged particles, at least one of them had a transverse momentum above 1.5 GeV/c, and the transverse energy of the event [4] exceeded 4 GeV/c.

[4]The transverse energy is defined as the sum of the absolute values of the transverse momenta of all particles in the event.

The main background processes rejected at this level were two-photon interactions (for which most of the energy is deposited in the forward regions of the detector), neutral or single track final states (like $e^+e^- \to \gamma\gamma$, $e\gamma \to e\gamma$) and beam-related backgrounds.

For chargino searches in nearly degenerate scenarios a looser version of the preselection was applied: at least two charged particles were required, as well as one isolated electromagnetic cluster with transverse energy above approximately 5 GeV and a mass recoiling against it above 90 GeV/c^2. Two-photon and beam-gas background was reduced by rejecting events with a large fraction of their total energy in the forward region of the detector.

5.1.3 Particle identification and reconstruction algorithms

The following criteria for particle and event classification were common to the different searches.

Particle jets were reconstructed using two different approaches:

- The `DURHAM` [28] algorithm was used to cluster the particles into a fixed number of jets: two or four.
- The `LUCLUS` [16] algorithm was applied with the critical distance set to d_{join} = 10 GeV/c or d_{join} = 2.5 GeV/c . The final number of jets is, thus, variable (and lower in the first case).
- A specific algorithm optimized for the low multiplicity jets resulting from τ decays was used for $\tilde{\tau}$ pair production searches and is described in section 5.4.2.

The presence of isolated leptons or photons in the event is often very important in distinguishing signal and background. In the present searches, two isolation criteria were defined, depending of the multiplicity of the event:

- In low multiplicity searches, charged tracks were classified as isolated if the total charged energy in a 10° cone around the track was below 2 GeV. Slightly tighter cuts in the impact parameters (1 cm and 5 cm in $r\phi$ and z respectively) and in the momentum error were also applied.
- In high multiplicity searches, a photon was considered isolated if its angular separation from any neutral or charged particle was greater than 15°. A lepton was tagged as isolated if its angular separation from all the jets (computed without the lepton using the LUCLUS algorithm with d_{join} = 40 GeV/c) was greater than 20°.

The identification of muons was provided primarily by the DELPHI standard algorithm described in [14] which relies on the association of charged particles to signals in the muon chambers and the HCAL.

Electron and photon identification was performed by the algorithm described in [29] which combines deposits in the EM calorimeters with tracking information and takes possible radiation and interaction effects into account by a clustering procedure in an angular region around the main shower. In low multiplicity topologies a looser electron identification based on the ratio E/p between the energy deposited in the EM calorimeter and the momentum of the associated charged track was also used.

e/γ separation inside the acceptance of the STIC luminometer is possible on a statistical basis, by using the veto information of the two planes of the scintillator counters placed in front of it.

Decays of b-quarks are tagged using a probabilistic method based on the impact parameters of tracks with respect to the main vertex [30]. $\mathcal{P}_E^+$ stands for the corresponding probability estimator for tracks with positive impact parameters, the sign of the impact parameter being defined by the jet direction. The combined probability $\mathcal{P}_{comb}$ includes in addition contributions from properties of reconstructed secondary vertices.

All searches made use of the information from the hermeticity taggers [15] to reject events with photons from initial state radiation lost in the otherwise insensitive region at polar angles around 40° and 140°. Events were rejected if there were active taggers in the direction of the missing momentum and not associated to reconstructed jets.

5.1.4 Analysis techniques

Likelihood ratio method

In the likelihood ratio method used, several discriminating variables are combined into one on the basis of their one-dimensional probability density functions (pdf). If the variables used are independent, this gives the best possible background suppression for a given signal efficiency [31]. For a set of variables $\{x_i\}$, the pdf's of these variables are estimated by normalized frequency distributions for the signal and the background samples. We denote the pdf's of these variables $f_i^S(x_i)$ for the signal events and $f_i^B(x_i)$ for the background events submitted to the same selection criteria. The likelihood ratio function is defined as $\mathcal{L}_R = \prod_{i=1}^{n} \frac{f_i^S(x_i)}{f_i^B(x_i)}$. Events with $\mathcal{L}_R > \mathcal{L}_{R_{CUT}}$ are selected as candidate signal events. The choice of variables and the value of $\mathcal{L}_{R_{CUT}}$ were optimized using simulated event samples by minimizing the signal cross-section that was expected to be excluded at 95% confidence level in the absence of a signal.

Neural networks

A neural network provides a different means of defining one discriminating variable from multidimensional distributions of event variables given as inputs. In the form used here it contains three layers of nodes: the input layer where each neuron corresponds to a discriminating variable, the hidden layer, and the output layer which is the response of the neural network. The program used in the squark analysis is SNNS [32]. A "feed forward" architecture is implemented and the "back-propagation" algorithm is used to train the network with simulated events. An independent validation sample was also used not to overtrain the network. A way of enhancing the efficiency of the network without increasing too much its number of parameters is to define a separate output node for each type of event that the neural network should separate.

5.2 Chargino searches

5.2.1 Standard search

The standard chargino search was designed to look for chargino pair production with $\tilde{\chi}_j^{\pm} \to \tilde{\chi}_1^0 \, \mathrm{f} \, \bar{\mathrm{f}}'$ or $\tilde{\chi}_j^{\pm} \to \tilde{\chi}_2^0 \, \mathrm{f} \, \bar{\mathrm{f}}'$, where both $\tilde{\chi}_2^0 \to \tilde{\chi}_1^0 \, \mathrm{f} \, \bar{\mathrm{f}}$ and $\tilde{\chi}_2^0 \to \tilde{\chi}_1^0 \gamma$ are considered.

The visible energy in the event and thus the properties of the chargino decay products are mainly governed by the value of the mass difference (ΔM) between the chargino and the lightest neutralino. This standard search covers scenarios in which the mass difference ΔM is above 3 GeV/c^2.

For low ΔM the signal events are similar to $\gamma\gamma$ events. For high ΔM they resemble four-fermion final states ($\mathrm{W}^+\mathrm{W}^-$, Z^0Z^0,..). For intermediate ΔM values, the background is composed of many SM processes in comparable proportions.

In order to cope with all the possible signatures of chargino decays, the signal and background events were divided into four mutually exclusive topologies:

- the $\ell\ell$ topology with no more than five charged particles and no isolated photons;
- the $jj\ell$ topology with more than five charged particles and at least one isolated lepton and no isolated photons;
- the *jets* topology with more than five charged particles and no isolated photons or leptons;
- the *rad* topology with at least one isolated photon.

The signal events selected in a given topology are mostly events of the corresponding decay channel, but events from other channels may also contribute. For instance, for low ΔM (and thus low visible energy) some events with hadronic decays are selected in the $\ell\ell$ topology, and some mixed decay events with the isolated lepton unidentified enter into the *jets* topology. This migration effect tends to disappear as ΔM increases. This effect was taken into account in the final efficiency and limit computations.

The signal events were simulated using the `SUSYGEN` generator for 126 combinations of $\tilde{\chi}_1^{\pm}$ and $\tilde{\chi}_1^0$ masses for nine chargino mass values ($M_{\tilde{\chi}_1^{\pm}} \approx$ 103, 102, 100, 98, 94, 85, 70, 50 and 45 GeV/c^2) and with ΔM ranging from 3 GeV/c^2 to 80 GeV/c^2. A total of 252000 chargino events (2000 per mass combination) was generated and passed through the complete simulation of the DELPHI detector. The kinematic properties (acoplanarity, E_{vis}, $\not\!\!P_t$,..) of the signal events were studied in terms of their mean value and standard deviation, and six ΔM regions were defined, each containing signal events with similar properties (table 2).

In each of these 24 windows (four topologies, six ΔM regions), a likelihood ratio function ($\mathcal{L}_R$) was defined. The variables $\{x_i\}$ used to build the $\mathcal{L}_R$ functions in the present analysis were [2]: the visible energy (E_{vis}), visible mass (M_{vis}), missing transverse momentum ($\not\!\!P_t$), polar angle of the missing momentum, number of charged particles, total number of particles, acoplanarity, acollinearity, ratio of electromagnetic energy to total energy, percentage of total energy within 30° of the beam axis, kinematic information concerning the isolated photons and leptons and two most energetic charged particles, and finally the jet characteristics.

The generation of these 24 likelihood ratio functions was performed in five steps:

- The signal distributions of all the variables $\{x_i\}$ were built with signal events generated with parameter sets giving rise to charginos and neutralinos with masses in the corresponding ΔM region. For each ΔM region the events were classified according to the above topological cuts. The background distributions were built with background events passing the same topological cuts.

- Preselection cuts, different for each ΔM region, were applied in order to reduce the high cross-section backgrounds (two-photon interactions and Bhabha events) and to generate the pdf's. The pdf's were then generated as mentioned in 5.1.4. Figures 1.a, 1.b and 1.c show the distributions of some event variables for the *jets*, $\ell\ell$ and *rad* topologies respectively, for real and simulated events.

- To reduce statistical fluctuations a smoothing was performed by passing the 24 sets of pdf's for signal and background through a triangular filter [33].

- In each window all the combinations of the pdf's were tested, starting from a minimal set of four variables. Every combination defined a $\mathcal{L}_R$ function (see section 5.1.4) and a $\mathcal{L}_{R_{CUT}}$ that minimized the expected excluded cross-section at 95% C.L. using the monochannel formula [34]. The parameters entering this computation were the number of expected background events and the efficiency of the chargino selection, defined as the number of events satisfying $\mathcal{L}_R > \mathcal{L}_{R_{CUT}}$ divided by the total number of chargino events satisfying the topological cuts. Figure 1.d shows the good agreement obtained between real and simulated events as a function of the likelihood ratio cut, for $25 \leq \Delta\mathrm{M} < 35$ GeV/c^2 in the $jj\ell$ topology.

- The combination of variables corresponding to the lowest excluded cross-section defined the $\mathcal{L}_R$ function and the $\mathcal{L}_{R_{CUT}}$ of this window.

Finally, for each window, the six likelihood ratio functions from the corresponding topology were combined by performing a logical 'or' of each possible subset (always including the likelihood ratio function from the considered window). The combination minimizing the expected cross-section limit was chosen. The detection efficiency was computed only using the chargino events belonging to the investigated window.

This analysis was applied to the data collected by DELPHI in 1999 and 2000. For the data recorded in 2000 only the first 3 regions of $\sqrt{s}$ defined in table 1 were investigated.

ΔM regions	
1	$3 \leq \Delta\mathrm{M} < 5$ GeV/c^2
2	$5 \leq \Delta\mathrm{M} < 10$ GeV/c^2
3	$10 \leq \Delta\mathrm{M} < 25$ GeV/c^2
4	$25 \leq \Delta\mathrm{M} < 35$ GeV/c^2
5	$35 \leq \Delta\mathrm{M} < 50$ GeV/c^2
6	50 GeV/$c^2 \leq \Delta$M

Table 2: Definition of the ΔM regions for the standard chargino search.

5.2.2 Nearly degenerate scenarios

The search for charginos in the nearly mass-degenerate scenarios uses several different techniques, depending on the lifetime of the chargino, which in turn depends on the mass difference ΔM between the chargino and the lightest neutralino (this is the only relevant dependence, at least in the heavy slepton hypothesis).

When ΔM is below the mass of the pion, the chargino lifetime is usually long enough to let it pass through the entire detector before decaying. This range of ΔM can be covered by the search for long-lived heavy charged particles. For ΔM $\sim$ few hundred MeV/c^2 the chargino can decay inside the main tracking devices of DELPHI. Therefore, a search for secondary vertices or kinks can be used to cover this region. As the mass difference increases, the mean lifetime shortens until the position of the $\tilde{\chi}_1^{\pm}$ decay can hardly be distinguished from the main event vertex. In this case, the tagging of a hard Initial State Radiation (ISR) photon can help in exploring the ΔM region between few hundred MeV/c^2 and 3 GeV/c^2.

The following selection criteria were applied to the data collected by DELPHI in the years 1999 and 2000. They are similar to the ones used in the analysis of previous data, which have been described in [3]. All data were finally combined to obtain the present results.

Search for quasi-stable charginos

The search for heavy stable charged particles is described in [11]. The method used to identify heavy stable particles relied on the ionisation loss measurements in the TPC and on the absence of signal in the DELPHI Čerenkov radiation detectors (RICH). The RICH detectors have two radiators (gas and liquid) with different refractive index and thus different velocity threshold. Heavy stable charged particles crossing the detector would be seen in the tracking system and have as distinctive signature the absence of Čerenkov radiation and an anomalous energy loss in the TPC. To fulfill the requirements of the search for charginos and to facilitate the combination with the results of the searches for shorter decay lengths, only the first three criteria described there were applied here. That is, a charged particle to be selected in the search had to fulfill at least one of the following requirements:

- momentum above 15 GeV/c, a gas veto and a liquid veto in the RICH;
- momentum above 5 GeV/c, high ionisation loss in the TPC and a gas veto in the RICH.
- momentum above 15 GeV/c, ionisation loss in the TPC at least 0.3 below the expectation for a proton, and a gas veto in the RICH;

Search for charginos decaying visibly

If a heavy charged particle decays inside the central tracking devices of DELPHI (at a radius between 10 cm and 1 m) then both the incoming and the outgoing track can be reconstructed, and the angle between the tracks can be calculated. Such a search for kinks was originally designed to search for long-lived staus in the GMSB scenario [11]. A similar technique was applied to search for mass-degenerate charginos, with some specific

features needed because the visible decay products carry very little momentum in the nearly mass-degenerate case.

Details of the selection criteria can be found in [3]. Here only a brief and qualitative summary of the most important selection cuts is given.

A set of rather loose general requirements was imposed on the events in order to suppress the low energy background (beam-gas, beam-wall, etc), two-photon, e^+e^- and hadronic events. For each event surviving the preselection cuts, all the charged particles were grouped in clusters according to their measured point closest to the interaction vertex (starting point). A cluster with only one track with momentum above 20 GeV/c was considered as a possible chargino candidate if it was compatible with a particle coming from the interaction point. For each single track cluster fulfilling the above conditions, a search was made for a second cluster possibly formed by the decay products of the $\tilde{\chi}_1^+$ and defining a secondary vertex or kink with the chargino candidate.

Reconstructed secondary vertices could also be the result of particles interacting in the detector material, or radiating and giving a particle trajectory reconstructed in two separate track segments. Additional requirements aiming at the rejection of this kind of background were applied to the events with a good crossing point (kink) [11]. Finally, for an event to be accepted, at least one charged particle had to be found in each hemisphere (defined by the plane containing the beam spot and perpendicular to the line connecting the beam spot to the kink).

Search for charginos with ISR photons

The visible particles resulting from a chargino decay when it is nearly mass-degenerate with the LSP have typically little energy and momentum. They are hard to trigger on in the experiment, and in addition they are overwhelmed by the background from two-photon events. The ISR photon tag improves detectability and, if the transverse energy of the photon is above some threshold which depends on the minimal polar angle acceptance of the experiment, it rejects most of the two-photon background.

After the preselection, which was summarized in 5.1.2, the following requirements were applied to the data and simulation samples.

- There had to be at least two and at most six good charged particles passing the quality criteria (see section 5.1.1) and no more than ten tracks in total.
- The transverse energy of the ISR photon was required to be greater than $(E_T^\gamma)^{\min}$, where $(E_T^\gamma)^{\min} \simeq 0.03 \cdot \sqrt{s}$.
- The mass recoiling against the photon had to be above $2M_{\tilde{\chi}_1^+} - \delta M$, where the term δM takes into account the energy resolution in the electromagnetic calorimeters.
- The photon had to be isolated by at least 30° with respect to any other charged or neutral particle in the event.
- The sum of the energies of the particles emitted within 30° of the beam axis (E_{30}) was required to be less than 25% of the total visible energy. If the photon was inside this angular region its energy was included neither in E_{30}, nor in the visible energy.

- If the ISR photon candidate was detected in the very forward DELPHI calorimeter (STIC), it had not to be correlated with a signal in the scintillators placed in front of the STIC.
- $(E_{\rm vis} - E_\gamma)/\sqrt{s}$ had to be below a kinematical threshold which depended on ΔM and on $M_{\tilde{\chi}_1^+}$ (and in any case below 6%).
- $\not{P}_t / E^T_{\rm vis}$ had to be above 0.40 if ΔM $>$ 300 MeV/c^2, and above 0.75 for smaller ΔM's.
- There had to be no signals from the hermeticity counters isolated with respect to the other charged and neutral particles in the event (with the same criteria as used in the standard chargino search).
- If ΔM $>$ 1 GeV/c^2 , at least two charged particles in the event had to be consistent with coming from the interaction vertex.

The distribution of some of the variables used in the final selection for the data, the MC simulation of standard processes, and the MC simulation of the signal, is shown in figure 2. Above a certain overall qualitative agreement of the various distributions, there is already an excess of data. On the other hand, it is known that the two-photon MC simulation lacks the events which have small $\gamma\gamma$ invariant mass, and that in some of the cases (namely, $\gamma\gamma \to e^+e^-$) there is also no ISR implemented at all. Moreover, background processes such as beam-gas interactions are not included in the simulation. As in the previous publications [3], the most likely explanation of such disagreement is therefore a deficit of standard MC events rather than an excess of data from possible new physics. As no attempt will be made in the following to account for the missing backgrounds in the simulation, the exclusion limits that will be obtained are conservative.

5.3 Neutralino searches

The neutralino searches were designed to cover both $\tilde{\chi}_k^0\tilde{\chi}_1^0$ production with $\tilde{\chi}_k^0 \to \tilde{\chi}_1^0 + \mathrm{f}\,\bar{\mathrm{f}}$, with a signature of acoplanar jets or leptons, and channels of the type $\tilde{\chi}_k^0\tilde{\chi}_j^0$ with k or $j > 2$, which can lead to neutralino cascade decays. To maximise the sensitivity several searches were used for different topologies, namely:

- a search for acoplanar jet events, as from $\tilde{\chi}_1^0\tilde{\chi}_2^0$ with $\tilde{\chi}_2^0 \to \tilde{\chi}_1^0 \mathrm{q}\,\bar{\mathrm{q}}$;
- a search for acoplanar lepton events, as from $\tilde{\chi}_1^0\tilde{\chi}_2^0$ with $\tilde{\chi}_2^0 \to \tilde{\chi}_1^0\,\ell^+\ell^-$;
- a search for multijet events, as from $\tilde{\chi}_i^0\tilde{\chi}_j^0, i = 1,2, j = 3,4$ with $\tilde{\chi}_j^0 \to \tilde{\chi}_2^0 \mathrm{q}\,\bar{\mathrm{q}}$ and $\tilde{\chi}_2^0$ decaying to $\tilde{\chi}_1^0 \mathrm{q}\,\bar{\mathrm{q}}$ or $\tilde{\chi}_1^0\gamma$;
- a search for multilepton events for the corresponding decays to lepton pairs;
- a search for cascade decays with tau leptons, e.g. $\tilde{\chi}_2^0\tilde{\chi}_1^0$ production with $\tilde{\chi}_2^0 \to \tilde{\tau}\tau$ and $\tilde{\tau} \to \tilde{\chi}_1^0\tau$.

The different searches, briefly described below, were designed to be mutually exclusive in order to allow easy combination of the results. Thus events selected in the likelihood-based searches for acoplanar leptons or jets of subsection 5.3.1 were explicitely rejected in the searches described in the subsequent sections.

5.3.1 Acoplanar jets and acoplanar leptons searches

As mentioned above, the acoplanar jets and acoplanar leptons topologies are dominant in most of the parameter space. For these cases, a search based on the likelihood ratio method was performed and the sequential cut analyses described in reference [4] were used as a cross-check.

The characteristics of the neutralino decays are mainly determined by the value of ΔM, here defined as the mass difference between the heavier of the produced neutralinos and the LSP ($\tilde{\chi}_1^0$). For low ΔM, the signal events are similar to $\gamma\gamma$ events, for high ΔM they resemble four-fermion final states (W^+W^-, Z^0Z^0,..), while for intermediate ΔM values the background is composed mainly of two-fermion processes. The total energy of the visible final state particles, $E_{\rm vis}$, was used to distinguish between regions of different signal and background characteristics in the optimisation of the selection.

Likelihood Ratio analysis

Earlier variations of this search at lower energies have been described in Refs. [5].

The first step of the analysis was to divide the events in three mutually exclusive topologies: ee, $\mu\mu$, and $q\bar{q}$. The ee topology was defined as events having exactly two isolated lepton candidates (see section 5.1.3). At least one of these had to be an identified electron, and neither identified as a muon. Similarly, the events of the $\mu\mu$ topology were required to contain at least one isolated muon candidate and no isolated electron. The $q\bar{q}$ topology was defined as events with more than five charged particles and no isolated photons or leptons.

In the second step, aimed at removing the dominant SM background processes, events which fulfilled all of the following criteria were selected:

- the polar angles of the most energetic neutral and charged particle were required to be greater than 10°;
- the missing transverse momentum had to exceed 2 GeV, or 4 GeV if the visible energy was less than 30 GeV;
- both the acoplanarity and acollinearity had to be greater than 3°;
- the event had to not be vetoed by the hermeticity taggers (see section 5.1.3);
- the total visible energy had to be less than $0.75\sqrt{s}$.

The first two requirements remove the bulk of the $\gamma\gamma$ events and off-momentum electrons. The third and fourth reject two-fermion processes. The last requirement removes mainly four-fermion events.

In the $q\bar{q}$ topology an additional selection was applied to suppress further the large $q\bar{q}(\gamma)$ background. This was based on the jets reconstructed using the Durham algorithm when forcing the number of jets to two. If the invariant mass of the event was within 40 GeV/c^2 of the Z mass, the acoplanarity of the two jets was required to be at least 10°.

The numbers of selected events in the different topologies at this stage of the analysis are summarized in table 3.

For different values of $E_{\rm vis}$ (typical of different values of ΔM), the kinematic properties of the signal were studied in terms of the mean value and standard deviation of several

Preselection Level					
$q\bar{q}$		ee		$\mu\mu$	
Data	MC	Data	MC	Data	MC
3049	2950±11	146	162 ± 4	377	402 ±5

Table 3: Selected events in real and simulated data at preselection level in the neutralino search for the $q\bar{q}$, ee, and $\mu\mu$ topologies

event variables. Five visible mass regions were defined each containing signal events with uniform properties and homogeneous SM background. These regions are given in table 4, together with the corresponding dominant SM background.

$E_{\rm vis}$ regions		main SM bkg
1	$5 \leq E_{\rm vis} < 20$ GeV/c^2	$\gamma\gamma$
2	$20 \leq E_{\rm vis} < 50$ GeV/c^2	$\gamma\gamma$, 2 fermions
3	$50 \leq E_{\rm vis} < 70$ GeV/c^2	2 fermions
4	$70 \leq E_{\rm vis} < 110$ GeV/c^2	2 and 4 fermions
5	110 GeV/$c^2 \leq E_{\rm vis}$	4 fermions

Table 4: Definitions of the visible mass regions for the neutralino search and the corresponding dominant SM backgrounds.

In the last step of the analysis, for each of the 15 windows (three topologies, five $E_{\rm vis}$ regions) thus defined, a likelihood ratio function was computed. The variables used in the likelihood definition are listed below:

- global variables (all topologies) comprising visible energy, transverse energy, missing momentum, energy and direction of the most energetic charged and neutral particles, transverse momentum with respect to the thrust axis, polar angle of the missing momentum, thrust value, thrust direction and acoplanarity;
- variables specific to the $q\bar{q}$ topology (calculated forcing the event into two jets) comprising jet directions, energies, widths, invariant mass and $y_{\rm cut}$ value;
- variable specific to the ee and $\mu\mu$ topologies, namely the invariant mass of the two charged particles.

For each variable used in the likelihood, the one-dimensional probability density function (pdf) was defined according to the procedure described in sections 5.1.4 and 5.2.1, and events with $\mathcal{L}_R > \mathcal{L}_{R_{CUT}}$ were selected as candidate signal events.

Some event variable distributions for real and simulated data before the likelihood selection are illustrated in figure 3. The visible energy of the events passing this selection is also shown for each topology.

Sequential analysis

The detailed selection criteria for the selection based on sequential cuts are given in reference [4] and have not been changed. This analysis was used as a cross-check of the likelihood ratio results. At the **final** selection level, criteria optimized for different

ΔM=$M_{\tilde{\chi}^0_2}$-$M_{\tilde{\chi}^0_1}$ regions were designed. They were used as independent selections in the derivation of results.

The numbers of events selected at the final step of the analysis at the various centre-of-mass energies for acoplanar leptons and acoplanar jets are listed in table 5.

The results of the sequential and likelihood ratio analyses were found to be comparable. The sequential analysis was less performant in the acoplanar jet search for large ΔM values, whereas their results were very similar in the acoplanar lepton channels and in the low ΔM region in general.

$\sqrt{s}$	low ΔM		medium ΔM		high ΔM	
(GeV)	Data	MC	Data	MC	Data	MC
ee selection						
205	0	0.8 ± 0.03	2	2.3 ± 0.07	3	3.2 ± 0.1
207	1	0.8 ± 0.1	3	3 ± 0.4	2	2.8 ± 0.4
208	0	0.3 ± 0.01	1	0.3 ± 0.05	1	0.3 ± 0.05
all	1	1.9 ± 0.1	6	5.6 ± 0.4	6	6.3 ± 0.4
$\mu\mu$ selection						
205	1	0.4 ± 0.01	1	1.4 ± 0.04	3	2.7 ± 0.09
207	1	0.4 ± 0.05	0	1.5 ± 0.2	2	2.7 ± 0.4
208	1	0.04± 0.01	0	0.1 ± 0.02	0	0.2 ± 0.04
all	3	0.8 ± 0.05	1	3.0 ± 0.2	5	5.6 ± 0.4
qq selection						
205	0	1.1 ± 0.3	3	5.4 ± 1.3	4	5.2 ± 1.2
207	1	1.2 ± 0.06	6	5.5 ± 0.3	5	4.7 ± 0.2
208	0	0.1 ± 0.01	1	0.5 ± 0.05	3	0.4 ± 0.04
all	1	2.4 ± 0.3	10	11.4 ± 1.3	12	10.3 ± 1.2

Table 5: Results of the acoplanar leptons and acoplanar jets searches based on sequential cuts at the final selection level for the different flavours, ΔM regions and centre-of-mass energies. The numbers of events selected in data and expected from the SM simulation are given. Simulation errors are statistical.

5.3.2 Multijet search

The multijet search was optimised for cascade decays of neutralinos with large mass splittings, giving high energy jets. Events with energetic photons, characteristic of the decay $\tilde{\chi}^0_2 \to \tilde{\chi}^0_1\gamma$, were treated separately.

This selection was similar to the acoplanar jet selection but required a rather large transverse energy and allowed any number of reconstructed jets. Events selected by the searches for acoplanar leptons or acoplanar jets were explicitly rejected.

The detailed selection criteria are similar to the ones described in reference [4]. Together with background studies based on earlier data and improved energy reconstruction, this motivated several changes in the selection procedure. Three selection stages (**preselection**, **intermediate** selection and **final** selection) are used in the figures and the tables. As compared to reference [4] the preselection, aimed at selecting well reconstructed purely hadronic events with significant jet activity, was more selective. In the following, the most important steps of the new search are summarised.

At **preselection** level, at least five well-reconstructed charged particles were required, at least one of them with a transverse momentum exceeding 2.5 GeV/c. The transverse

energy of the event had to be greater than 25 GeV, the visible energy of the event was required to be less than $0.55\sqrt{s}$, and the missing momentum had to be less than $0.4\sqrt{s}$. There were several requirements aimed at selecting events with clear jets which were not dominated by single particles with large reconstructed energy. The upper plots in figure 4 show the distributions of the visible mass divided by the centre-of-mass energy for real data and simulated background events passing the above selection.

At the **intermediate** selection level, radiative return, two-photon, and Bhabha background was reduced by excluding events with large energy deposits in the EM calorimeters (above 60 GeV) or large amounts of energy in the forward region of the detector (more than 60% of the visible energy within 30° of the beam). Also, the transverse momentum had to exceed 6 GeV/c. The total momentum and the most energetic shower in the event were both required not to be close to the beam direction. A comparison of the $p_{\mathrm{T}}/\sqrt{s}$-distributions for real data and simulated background following the above selection is shown in the middle plots in figure 4.

At the **final** level of the selection the acollinearity and scaled acoplanarity (in a forced 2-jet configuration) [5] had to be greater than 30° and 10°, respectively. To reject WW background it was required that there be no charged particle with a momentum above 30 GeV/c, and no isolated leptons of significant energy. In addition, the mass recoiling against the system of visible particles had to be greater 50 GeV/c^2.

Events with a photon signature were then selected on the basis of reconstructed photons in the polar angle range between 20° and 160°, isolated by more than 20° from the nearest charged particle track. If there was only one such photon its energy was required to be between 10 GeV and 40 GeV; if more than one photon, at least two had to have energy greater than 10 GeV.

For the complementary sample, without a photon signature, several of the criteria above were made stricter in order to reject $\mathrm{Z}\gamma$ events. In addition, all jets with energy above 20 GeV had to have a ratio of energy in charged particles to energy in neutral particles which was above 0.15, and no isolated neutrals with energy greater than 40 GeVwere allowed.

The numbers of events selected at the initial, intermediate and final steps of the analysis at the various centre-of-mass energies are given in tables 6 and 7 for the multijet selection without and with photons respectively. The lower plots in figure 4 show the distribution of scaled acoplanarity for real and simulated data at the final selection level.

$\sqrt{s}$ (GeV)	Selection Level					
	Preselection		Intermediate		Final	
	Data	MC	Data	MC	Data	MC
205	2663	2642 ±16	371	349.4 ±5.2	18	16.3 ±0.5
207	2662	2693 ±9	408	363.8 ±2.7	22	17.6 ±0.7
208	247	244 ±1	36	33.1 ±0.3	3	1.7 ±0.1
all	5572	5579 ±18	815	746 ± 6	43	36 ±1

Table 6: Results of the search in the multijet without γ topology at the different selection levels and centre-of-mass energies. The numbers of events selected in data and expected from the SM simulation are given. Simulation errors are statistical.

[5] The scaled acoplanarity is the acoplanarity of the two jets multiplied by the sine of the minimum angle between a jet and the beam axis.

$\sqrt{s}$ (GeV)	Selection Level					
	Preselection		Intermediate		Final	
	Data	MC	Data	MC	Data	MC
205	27	29.5 ±0.8	4	7.8 ±0.3	2	1.2 ±0.1
207	32	30.3 ±0.9	7	7.6 ±0.3	0	1.1 ±0.1
208	2	2.8 ±0.1	1	0.6 ±0.04	0	0.1 ±0.02
all	61	63 ±1	12	16 ±0.4	2	2.4 ±0.1

Table 7: Results of the search in the multijet with γ topology at the different selection levels and centre-of-mass energies. The numbers of events selected in data and expected from the SM simulation are given. Simulation errors are statistical.

5.3.3 Multilepton search

The multilepton search is sensitive to cascade decays involving leptons, which can dominate if there are light sleptons. The selection of reference [4] was basically left unchanged.

At the **preselection** level, well reconstructed low multiplicity events with missing energy and missing mass were selected. In particular, the total visible energy including badly reconstructed tracks was required to be less than 140 GeV, the number of charged particles was required to be at least two and at most eight, and events with more than four neutral particles were rejected. The top left plot in figure 5 shows a comparison between the visible mass divided by the centre-of-mass energy distributions for real and simulated events passing the preselection.

The selection at the **intermediate** level served mainly to reject $Z\gamma$, two-photon, and Bhabha events by requiring significant transverse momentum and transverse energy ($E^T_{\rm vis}>$ 25 GeV). The distributions of $p_{\rm T}/\sqrt{s}$ for real and simulated data, following the intermediate selection are compared in the middle left plot in figure 5.

At the **final** selection level events with two or more well-reconstructed charged particles were subjected to criteria designed to reject Bhabha events and the charge asymmetry for the two most energetic such tracks was used to reject W pairs decaying leptonically. In events with four or more tracks the LUCLUS jet algorithm was applied, and events with exactly two reconstructed jets were rejected if their scaled acoplanarity was less than 15°.

The numbers of events selected at the initial, intermediate and final steps of the analysis at the various centre-of-mass energies are given in table 8

$\sqrt{s}$ (GeV)	Selection Level					
	Preselection		Intermediate		Final	
	Data	MC	Data	MC	Data	MC
205	5606	5192 ±48	58	63 ±3	13	11 ±1
207	5586	5186 ±39	57	61 ±5	22	16±1
208	512	478 ±4	7	5.6 ±0.3	0	0.9 ±0.1
all	11704	10856 ±62	248	200 ±8	35	28 ±1

Table 8: Results of the multilepton search at the different selection levels and centre-of-mass energies. The numbers of events selected in data and expected from the SM simulation are given. Simulation errors are statistical.

5.3.4 Tau cascade search

The tau cascade search is sensitive to $\tilde{\chi}^0_1\tilde{\chi}^0_2$ production with $\tilde{\chi}^0_2 \to \tilde{\tau}\tau$ and $\tilde{\tau} \to \tilde{\chi}^0_1\tau$, where the second τ produced has very low energy. This search was described in reference [4] and is briefly summarised here. A dedicated search for tau cascades in $\tilde{\chi}^0_2\tilde{\chi}^0_2$ production is described in section 5.4.2.

At the **preselection** level, well reconstructed low multiplicity events with missing energy and missing mass were selected. The selection was the same as for the multilepton search (section 5.3.3), with the additional requirement of no more than two reconstructed jets. Two or more of the charged particles also had to satisfy stricter criteria on reconstruction and impact parameters. The distributions of the visible mass divided by the centre-of-mass energy for real and simulated data at this level are shown in figure 5 (upper right plot).

At the **intermediate** selection level, the highest and second highest momenta of charged particles were required to be below 50 GeV/c and 25 GeV/c, respectively, and at least one charged particle had to have a transverse momentum above 2.5 GeV/c. The criteria to reject $Z\gamma$, two-photon, and Bhabha events were similar to those used in the multilepton search, except for the removal of the transverse energy requirement. Figure 5 (middle right plot) shows the distributions of $p_T/\sqrt{s}$ for real and simulated data at the intermediate selection level.

At the **final** selection level, events with exactly two isolated, well-reconstructed, oppositely charged particles were required to have acollinearity and acoplanarity above 60°. The smaller of the two momenta had to be below 70% of the greater one, and below 10 GeV/c. For events with two reconstructed jets the scaled acoplanarity was required to be greater than 20°, and the acoplanarity and the acollinearity greater than 60°. The acoplanarity distributions for the resulting samples of real and simulated data events are shown in figure 5 (lower right plot), and the numbers of events selected at the different selection levels are given in table 9.

CM Energy (GeV)	Selection Level					
	Preselection		Intermediate		Final	
	Data	MC	Data	MC	Data	MC
205	5358	5876 ±44	55	52 ±4	1	1.5 ±0.8
207	5366	5899 ±44	54	51 ±3	6	1.4 ±0.8
208	512	545 ±4	4	4.5 ±0.3	0	0.1 ±0.1
all	11236	12320 ±62	113	108 ±5	7	3 ±1

Table 9: Results of the asymmetric tau search at the different selection levels and centre-of-mass energies. The number of events selected in data and expected from the SM simulation are given. MC errors are statistical.

5.4 Slepton searches

5.4.1 Selectron and smuon searches

The data collected at centre-of-mass energies between 183 and 208 GeV were used to search for the supersymmetric partners of electrons and muons. The complete year 2000

data set was analysed, but all tracks in the region of the damaged sector of the TPC were ignored, and the estimated slepton efficiency was reduced accordingly.

The analysis was performed in two stages. Firstly, a loose preselection was used to obtain a sample of events containing two oppositely charged tracks. At this stage, various data distributions were compared with those from simulated Standard Model processes and variables well described by the Monte-Carlo were identified for use in further stages of the analysis. Comparing the simulated background and signal events, selections were made in order to reduce the expected SM backgrounds whilst keeping a reasonable efficiency for the signal over a wide region of the slepton-neutralino mass plane.

The selectron search

To search for selectrons, the general topology required was two acoplanar electrons and missing energy. The preselection kept all candidates with exactly two well-reconstructed oppositely charged isolated tracks with momentum above 1 GeV/c according to the definition described in section 5.1.3. One of the two charged tracks was required to be identified as an electron, rejecting events if the other was identified as a muon. At this stage of the selection the sample consisted mainly of Bhabha and two-photon events. Satisfactory agreement was observed between the data and simulated background, as shown in Figure 6.

To further reduce the SM backgrounds, tighter cuts were then applied. As 2-photon events are predominantly at low polar angles and with low momentum, it was required that the visible energy be greater than 15 GeV and that the energy deposited in the low angle STIC calorimeter be less than 4 GeV. As a further constraint, the invariant mass of the two tracks was required to be greater than 4.5 GeV/c^2 and the total transverse momentum with respect to the beam axis greater than 5 GeV/c. To reduce the number of Bhabha events an upper limit on the visible energy of 100 GeV was imposed, whilst also requiring that the neutral energy not associated to the charged tracks be less than 30 GeV. Events were also rejected if there were more than four neutral clusters in total, each with energy above 500 MeV. Bhabha events are coplanar with a large opening angle, hence it was demanded that the acoplanarity and acollinearity be greater than 15°. Constraints were also imposed on the momenta of the two tracks, requiring that both tracks had momentum greater than 2 GeV/c. It was further required that the missing momentum vector pointed to an active region of the detector.

The smuon search

As a preselection, exactly two well reconstructed oppositely charged particles with momenta above 1 GeV were required (see section 5.1.3). At least one of the tracks had to be identified as a muon. It was further required that neither track be identified as an electron. The preselection sample consisted mainly of two-photon events and good agreement between real data and simulated background was observed (figure 7).

To further reduce the SM background a series of tighter cuts were applied. To remove 2-photon events, the visible energy was required to be greater than 10 GeV. Also, the energy in the STIC had to be less than 1 GeV. It was also demanded that the invariant mass of the two tracks be greater than 4.5 GeV/c^2 and the transverse momentum be greater than 5 GeV/c. To remove $e^+e^- \rightarrow \mu^+\mu^-$ events, an upper limit of 120 GeV on the visible energy was imposed whilst also requiring the unassociated neutral energy to

be less than 10 GeV, with no more than 2 neutral clusters. This background was further suppressed by accepting only events in which the opening angle between the tracks was less than 165° and the acoplanarity was greater than 15°. To reduce W pair contamination, events were rejected if the positively charge muon was within 40° of the e^+ beam direction, or the negatively charged muon was within 40° degrees of the e^- beam direction.

5.4.2 Stau searches

The signature of stau-pair production are events with two acoplanar taus and high missing energy. The signature of staus produced in the process $\tilde{\chi}_2^0\tilde{\chi}_2^0 \rightarrow \tilde{\tau}\tau\ \tilde{\tau}\tau$, with the stau nearly degenerate with the $\tilde{\chi}_1^0$, is similar: the two acoplanar taus are accompanied by two low energy ones. To select such topologies, events with less than 10 charged tracks, a transverse momentum imbalance exceeding 4 GeV/c, and a visible invariant mass above 4.5 GeV/c^2 were retained for further analysis. A comparison of data and simulated Standard Model background at this stage is shown in figure 8.

Particle selection

Charged tracks passing the criteria presented in 5.1.1 were used, if in addition they had an angle to the beam exceeding 15°, a relative momentum error less than 100 %, and either at least 4 of the 16 pad-rows of the TPC or all three of the detectors VD, ID and OD were used in the reconstruction of the track. Neutral clusters passing the criteria of 5.1.1 were used if they also had angle to the beam above 15°, and passed cuts removing clusters created by ambient radioactivity in the HPC or by cosmics.

In addition, at least two tracks in the event were required to have momentum above 1 GeV/c, with a relative error less than 30 %. These two tracks had to be either above 30° to the beam or isolated (no neutral or charged activity in a 20° cone around the track). Their calorimetric energy should not exceed their momentum by more than three times the expected error on the calorimetric measurement.

Particle identification

Charged particles were classified as electrons, muons or hadrons, either tightly or loosely. Tight identifications were unambiguous, while a particle could simultaneously be loosely identified as several different species.

Tight electrons and muons were defined with the standard DELPHI algorithms (see section 5). A particle was considered as a tight hadron if was not classified as a muon or electron, and had an associated hadron calorimetric energy exceeding 50% of its momentum. In addition, if a particle had a loose identification for one species, and was vetoed for the other two, it was also considered as tightly identified.

The standard DELPHI algorithms were also used for loose identification of electrons and muons. A particle was considered as a loose hadron if any hadronic energy was associated and it was not tightly identified as a muon or electron. If both the electromagnetic and hadronic energies were small (less than 1 and 6 GeV respectively), and the difference between hadronic energy and the track momentum was above 10 GeV, the track was assigned both the loose muon and loose hadron code.

If the track pointed to a gap in the electromagnetic calorimetry, it was considered as a loose electron, even if the DELPHI algorithm vetoed the electron hypothesis.

Tracks with no identification information were treated as loose electrons.

The clustering procedure

The clustering method considered all possible ways to group the charged particles in the event into two groups. Tightly identified leptons were forced to form a single-particle group, as leptonic τ-decays are always in the 1-prong topology. However, pairs of oppositely charged, well identified electrons close together were allowed to be grouped with other tracks, since they would be likely to originate from a photon from a π^0-decay, converted in the beam-pipe or the VD. When more than one way of obtaining two groups both with invariant mass below 2.0 GeV/c^2 was found, the grouping yielding the lowest sum of masses was retained.

Once the best grouping of the charged tracks was found, it was attempted to associate the neutrals in the event to the particle groups. Also in this step, the grouping yielding the lowest sum of masses was chosen, if more than one possibility was at hand. If a neutral particle could not be merged into any of the groups, without the invariant mass exceeding 2.0 GeV/c^2, it was treated as an *isolated neutral* in the subsequent analysis. As very few hadrons are expected in τ-decays, neutral hadronic clusters were never included in the clusters. A special procedure was performed in order to identify neutral clusters that were likely to be either bremsstrahlung photons off an electron, or a shower induced by an electron that was not correctly assigned to the track by the reconstruction program. This procedure uses the fact that bremsstrahlung photons are collinear to the track at the point of production. Most of the material in the central part of DELPHI was at the outer field-cage of the TPC, or the inner field-cage, liquid radiators or drift-tubes of the barrel RICH, i.e. at a radius of around 135 cm. Assuming that the radiation originated at this radius, the impact-point on the HPC was predicted. Any neutral found close to this position was rejected. Its energy was then was subtracted from the momentum of the track, and the subsequent curvature of the track re-evaluated. The track-helix was extrapolated to its intersection with the HPC, and any neutral cluster found near to this point was also rejected.

Event selection for the stau-pair search

Events with exactly two particle clusters (possibly in company with isolated neutral particles) were considered further if there were no more than 6 charged tracks in the event and these gave a total charge of 0 or ± 1. At least one of the two particle-clusters should have a total momentum greater than 4% of the beam momentum. There should be no identified hadronic secondary interactions inside the tracking system.

To suppress the remaining 2-photon events, the pre-selection condition on transverse momentum imbalance was supplemented by the requirement that the the total calorimetric energy below 30° did not exceed 12% of the beam momentum, and the orientation of the event had to be well in the barrel region: $\theta(\Sigma\vec{p}) > 35°$.

To reduce the background from radiative return to the Z, none of the clusters were allowed to have a total momentum (p^{JET}) above 70% of the beam momentum, isolated photons had to be below 15% of the beam momentum, there had to be no signal in any isolated hermiticity tagger, the acoplanarity was required to be above 10°. In $\mathrm{e^+e^-} \to \mathrm{Z}/\gamma \to \tau^+\tau^-$events it was not sufficient to remove events with low acoplanarity and low missing transverse momentum: if the decay of one τ yielded visible products with large

momentum, while the other decay yielded soft products, both these quantities would be large. However, unlike a possible signal, the momentum transverse to the thrust axis (δ) tends to be small even for large acoplanarities in such events. Therefore δ had to exceed 0.9 GeV/c.

To suppress the WW background, the events were analysed as if they were indeed WW events, and the θ angle of the positive W was estimated (θ_{W^+}). If the momenta of the charged leptons from both the W decays are known, θ_{W^+} can be calculated exactly, albeit usually with two-fold ambiguity. If either W decays to a τ, the momentum of the τ is unknown, so the solution is approximate. Hence, two cases could be distinguished: either the W decayed to a muon or an electron, or to a τ. The treatment of the two cases differed in what absolute momentum was assigned to the lepton (in both cases, the direction of the W-decay product was estimated by the measured jet-direction). In the first case, which could be recognised by the presence of at least one 1-prong with at least a loose lepton identification and a momentum above the lowest possible momentum for the charged lepton from the decay of an on-shell W, the momentum of the initial lepton was assigned the measured jet-momentum. In the second case, the momentum of the initial τ was estimated by the expected momentum of the W decay products, given by the kinematics of $W \to \tau\nu$, with the additional condition that the τ-momentum could not be lower than the measured jet-momentum.

W pair-production is highly asymmetric, while the signal is isotropic. The W pair-production process tends to have higher values of the higher of the two jet momenta ($p_{high}^{\rm JET}$), and in addition θ_{W^+} and $p_{high}^{\rm JET}$ are correlated in such processes, while they are independent in $\tilde{\tau}$ production. In order to exploit the difference in the distribution and correlation of these observables, a cut was applied in the θ_{W^+} - $p_{high}^{\rm JET}$ plane: it was demanded that reconstructed angle was below a curve given by:

$$\theta_{W^+} = \begin{cases} -5.0x + 3.725 & \text{if } x < 0.325 \\ 2.1 & \text{if } 0.325 \leq x < 0.52 \\ -3.6x + 3.972 & \text{if } x \geq 0.52 \end{cases}$$

where $x = p_{high}^{\rm JET}/p_{beam}$. This curve closely follows a curve of equal ratio between the probability density functions for signal and for background, ie. the Likelihood ratio.

This selection was supplemented by cuts that depended on the region of the ($M_{\tilde{\tau}}$,M_{LSP}) plane considered. For high ΔM= $M_{\tilde{\tau}}$-M_{LSP}, the remaining background from two-photon events can be removed by a strong cut on transverse momentum imbalance. At lower values of ΔM such a cut would dramatically reduce the signal detection efficiency, and other methods must be employed to reduce this source of background. For the remaining two- and four-fermion background, the situation was the opposite: the requirement that the events should be kinematically compatible with a low ΔM signal imposes a strong cut on $p_{high}^{\rm JET}$, while other methods must be used for high ΔM, not to reduce the signal efficiency.

Therefore, if ΔM was below (above) 20 GeV/c^2 the total missing transverse momentum ($p_T^{\rm miss}$) had to exceed 0.9 (1.2) times the maximal transverse momentum a $\gamma\gamma$ event could have without one of the beam-remnant electrons being deflected into the STIC (ie. by an angle greater than $\theta_{min} = 1.82^\circ$). This limit depended on the centre-of-mass energy: $p_T^{\rm lim} = \sqrt{s}\sin\theta_{min}/(1+\sin\theta_{min}) = 0.031\ \sqrt{s}$. [6] To reduce the two-photon background in the lower ΔM region, there should be no calorimetric energy below 30°, and $\theta(\Sigma\vec{p}) > 45^\circ$.

[6] The missing transverse momentum was estimated in four different ways: as the transverse momentum

To reduce the two- and four-fermion background in the higher region, there should not be more than one identified electron or muon in the event and $p_{high}^{\rm JET}$ should be above 8% of the beam momentum. Electrons and muons in WW events might come either directly from the W-decay, or indirectly from τ-decays. In the former case, the momentum of the detected lepton tends to be higher than in the latter case. It was therefore demanded that the highest momentum of any tightly or loosely identified lepton in the event was less than 22 (19)% of the beam momentum in the high (low) ΔM region.

Event selection for the search for staus in $\tilde{\chi}_2^0\tilde{\chi}_2^0$ production

The final state of $\tilde{\chi}_2^0\tilde{\chi}_2^0 \to \tilde{\tau}\tau\ \tilde{\tau}\tau$ is quite similar to what is searched for in stau-pair production, the only difference being the presence of two soft taus from the stau-decay. The procedure used in the stau-pair search was therefore adopted for the search for $\tilde{\chi}_2^0\tilde{\chi}_2^0 \to \tilde{\tau}\tau\ \tilde{\tau}\tau$ as well, with the following modifications: rather than requesting exactly two τ-candidates in the event, it was requested that more than two such candidates were present. It was demanded that the third most energetic τ-candidate was soft: its momentum should not exceed 4% of the beam momentum. The cut on the maximal number of tracks in the event was increased from seven to eight. As there is virtually no $\mathrm{W^+W^-}$ background to this channel, the bi-dimensional cut in the θ_{W^+} - $p_{high}^{\rm JET}$ plane was removed. Because the only SM processes yielding final states with four taus are ZZ, ZZ^* or $Z\gamma^*$, it was demanded that the invariant mass of the two most energetic τ-candidates be below 40 GeV/c^2, i.e. well below $m_{\rm Z}$. Variables – such as the acoplanarity – that were intrinsically related to the two-jet topology were evaluated using the two most energetic τ candidates only. All other cuts were taken from the stau-pair search. For cuts that in the stau-pair search depended on the mass-difference between the stau and the LSP, the value corresponding to the looser cut was retained.

5.5 Squark searches

Supersymmetric partners of top and bottom quarks were searched for in data collected by DELPHI from 1998 to 2000 at centre-of-mass energies from 189 to 208 GeV. The data samples correspond to a total integrated luminosity of 606 pb^{-1}. The dominant decays of the stop and sbottom squarks are assumed to be $\tilde{\rm t}_1 \to c\tilde{\chi}_1^0$ and $\tilde{\rm b}_1 \to b\tilde{\chi}_1^0$, respectively, and the final topology is two acoplanar jets and missing energy. In the non-degenerate scenario ($\Delta M > 10$ GeV/c^2), the neural network analysis has already been presented in [9, 10]. This analysis has been extended down to $\Delta M = 5$ GeV/c^2. In addition, a new analysis based on a sequential cut approach has been developed to search for stop almost degenerate in mass with the LSP. DELPHI 1998 and 1999 data were re-analysed in this new framework.

5.5.1 Non-degenerate scenarios

After the track selection and the event preselection of section 5.1, events were forced into two jets using the Durham algorithm. A common preselection was then applied for both

of the two jets, as that of all particles passing the quality cuts, as that of all reconstructed particles except those identified as bremsstrahlung photons by the method outlined above, and as that of all reconstructed particles. The cut was applied on the smallest of these. This way one obtained stability against possible errors in reconstruction, in corrections, and against the presence of noise or cosmics.

stop and sbottom analyses. To select hadronic events, the number of charged particles reconstructed with the TPC was required to be greater than three, and the energy in the STIC to be less than 70% of the total energy. The polar angle of the thrust axis had to be between 20° and 160°. Then, the following event quality cuts were applied. The percentage of good tracks, the ratio of the number of charged tracks after the particle selection to the number before, had to be greater than 35%. In addition, the scalar sum of charged particle momenta reconstructed with the TPC was required to be greater than 55% of the total energy in the event, and the total number of charged particles to be greater than 6. A veto algorithm based on the hermeticity taggers was applied to reject events with badly measured energetic photons.

To remove radiative return events, the energy of the most energetic neutral particle was required to be less than 40 GeV. Additional cuts were then applied to restrict the selection to events with missing energy. The transverse missing momentum had to be greater than 4 GeV/c, the polar angle of the missing momentum had to be between 20° and 160°, and the energy in a 40° cone around the z axis was required to be less than 40% of the event energy. Finally, the visible mass of the events was required to be less than 95 GeV/c^2.

The number of events selected by this preselection was 2178 for 2143±8 expected (combined data from $\sqrt{s}$ =189 to 208 GeV). Figure 9 shows the Monte-Carlo comparison to the data. At this level, stop signal efficiencies were ranging from 20% to 70% depending on the mass difference between the stop and the neutralino. Sbottom efficiencies were quite similar except at low ΔM where, for example, the efficiency for $M_{\tilde{b}_1}$=90 GeV/c^2 and $M_{\tilde{\chi}^0_1}$=85 GeV/c^2 was close to zero, because the $\tilde{b}$squarks are produced almost at rest.

The final selection of events was performed using neural network techniques. Separate searches were made for two different ranges of ΔM: $\Delta M > 20$ GeV/c^2 and $5 < \Delta M \leq 20$ GeV/c^2. The neural network structure was the same for the stop and the sbottom searches. There were 10 input nodes (variables), 10 hidden nodes (in one layer) and 3 output nodes. The 10 input variables were: the ratio between the transverse missing momentum and the visible energy, the transverse energy, the visible mass, the softness defined as $M_{jet1}/E_{jet1} + M_{jet2}/E_{jet2}$, the acollinearity, the quadratic sum of the transverse momenta of the jets $\sqrt{(P_t^{jet1})^2 + (P_t^{jet2})^2}$, the acoplanarity, the sum of the first and third Fox-Wolfram moments, the polar angle of the missing momentum and finally the combined b-tagging probability. For each window of the stop and sbottom analyses the network was trained to discriminate the signal from the combined two-fermion and four-fermion backgrounds, and from the $\gamma\gamma$ interactions leading to hadronic final states.

	node 1	node 2	node 3
$\tilde{q}_1$ Signal	1	0	0
$\begin{cases} 2-\text{fermions} \\ 4-\text{fermions} \end{cases}$	0	1	0
$\gamma\gamma \rightarrow$ hadrons	0	0	1

Table 10: Values of the three output nodes used in the training of the neural networks of the non-degenerate squark analysis.

Although the three output nodes proved useful in training the network, the selection

was made according to the output of the signal node only. Figure 10 shows the number of events as a function of the signal efficiency for the two mass analysis windows of the stop and the sbottom searches. The number of events in the data is in agreement with the Standard Model background predictions over the full range of neural network outputs. The optimisation of the final cuts was performed by minimising the expected confidence level of the signal hypothesis, CL_s [36].

5.5.2 Nearly mass-degenerate scenarios

The stop ($\tilde{t_1}$) and the sbottom ($\tilde{b_1}$) can be nearly degenerate in mass with the LSP, without requiring special theoretical assumptions.

The width of the decay $\tilde{\mathrm{t}} \rightarrow c\tilde{\chi}_1^0$ is proportional to $m_{\tilde{t}}(1 - m_{\tilde{\chi}}^2/m_{\tilde{t}}^2)^2$, and therefore proportional to ΔM. So if ΔM gets small enough, the stop acquires a sizeable lifetime and may form a quasi-stable (decaying inside the tracking volume) or even stable stop hadron. These two cases are still under study, as well as the analysis of the nearly-degenerate mass scenario for the sbottom. The current analysis focusses on a stop decaying promptly into a charm and the LSP.

The event preselection required, in addition to the criteria described in section 5.1.2 that not more than 30% of the total visible energy was contributed to by tracks seen in the VD and ID only. To eliminate Bhabhas and leptonic $\gamma\gamma$ backgrounds, the charged multiplicity was required be greater than five. The $\gamma\gamma$ background was further suppressed by requiring the energy in a forward cone of 30° around the beam direction to be at most 40% of the total visible energy and smaller than 2 GeV and that no energy was deposited in the STIC calorimeter. To avoid the relatively low hadronic energy region, where the $\gamma\gamma$ background is¡ not well reproduced by the MC, the total transverse charged energy had to be greater than 7 GeV, the total transverse energy measured in the TPC and the total transverse momentum had to be greater than 4 GeV and 3.5 GeV/c, respectively, and the number of tracks with TPC information had to be at least 4.

Finally an hermiticity cut was applied using the taggers. The agreement between data and MC after this preselection is shown in table 11 and in figure 11.

Figure 11 also demonstrates that the two-fermion and four-fermion backgrounds dominate at this stage of the selection, and that the small contribution from two-photon interactions may be easily identified in the data.

A further selection was performed in order to reduce the remaining backgrounds. Firstly, events having mainly barrel activity were selected. This was achieved by requiring that the energy within a cone of 60° around the beam direction was less than 10 GeV and that the polar angle of the missing momentum was between 45 ° and 135 °. Secondly by demanding that the transverse momentum of the leading particle was less than 10 GeV/c and that the total transverse energy was less than 40 GeV, most of the remaining two- and four-fermion background was rejected. Finally, the total transverse momentum was required to be greater than 5 GeV/c and the scaled acoplanarity greater than 20 °. This cut removes most of the remaining background from 2-photon processes.

6 Results and limits

In this section the number of events selected and expected at the final event selections and the expected signal efficiencies are presented for each channel. No evidence of a significant

Stop (nearly-degenerate scenario)		
$\mathbf{\Delta M \leq\ 10}$ GeV/c^2		
$\sqrt{s}$	data	MC
188.7	3717	3717
191.6	527	599
195.6	1620	1623
199.6	1667	1679
201.7	867	793
205	1469	1492
207	1423	1468
208	138	133
206.5(*)	1023	1133

Table 11: Data MC comparison at the preselection level. (*) indicates 2000 data taken with the sector 6 of the TPC off.

excess with respect to the SM expectation is found in any of the channel. Thus, exclusion limits at 95% CL can be set. In a relatively model-independent approach, cross-section limits are derived. Sparticle mass limits are then obtained, with assumptions that depend on the channel and will be specified case by case.

6.1 Limit computation

Depending on the searches, limits were derived using the multichannel Bayesian method [35] or the modified frequentist likelihood ratio method [36]. Multichannel approaches allow to combine different search channels while preserving the information about efficiency, expected background, number of candidates and centre-of-mass energy in each of them.

Expected exclusion limits were calculated using exaclty the same algorithms and assuming the observation to be equal to the expectation in the absence of signal.

The two methods typically give similar results. Both methods take a posteriori knowledge about the background into account, and thus give physically reasonable and conservative results in the case of downward fluctuations of the background. Background fluctuations could nevertheless significantly affect the range of exclusion, and for this reason limits expected in the absence of a signal are also given below.

6.2 Chargino searches

6.2.1 Standard search

Efficiencies and selected events

The total numbers of background events expected in the different windows are shown in tables 12 and 13 together with the numbers of events selected in the data collected in 1999 and 2000. The method used to compute the asymmetric errors is described in Ref. [2].

Stable $\tilde{\chi}_1^0$ 1999 data, $\mathcal{L} = 227\ pb^{-1}$

Topology:	$jj\ell$	$\ell\ell$	*jets*	rad	Total
	$3 \leq \Delta M < 5$ GeV/c^2				
Obs. events:	4	58	5	10	77
Expect. events:	$2.4\ ^{+1.2}_{-0.1}$	$71.5\ ^{+3.1}_{-2.2}$	$9.8\ ^{+1.3}_{-0.6}$	$7.8\ ^{+1.2}_{-0.4}$	$91.7\ ^{+3.8}_{-2.4}$
	$5 \leq \Delta M < 10$ GeV/c^2				
Obs. events:	4	13	5	10	32
Expect. events:	$2.4\ ^{+1.2}_{-0.1}$	$11.3\ ^{+1.6}_{-0.6}$	$10.1\ ^{+1.4}_{-0.6}$	$7.8\ ^{+1.2}_{-0.4}$	$31.7\ ^{+2.7}_{-1.0}$
	$10 \leq \Delta M < 25$ GeV/c^2				
Obs. events:	4	22	17	10	53
Expect. events:	$2.4\ ^{+1.2}_{-0.1}$	$18.9\ ^{+1.6}_{-0.6}$	$16.6\ ^{+1.4}_{-0.7}$	$7.8\ ^{+1.2}_{-0.4}$	$45.8\ ^{+2.7}_{-1.0}$
	$25 \leq \Delta M < 35$ GeV/c^2				
Obs. events:	6	24	10	10	50
Expect. events:	$2.2\ ^{+1.1}_{-0.1}$	$27.4\ ^{+1.6}_{-0.6}$	$9.3\ ^{+1.2}_{-0.3}$	$7.8\ ^{+1.2}_{-0.4}$	$46.8\ ^{+2.6}_{-0.8}$
	$35 \leq \Delta M < 50$ GeV/c^2				
Obs. events:	4	44	29	16	93
Expect. events:	$2.9\ ^{+1.1}_{-0.1}$	$47.9\ ^{+1.7}_{-0.7}$	$25.2\ ^{+1.2}_{-0.4}$	$19.2\ ^{+1.2}_{-0.4}$	$95.3\ ^{+2.7}_{-0.9}$
	50 GeV/$c^2 \leq \Delta M$				
Obs. events:	9	67	37	16	129
Expect. events:	$8.1\ ^{+1.2}_{-0.2}$	$71.3\ ^{+1.8}_{-0.9}$	$38.3\ ^{+1.3}_{-0.5}$	$19.2\ ^{+1.2}_{-0.4}$	$137.0\ ^{+2.8}_{-1.1}$
	TOTAL (logical .OR. between different ΔM windows)				
Obs. events:	14	127	55	22	218
Expect. events:	$10.2\ ^{+1.2}_{-0.3}$	$147.8\ ^{+3.5}_{-2.5}$	$57.4\ ^{+1.7}_{-1.0}$	$22.9\ ^{+1.3}_{-0.5}$	$238.4\ ^{+4.3}_{-2.8}$

Table 12: Number of events observed in data and the expected number of background events in the different chargino search channels under the hypothesis of a stable neutralino for all the data collected in 1999.

Stable $\tilde{\chi}_1^0$ 2000 data, $\mathcal{L} = 164.4\ pb^{-1}$

Topology:	$jj\ell$	$\ell\ell$	*jets*	rad	Total
	$3 \leq \Delta M < 5$ GeV/c^2				
Obs. events:	1	54	1	6	62
Expect. events:	$3.3\ ^{+1.9}_{-0.6}$	$54.8\ ^{+4.6}_{-3.3}$	$2.5\ ^{+1.8}_{-0.5}$	$4.2\ ^{+1.8}_{-0.4}$	$64.9\ ^{+5.6}_{-3.4}$
	$5 \leq \Delta M < 10$ GeV/c^2				
Obs. events:	1	16	4	6	27
Expect. events:	$3.3\ ^{+1.9}_{-0.6}$	$10.5\ ^{+2.4}_{-1.1}$	$6.2\ ^{+2.1}_{-0.9}$	$4.2\ ^{+1.8}_{-0.4}$	$24.3\ ^{+4.1}_{-1.6}$
	$10 \leq \Delta M < 25$ GeV/c^2				
Obs. events:	1	12	8	6	27
Expect. events:	$3.3\ ^{+1.9}_{-0.6}$	$11.3\ ^{+2.1}_{-0.8}$	$10.7\ ^{+2.1}_{-1.0}$	$4.2\ ^{+1.8}_{-0.4}$	$29.6\ ^{+4.0}_{-1.5}$
	$25 \leq \Delta M < 35$ GeV/c^2				
Obs. events:	2	26	7	6	41
Expect. events:	$2.7\ ^{+1.7}_{-0.3}$	$21.2\ ^{+2.3}_{-1.0}$	$5.7\ ^{+1.7}_{-0.3}$	$4.2\ ^{+1.8}_{-0.4}$	$33.9\ ^{+3.8}_{-1.2}$
	$35 \leq \Delta M < 50$ GeV/c^2				
Obs. events:	2	30	16	14	62
Expect. events:	$2.1\ ^{+1.5}_{-0.1}$	$36.4\ ^{+2.5}_{-1.2}$	$14.6\ ^{+1.6}_{-0.4}$	$13.5\ ^{+1.8}_{-0.5}$	$66.7\ ^{+3.8}_{-1.4}$
	50 GeV/$c^2 \leq \Delta M$				
Obs. events:	5	44	26	14	89
Expect. events:	$7.9\ ^{+1.7}_{-0.4}$	$47.7\ ^{+2.4}_{-1.2}$	$25.0\ ^{+1.7}_{-0.5}$	$13.5\ ^{+1.8}_{-0.5}$	$94.2\ ^{+3.9}_{-1.5}$
	TOTAL (logical .OR. between different ΔM windows)				
Obs. events:	7	101	37	15	160
Expect. events:	$11.6\ ^{+2.1}_{-0.8}$	$105.6\ ^{+4.9}_{-3.6}$	$36.8\ ^{+2.5}_{-1.5}$	$15.1\ ^{+1.9}_{-0.7}$	$169.3\ ^{+6.2}_{-4.1}$

Table 13: The number of events observed in data and the expected number of background events in the different chargino search channels under the hypothesis of a stable neutralino for all the events recorded in 2000 with the DELPHI detector fully operational ($< E_{cm} > = 206$ GeV).

The efficiencies of the chargino selection in the four topologies were computed separately for the 126 MSSM points using the $\mathcal{L}_R$ function and the $\mathcal{L}_{R_{CUT}}$ of the corresponding topology and ΔM region. To pass from the efficiencies of the chargino selection in the four topologies to the efficiencies in the four decay channels, all the migration effects were computed for all the generated points of the signal simulation. Then the efficiencies of the selection in the four decay channels were interpolated in the ($M_{\tilde{\chi}_1^\pm}$,$M_{\tilde{\chi}_1^0}$) plane using the same method as in Ref. [2]. These efficiencies as functions of $M_{\tilde{\chi}_1^\pm}$ and $M_{\tilde{\chi}_1^0}$ are shown in Figure 12 for a mean centre-of-mass energy of 206 GeV.

All the selected events in the real data are compatible with the expectation from the background simulation. As no evidence for a signal is found, exclusion limits are set.

Results and limits

The simulated points were used to parameterize the efficiencies of the chargino selection criteria described in section 5.2.1 in terms of ΔM and the mass of the chargino. Then a large number of SUSY points were investigated and the values of ΔM, the chargino and neutralino masses and the various decay branching ratios were determined for each point. By applying the appropriate efficiency (from the interpolation) and branching ratios and cross-sections for each channel decay, the number of expected signal events can be calcu-

lated. Taking into account the expected background and the number of observed events, the corresponding point in the MSSM parameter space (μ, M_2, $\tan\beta$) can be excluded if the number of expected signal events is greater than the upper limit on the number of observed events of the corresponding ΔM region computed at 95% CL using the multi-channel Bayesian formula [35] taking into account the branching ratio and the efficiency of each decay channel.

Figure 13 shows the chargino production cross-sections as obtained in the MSSM at $\sqrt{s} = 205.9$ GeV for different chargino masses for the high ΔM (ΔM > 10 GeV/c^2) and low ΔM cases (ΔM = 3 GeV/c^2). The parameters M_2 and μ were varied randomly in the ranges 0 GeV/c^2 < M_2 < 3000 GeV/c^2 and -200 GeV/c^2 < μ < 200 GeV/c^2 for three fixed different values of $\tan\beta$, namely 1, 1.5 and 35. The random generation of the parameters led to an accuracy on the mass limit computation of the order of 10 MeV/c^2. Two different cases were considered for the sneutrino mass: $m_{\tilde{\nu}} > 300$ GeV/c^2 (for ΔM > 10 GeV/c^2) and $m_{\tilde{\nu}} > M_{\tilde{\chi}_1^\pm}$ (for ΔM = 3 GeV/c^2).

The chargino mass limits are summarized in Table 14. The table also gives, for each case, the minimal MSSM cross-section for which $M_{\tilde{\chi}_1^\pm}$ is below the corresponding mass limit. These cross-section values are also displayed in figure 13. The chargino mass limit versus ΔM assuming a heavy sneutrino is shown in figure 14. The behaviour of the curve in figure 14 depends very weakly on the relation between M_1 and M_2.

For ΔM > 10 GeV/c^2 with a large sneutrino mass (> 300 GeV/c^2), the lower limit for the chargino ranges between 102.5 GeV/c^2 (for a mostly higgsino-like chargino) and 102.8 GeV/c^2 (for a mostly wino-like chargino). The minimal excluded MSSM cross-section at $<\sqrt{s}> = 205.9$ GeV is 0.21 pb, deriving from a chargino mass limit of 102.5 GeV/c^2.

For ΔM = 3 GeV/c^2 , the cross-section does not depend significantly on the sneutrino mass, since the chargino is higgsino-like under the assumption of gaugino mass unification. The lower limit for the chargino mass, shown in figure 13, is 97.3 GeV/c^2. The minimal excluded cross-section is in this case 1.09 pb at $<\sqrt{s}> = 205.9$ GeV.

The systematic error on the given mass limits is less than 0.5% for ΔM = 3 GeV/c^2 and less than 0.1% for ΔM > 20 GeV/c^2. The method used to compute these systematic errors is similar to that used at $\sqrt{s} = 189$ GeV [2].

The results can be translated into a limit on the mass of the lightest neutralino [2] also shown in the ($M_{\tilde{\chi}_1^\pm}$,$M_{\tilde{\chi}_1^0}$) plane in figure 15. A lower limit of 37.8 GeV/c^2 on the lightest neutralino mass is obtained, valid for $\tan\beta \geq 1$ and a heavy sneutrino. This limit is reached for $\tan\beta = 1$, $\mu = -64.5$ GeV/c^2, $M_2 = 64.4$ GeV/c^2.

6.2.2 Nearly degenerate scenarios

Efficiencies and selected events

In the search for heavy stable charged particles, only the first three windows described in [11] were searched for mass-degenerate charginos. In those windows, no events were found in the 1999 and 2000 data, where 0.51 ± 0.08 and 0.15 ± 0.03 events were expected, respectively. The efficiency for selecting a single chargino track by using this technique is shown in figure 16, as function of the mass of the chargino and at the various centre-of-mass energies.

Case	$m_{\tilde{\nu}}$ (GeV/c^2)	$M_{\chi^{\pm}}^{min}$ (GeV/c^2)	σ^{max} (pb)	$N_{95\%}$
Stable $\tilde{\chi}_1^0$ $< E_{cm} >$ = 191.6-205.9 GeV				
ΔM $>$ 10 GeV/c^2	> 300	102.5	0.21	11.9
ΔM $>$ 5 GeV/c^2	> 300	99.4	0.81	13.2
ΔM = 3 GeV/c^2	$>M_{\tilde{\chi}_1^{\pm}}$	97.3	1.09	14.9

Table 14: 95% confidence level lower limits for the chargino mass, the corresponding pair production cross-sections at 205.9 GeV and the 95% confidence level upper limit on number of observed events. The scenario of a stable $\tilde{\chi}_1^0$ is considered.

In the search for kinks, 42000 chargino events with masses comprised between 60 and 100 GeV/c^2 and mean decay length of 50 cm were generated at the centre-of-mass energies between 192 and 206 GeV. The events were used to map the selection and trigger efficiency for the single chargino, as function of its mass and decay position. As an example, the efficiencies for a 75 GeV/c^2chargino at $\sqrt{s}$=196 GeV are plotted in figure 17. In the data of 1999 (2000 with full TPC, 2000 without the sector 6 of TPC) 5 (3, 1) events survived the cuts, while 3.7 ± 1.0 (1.2 ± 0.6, 0.5 ± 0.2) were expected from the standard sources.

In the search with the ISR photon tag a total of almost 3 million $\tilde{\chi}_1^+\tilde{\chi}_1^-$ events was generated at the centre-of-mass energies between 192 and 206 GeV; about 100 000 of them had an high $p_{\rm t}$ photon within the detector acceptance and were produced with full detector simulation. The mass of the generated charginos ranged from 60 to 95 GeV, and ΔM from 150 MeV/c^2 to 3 GeV/c^2. The selection efficiency was computed applying the selection cuts to the samples of simulated events. The trigger efficiency, instead, was parameterized on the real data themselves separately for the isolated photon and for the system of few low momentum particles, then the parameterization was applied on the simulation (both signal and background events). Detection and trigger efficiency vary widely with $M_{\tilde{\chi}_1^+}$ and ΔM; they also depend on the gauge composition of the chargino, since the spectrum of the ISR radiation is different for higgsinos and gauginos. The selection times trigger efficiency for a signal (higgsino) at 206 GeV is shown in figure 18. The small probability of radiating a photon with transverse energy E_T^{γ} above the chosen threshold is the main reason for having such a low efficiency. As the selection cuts varied across the plane ($M_{\tilde{\chi}_1^+}$, ΔM), so did the number of candidate events remaining in the data and the amount of background expected from the standard MC simulations available. Figure 19 shows, as an example, the number of events remaining in data and MC for the year 2000 statistics with full TPC, as a function of the position on the plane ($M_{\tilde{\chi}_1^+}$, ΔM). The number of events remaining after the dedicated preselection and at the final step after the logical OR of all selections, together with the integrated luminosity used for the analysis, are given in table 15. The excess of events seen in the data is of

the same kind as the excess observed in the analyses done at lower energies [3] and, as in the past, it can be qualitatively explained by the incomplete phase space coverage of the standard simulation used, plus possibly some noise events like beam-gas collisions, as already discussed at the end of section 5.2.2. The excess at the preselection level has been verified to be almost entirely due to the cuts done at the generator level in the (hadronic) two-photon simulation used (in 1999 tighter cuts in the generation were applied to the hadronic $\gamma\gamma$ samples).

$\sqrt{s}$	$\int \mathcal{L}$	Preselection		Final sel.	
(GeV)	(pb^{-1})	Data	MC	Data	MC
192	25.4	75	40 ± 2	0	0.6 ± 0.1
196	76.2	162	118 ± 4	4	1.3 ± 0.3
200	84.0	201	123 ± 4	0	1.4 ± 0.3
202	40.4	109	55 ± 2	0	0.6 ± 0.1
206	221.5	553	506 ± 18	13	4.6 ± 1.4
all		1100	842 ± 19	17	8.4 ± 1.5

Table 15: Numbers of events selected in data and expected from the SM simulation in the search for nearly mass degenerate chargino and neutralino at the preselection and at the final selection level, for the different centre-of-mass energies collected during the years 1999 and 2000. All year 2000 data were considered at the mean centre-of-mass energy of 206 GeV. Simulation errors are statistical.

Results and limits

Having no evidence of excess above the expectations in any of the three experimental methods used to search for charginos nearly mass degenerate with the lightest neutralino, regions in the plane $(M_{\tilde{\chi}_1^+}, \Delta\mathrm{M})$ can be excluded at the 95% CL. First, the two searches for long-lived charginos were combined, assuming that in a $\tilde{\chi}_1^+\tilde{\chi}_1^-$ event any of the two long-lived charginos can be tagged either as a kink or as a stable particle, according to its decay length. Then the search with the ISR photon was considered for all events in which the chargino decay length was shorter than that required by the two other methods. In all cases, the data collected in the years 1999 and 2000 were further combined with all previous data from the high energy phase of LEP [3].

The limits obtained in this way are certainly model dependent: in fact cross-sections, decay modes, and the spectrum of the ISR radiation itself all depend on the gauge composition of the chargino. They were obtained in the two SUSY scenarios in which a near mass-degeneracy between the lightest chargino and neutralino is possible: the $M_2 \gg \mu$ scenario in which the lightest chargino and neutralino are both almost pure higgsinos; and the $\mu \gg M_2$ scenario in which the lightest chargino and neutralino are both almost pure gauginos. In the gaugino scenario, the gaugino mass unification at large scale must be violated in order to obtain low ΔM; in the higgsino scenario this is not mandatory, therefore this is the scenario to be taken into account in the constrained SUSY models. Those limits are shown in figure 20, separately for the different techniques. In the same figure, they are compared with the exclusion obtained in the search for higher ΔM charginos in DELPHI.

With these new results, the ΔM independent 95% CL lower limit of DELPHI on the mass of the chargino becomes: $M_{\tilde{\chi}_1^+} > 75$ GeV/c^2 in the higgsino scenario and $M_{\tilde{\chi}_1^+} >$

70 GeV/c^2in the gaugino scenario with heavy sneutrinos.

Both limits take into account a variation of $\tan\beta$ between 1 and 50, and a variation of M_1, M_2 and μ such that the mass difference between the chargino and the neutralino remains below 3 GeV/c^2 and $M_2 \leq 2M_1 \leq 10M_2$. In the higgsino scenario all sfermions are just required to be heavier than the chargino, while in the gaugino scenario they must be heavy enough not to modify significantly the cross-section (only the sneutrino can, and it was required to be heavier than 500 GeV/c^2) or the decay modes and widths.

Uncertainties in the selection efficiencies and in the expected backgrounds were taken into account in a bayesian way by convoluting their expected distributions with the Poissonian distribution of the number of observed events while computing the limits (see [3]). The most important of these systematics is the uncertainty in the background content: depending on the point, the exclusion limits may vary as much as 2-3 GeV/c^2. Other systematics, like uncertainties in the trigger efficiencies and background components not accounted for in the simulation, were taken into account by considering the scenario which lead to the most conservative limit.

6.3 Neutralino searches

6.3.1 Efficiencies and selected events

Table 16 shows the number of events selected in the different neutralino searches in real data and the numbers expected from the Standard Model background. Also shown are the main background sources contributing in each channel and the typical efficiency of each search for MSSM points where it is relevant.

	205 GeV		207 GeV		208 GeV			
Search	Data	Tot bkg.	Data	Tot bkg.	Data	Tot bkg.	Main bkg.	Eff. (%)
Acopl jets	14	12.7±1.4	15	13.0±1.4	2	1.2±0.2	W^+W^-,ZZ	10 – 30
Acopl electrons	18	14.9±0.7	9	15.0±0.7	3	1.4±0.1	W^+W^-,$\gamma\gamma$	10 – 40
Acopl muons	18	19.5±1.0	20	19.8±1.1	3	1.8±0.2	W^+W^-,$\gamma\gamma$	10 – 40
Multijets, γ's	2	1.2±0.1	0	1.1±0.1	0	0.1±0.02	Zγ	10 – 20
Multijets, no γ	18	16.3±0.5	22	17.6±0.7	3	1.7±0.1	Zγ, W^+W^-	10 – 40
Multileptons	13	11±1.0	14	10.7±1.0	0	0.9±0.1	W^+W^-	30 – 50
Tau cascades	1	1.5±0.8	6	1.4±0.8	0	0.1±0.1	WW,ee,$\mu\mu$	13–19
All	84	77±2	88	79±2	11	7.2±0.1		

Table 16: Results of the different searches. The typical efficiency of each search for MSSM points where it is relevant is shown. The efficiencies depend typically on the masses of the sparticles involved in the process. For any given search, events are explicitly rejected if accepted by one of the searches appearing earlier in the table.

More than 1.2 million $\tilde{\chi}^0_1\tilde{\chi}^0_2$ events were simulated for different combinations of masses with $M_{\tilde{\chi}^0_1}$ and $M_{\tilde{\chi}^0_2}$ ranging from 5 GeV/c^2 to 100 GeV/c^2 and from 10 GeV/c^2 to 200 GeV/c^2, respectively, and for different $\tilde{\chi}^0_2$ decay modes ($\mathrm{q\,\bar{q}}\tilde{\chi}^0_1$, $\mu^+\mu^-\tilde{\chi}^0_1$, $\mathrm{e^+e^-}\tilde{\chi}^0_1$, $\tilde{\tau}\tau$). The efficiencies were computed for the the mass combinations and parameterised as functions of the two masses. In addition, around 300 000 $\tilde{\chi}^0_2\tilde{\chi}^0_{3,4}$ events with cascade decays were simulated. For cascade processes, the efficiencies were parameterised as functions of $M_{\tilde{\chi}^0_1}$ and a second parameter chosen to be $M_{\tilde{\chi}^0_4,3}$+$M_{\tilde{\chi}^0_2}$ when considering the decay modes $M_{\tilde{\chi}^0_2} \to \tilde{\chi}^0_1\gamma$, $M_{\tilde{\chi}^0_4,3} \to \mathrm{q\,\bar{q}}\tilde{\chi}^0_1$, and $M_{\tilde{\chi}^0_4,3}$-$M_{\tilde{\chi}^0_2}$ when considering the decay modes

$M_{\tilde{\chi}^0_2} \to \mathrm{q}\,\bar{\mathrm{q}}\tilde{\chi}^0_1$, $M_{\tilde{\chi}^0_{4,3}} \to \mathrm{q}\,\bar{\mathrm{q}}\tilde{\chi}^0_1$. The dependence on remaining parameters was found to be small in the relevant mass ranges and the efficiencies were averaged over them.

As discussed in section 6.4.2, in the search for $\tilde{\chi}^0_2\tilde{\chi}^0_2 \to \tilde{\tau}\tau\ \tilde{\tau}\tau$ the total expected background was 1.10 ± 0.19 events, and no candidates were found in the data. The selection efficiency ranged between 10 % and 20 % growing with decreasing $M_{\tilde{\tau}}$-$M_{\tilde{\chi}^0_1}$ and increasing $M_{\tilde{\chi}^0_1}$.

6.3.2 Results

In the absence of a signal, limits on neutralino production cross-sections were derived, using the dependence of the calculated efficiencies on the masses involved.

The limits for $\tilde{\chi}^0_1\tilde{\chi}^0_2$ production, as obtained from the searches for acoplanar leptons and jets, are shown in Figs. 21 assuming different branching ratios.

Similarly, Figs. 22(a,b) show cross-section limits for $\tilde{\chi}^0_2\tilde{\chi}^0_i$ production ($i = 3$ or 4). In the white regions marked "Not allowed", no such points were found. Figure 22(a) shows the limit obtained using a Bayesian combination [35] of the results from the multijet and acoplanar jet searches in the case where $\tilde{\chi}^0_i \to \tilde{\chi}^0_2 \mathrm{q}\,\bar{\mathrm{q}}$ and $\tilde{\chi}^0_2 \to \tilde{\chi}^0_1 \mathrm{q}\,\bar{\mathrm{q}}$. Figure 22(b) gives the corresponding limits when $\tilde{\chi}^0_2 \to \tilde{\chi}^0_1\gamma$, as obtained from the search for multijet events with a photon signature.

From the results of the search for $\tilde{\chi}^0_2\tilde{\chi}^0_2 \to \tilde{\tau}\tau\ \tilde{\tau}\tau$ described in section 5.4.2 , an equivalent production cross-section at $\sqrt{s} = 206.7$ GeV larger than 63 fb can be excluded. This limit is valid for 30 GeV/$c^2 \leq M_{\tilde{\chi}^0_1} \leq$ 50 GeV/$c^2$and $M_{\tilde{\tau}}$-$M_{\tilde{\chi}^0_1} \leq$ 5 GeV/c^2in the gaugino region $|\mu| >> M_2$, where this channel is important for setting a limit on the LSP mass. The cross-section dependence on $\sqrt{s}$ as given by `SUSYGEN` was assumed. The corresponding expected limit was 68 fb.

6.4 Slepton searches

6.4.1 Smuon and selectron searches

Efficiencies and selected events

The efficiency for the signal detection depends on the masses of the slepton and neutralino. The cuts used to reject the backgrounds resulted in typical signal efficiencies of 50% both for the selectron and the smuon channels.

The number of events selected at each energy in the data, together with the estimate of the background is shown in Table 17 for the selectron and smuon analyses. It can be seen that the principal background arises from leptonic decays of W pairs. No evidence of a selectron or smuon signal is apparent in the data.

Results

The results are presented in terms of exclusion regions in the slepton-neutralino mass plane.

Limits on slepton masses can be derived using several assumptions. In the MSSM model, right handed sleptons are expected to have lower masses and lower cross-sections for a given mass. Hence we have assumed that only right handed selectrons and smuons

	Selectrons			Smuons		
year	1998	1999	2000	1998	1999	2000
2-fermion events	5.6	8.4	4.2	0.1	2.2	1.4
4-fermion events	29.7	40.9	34.4	18.8	25.5	20.9
$\gamma\gamma$ events	1.7	2.5	2.2	0.5	1.1	2.6
Total	37.0	51.8	40.8	21.4	28.3	23.9
data	40	52	49	19	23	28

Table 17: Selectron and smuon candidates in the different data sets, together with the number of background events expected.

are sufficiently low in mass to be pair produced at LEP. This leads to conservative mass limits.

Exclusion limits for slepton pair production were obtained taking into account the signal efficiencies for each slepton-neutralino mass point, the cross-section for right-handed slepton production and the branching-ratios squared for the direct decay $\tilde{\ell} \to \ell\chi_1^0$, together with the number of data and background events kinematically compatible with the mass combination under test. The estimate of the SUSY cross-section and branching-ratios for each mass point was determined with the SUSY parameters tan β=1.5 and μ=-200 GeV/c^2.

Figure 23 shows the 95% CL exclusion region for $\tilde{e}_R\tilde{e}_R$ production, obtained using the full set of data taken during 2000, combined with data taken over previous years at lower energies. For a mass difference between the selectron and the neutralino above 5 GeV/c^2. and a neutralino mass up to 60 GeV/c^2 right-handed selectrons up to masses of 98 GeV/c^2.

Figure 24 shows the 95% CL exclusion regions for $\tilde{\mu}_R\tilde{\mu}_R$ production, obtained by combining the year 2000 data with that taken previously. For the smuons we exclude masses up to 85 GeV/c^2, provided the mass difference between the smuon and the neutralino is above 5 GeV/c^2.

6.4.2 Stau search

Efficiencies and selected events

For the stau-pair search, table 18 summarises the number of accepted events in the data together with the expected numbers of events from the different background channels. In both ΔM regions, good agreement with the Standard model expectation was observed. Most of the selected SM events in the simulation contained one (17%) or two (67%) τ:s. In most (65%) of the events with less than two τ:s, the lepton mistakenly taken as coming from a τ-decay had low momentum, i.e. was indistinguishable from a secondary lepton from a τ-decay.

The efficiencies have been determined using 5000 events for each point of a 1 GeV/c^2 $\times$ 1 GeV/c^2 grid in the ($M_{\tilde{\tau}}$,M_{LSP}) plane, using a fast detector simulation, and ranges between 20 and 30 percent for ΔM$>$ 20 GeV/c^2. The results have been verified with the full detector simulation and analysis chain (figure 25).

In the search for staus in $\tilde{\chi}_2^0\tilde{\chi}_2^0$ production, all data recorded between 1998 and 2000

$\mathcal{L}$ (pb^{-1})	221.4	
ΔM(GeV/c^2)	< 20	≥ 20
2-fermion events	0.3 ± 0.1	0.6 ± 0.1
4-fermion events	6.2 ± 0.2	9.1 ± 0.3
$\gamma\gamma$ events	0.2 ± 0.1	1.9 ± 0.7
Total Background	6.7 ± 0.3	11.6 ± 0.7
Candidates	5	12

Table 18: Stau candidates, together with the number of background events expected. The quoted integrated luminosity is the useful value after run-quality checks, and include data from both the period when the TPC was fully operational and the period when one sector was broken. Note that a large fraction of the four-fermion events were not kinematically compatible with low ΔM – they had too large p_{high}^{JET} – and did not enter when evaluating the limiting cross-section in that region.

(at CMS energies from 189 to 208 GeV) was analysed. The number of observed and expected candidates are summarised in table 19. The total expected background over the three years was 1.10 ± 0.19 events, 55 % of which was two-fermion events, the reminder being four-fermion events.

E_{CMS} (GeV)	Data	Background
189	0	0.42 ± 0.17
192	0	0.02 ± 0.06
196	0	0.06 ± 0.02
200	0	0.25 ± 0.11
202	0	0.13 ± 0.05
205.9	0	0.21 ± 0.04
Total	0	1.10 ± 0.19

Table 19: Background and candidates in the $\tilde{\chi}_2^0\tilde{\chi}_2^0 \to \tilde{\tau}\tau\ \tilde{\tau}\tau$ analysis. In this analysis, the period of the data-taking in 2000 when one sector of the TPC was broken was not used.

The efficiency for $\tilde{\chi}_2^0\tilde{\chi}_2^0 \to \tilde{\tau}\tau\ \tilde{\tau}\tau$ was evaluated in a number of points with $M_{\tilde{\chi}_1^0}$ between 30 and 50 GeV/c^2, and mass-differences between the stau and the $\tilde{\chi}_1^0$ ranging from 2 to 5 GeV/c^2. The $\tilde{\chi}_2^0$ mass exceeded $\tilde{\chi}_1^0$ mass by 30 to 45 GeV/c^2. These points were chosen because they correspond to a region in the CMSSM parameter space which cannot be excluded by the chargino search, nor – due to the low mass difference – by the stau search. Efficiencies between 10 and 20% were found, varying little with the chosen masses. These values were obtained by the fast simulation and verified with the full simulation in a sub-set of points.

Results

Limits on sfermion masses can be derived using several different assumptions. Scalar mass unification suggests lower masses and cross sections for the partners of right handed fermions. For third generation sfermions, Yukawa couplings can be large, leading to an

appreciable mixing between the pure weak hypercharge states. The production cross-section depends on the mixing angle, due to the variation in strength of the coupling to the Z component of the weak current, and has a minimum close to 45°. For the staus, we therefore present results also for this case.

For each $M_{\tilde{\tau}}$- M_{LSP} mass combination, we compare the predicted number of SUSY events taking into account the signal efficiencies with the observed number of kinematically compatible data and background candidates. When determining whether data or background events were kinematically compatible with the mass-point, the upper end-point of the expected momentum spectrum of the visible reconstructed τ was used. A mass combination is excluded at 95% CL if the SUSY prediction is incompatible with the data. Figure 26 shows the 95% CL $\tilde{\tau}_R$ exclusion region obtained by combining the previous data at 130 to 202 GeV with the data taken in 2000 up to 208 GeV. Figure 27 shows the exclusion regions in the case of the mixing corresponding to the minimal production cross-section. In the latter plot, the region below $M_{\tilde{\tau}} = 25$ GeV/c^2 does not include the data from 1999-2000. Due to the vanishing coupling to the Z at this mixing angle, no limit can be inferred from the precision measurements at LEPI in this case.

In summary, a stau mass limit can be set at 82.5 to 83.6 GeV/c^2 (depending on mixing) for LSP masses below 60 GeV/c^2 and mass-differences between the stau and the LSP above 6 GeV/c^2. The expected limit in the same region ranges from 80.4 to 81.7 GeV/c^2. The results of the search for staus in $\tilde{\chi}_2^0\tilde{\chi}_2^0$ production are more relevant for the neutralino searches, and were given in section 6.3.2.

6.5 Squark searches

6.5.1 Efficiencies and selected events

In the non-degenerate scenario, the efficiencies of the stop and sbottom signal selection are summarised in figure 28. For the second part of the 2000 data taking, in which the TPC was no longer fully operational, signal samples were simulated with the modified version of the reconstruction program used for real data and standard processes. The number of candidates found and the expected background levels are shown in Table 20.

In the degenerate scenario, the efficiency for the stop signal is summarized in Figure 29. The figure shows the variation of the efficiency of the signal selection as a function of ΔM and of the stop mass for two different values of the centre-of-mass energy. Some examples of the detection efficiency obtained by the degenerate analysis are quoted below: for a ΔM of 2 GeV/c^2, and a stop mass of 70 GeV/c^2, an efficiency of 2.4% is obtained at $\sqrt{s} = 189$ GeV and of 4.8% at $\sqrt{s} = 206$ GeV. For a ΔM of 4 GeV/c^2 and a stop mass of 80 GeV/c^2, an efficiency of 4.0% is achieved at $\sqrt{s} = 189$ GeV and of 7.7% at $\sqrt{s} =$ 206 GeV. Furthermore when getting close to the limit of the degenerate scenario, as for instance, at $\Delta M = 10$ GeV/c^2 and for a stop mass of 90 GeV/c^2, at $\sqrt{s} = 189$ GeV the efficiency reaches 28.5% and at $\sqrt{s} = 206$ GeV, the efficiency is 26.5%. One should note that for higher values of ΔM and of the stop mass, some cuts, such as the total visible energy cut, are removing more events at higher c.m. energies than at lower ones. This explains that the efficiency is slightly better at 189 GeV than at 206 GeV in the latter mentioned case.

It should be noted that so far, in the degenerate scenario analysis, only the statistical errors are taken into account.

Sbottom Analysis				
	$\mathbf{\Delta M \geq\ 20}$GeV/$c^2$		$\mathbf{5 < \Delta M < 20}$GeV/$c^2$	
$\sqrt{s}$	data	MC	data	MC
188.7	2	$0.43 \pm 0.08^{+0.12}_{-0.03}$	1	$0.47 \pm 0.20^{+0.19}_{-0.05}$
191.6	0	$0.05 \pm 0.009^{+0.02}_{-0.02}$	0	$0.06 \pm 0.024^{+0.01}_{-0.03}$
195.6	0	$0.17 \pm 0.04^{+0.03}_{-0.03}$	1	$0.22 \pm 0.08^{+0.02}_{-0.07}$
199.6	0	$0.14 \pm 0.03^{+0.02}_{-0.03}$	0	$0.27 \pm 0.08^{+0.05}_{-0.3}$
201.7	0	$0.07 \pm 0.02^{+0.03}_{-0.01}$	1	$0.13 \pm 0.04^{+0.04}_{-0.03}$
205	0	$0.49 \pm 0.05^{+0.05}_{-0.06}$	0	$0.43 \pm 0.17^{+0.05}_{-0.23}$
207	0	$0.36 \pm 0.04^{+0.07}_{-0.03}$	0	$0.38 \pm 0.17^{+0.13}_{-0.16}$
208	0	$0.05 \pm 0.007^{+0.073}_{-0.001}$	0	$0.04 \pm 0.017^{+0.063}_{-0.008}$
206.5(*)	0	$0.33 \pm 0.04^{+0.01}_{-0.10}$	0	$0.12 \pm 0.03^{+0.02}_{-0.05}$
Total	2	$2.10 \pm 0.12^{+0.17}_{-0.13}$	3	$2.12 \pm 0.34^{+0.25}_{-0.42}$

Stop Analysis				
	$\mathbf{\Delta M \geq\ 20}$GeV/$c^2$		$\mathbf{10 < \Delta M < 20}$GeV/$c^2$	
$\sqrt{s}$	data	MC	data	MC
188.7	3	$2.28 \pm 0.22^{+0.78}_{-0.01}$	3	$0.87 \pm 0.21^{+0.28}_{-0.02}$
191.6	2	$0.92 \pm 0.11^{+0.17}_{-0.40}$	0	$0.27 \pm 0.07^{+0.01}_{-0.10}$
195.6	0	$2.35 \pm 0.22^{+0.34}_{-0.24}$	3	$0.78 \pm 0.15^{+0.08}_{-0.20}$
199.6	1	$2.14 \pm 0.13^{+0.07}_{-0.39}$	0	$0.91 \pm 0.16^{+0.13}_{-0.11}$
201.7	1	$1.16 \pm 0.07^{+0.49}_{-0.12}$	0	$0.49 \pm 0.08^{+0.18}_{-0.12}$
205	5	$2.00 \pm 0.11^{+0.34}_{-0.28}$	0	$0.75 \pm 0.18^{+0.07}_{-0.42}$
207	1	$2.32 \pm 0.11^{+0.43}_{-0.10}$	1	$0.78 \pm 0.18^{+0.16}_{-0.27}$
208	0	$0.19 \pm 0.01^{+0.26}_{-0.01}$	0	$0.08 \pm 0.018^{+0.14}_{-0.003}$
206.5(*)	1	$2.67 \pm 0.11^{+0.01}_{-0.89}$	0	$0.41 \pm 0.04^{+0.03}_{-0.18}$
Total	14	$16.03 \pm 0.41^{+1.2}_{-1.1}$	7	$5.34 \pm 0.41^{+0.43}_{-0.60}$

Table 20: Number of events selected by the squark analysis in the non-degenerate scenarios. The first errors are statistical and the second ones are systematic. (*) indicates the 2000 data taken with the sector 6 of the TPC off.

6.5.2 Evaluation of systematics

Three kinds of systematic errors were evaluated. The first comes from imperfect simulations of the detector response. A method to re-weight the simulated events was developed to make a conservative estimate of these errors:

- After the preselection level, each of the 10 neural network input variables was separated into 25 bins. For each variable, the re-weighting factor giving perfect superposition of the Monte-Carlo on the real data was calculated for each bin where the number of Monte Carlo events was at least 1% of the total and the number of real events was not equal to zero.

- The background was then re-estimated for each variable in turn applying the relevant re-weighting factor to each Monte-Carlo event passing the neural network cut ($N_{MC}(i), i = 1\ to\ 10$).

Stop (nearly degenerate)		
$\mathbf{\Delta M \leq\ 10}$GeV/$c^2$		
$\sqrt{s}$	data	MC
188.7	3	3.18 ± 0.51
191.6	0	0.52 ± 0.09
195.6	2	1.23 ± 0.23
199.6	0	1.36 ± 0.25
201.7	0	0.75 ± 0.12
205	1	1.43 ± 0.35
207	2	1.45 ± 0.36
208	1	0.13 ± 0.03
206.5(*)	0	1.12 ± 0.28
Total	9	11.17 ± 2.22

Table 21: Number of events selected by the stop analysis in the degenerate scenario with statistical errors. (*) indicates 2000 data taken whit the sector 6 of the TPC off.

- A positive and a negative systematic error were then defined as:

$$\epsilon_+ = \sqrt{\sum_{i,N_{MC}(i)>N_{MC}} (N_{MC}(i) - N_{MC})^2}$$
$$\epsilon_- = \sqrt{\sum_{i,N_{MC}(i)<N_{MC}} (N_{MC}(i) - N_{MC})^2}$$

  where N_{MC} is the result obtained without re-weighting.

This method has the advantage to keep exactly the same events at the end to evaluate the background contribution. Each variable is studied separately. The correlations are not taken into account, but as the quadratic sum is performed over all results, these systematic errors are overestimated. It has been applied in the 4 neural network analysis at each centre-of-mass energy from 189 to 208 GeV. These systematic errors took relative values between 15 and 60%, which are relatively high. However, the aim is to remain conservative and, as it will shown, their effects on the final results (mass limits) are negligible.

The second kind of systematic error comes from background generators. For the 2 and 4-fermions, they are relatively low as compared to the first type of errors and were not taken into account. For the hadronic $\gamma\gamma$ background, PYTHIA results were cross-checked with the TWOGAM generator. A relative difference of 15% between the two generators was observed at the preselection level. Is known that TWOGAM underestimates this background [38], hence this number is conservative.

Finally, systematic errors in the signal simulation were estimated. The main error comes from the stop hadronization scheme, which is important for low ΔM values. Stop events were generated with two other generators: SUSYGEN [25] where the stop hadronization is not performed, and STOPGEN, a specially developed generator in which the stop hadronization is performed non-perturbatively, and the ϵ parameter of the Peterson function which regulates the stop fragmentation and hadronization can be varied. The analyses were applied to these signal samples and the results were compared. In the stop analysis, relative systematic errors coming from the signal simulation were estimated

to be 7% for $\Delta M > 10\text{GeV}/c^2$ and 10% for $\Delta M \leq 10\text{GeV}/c^2$. For the sbottom analysis, 7% was used as a conservative number for all ΔM.

6.5.3 Results

Stop and sbottom cross-sections were calculated with the SUSYGEN program for two squark mixing angles. For purely left-handed squarks ($\theta_{\tilde{q}} = 0°$), the cross-section is maximal. The squark mixing angle which corresponds to the Z decoupling is 56° for the stop and 68° for the sbottom and it corresponds approximately to the minimal cross-section. The program ALRMC [36] was used to determine the confidence level in the signal hypothesis, CL_s, based on the observed events and expected backgrounds. A point is excluded if $1 - CL_s$ is greater than 95%. Systematic errors were taken into account in the definition of CL_s.

Figures 30 and 31 show the ($M_{\tilde{q}}$,$\tilde{\chi}_1^0$) regions excluded at 95% confidence level by the search for $\tilde{t} \to c\tilde{\chi}_1^0$ and $\tilde{b} \to b\tilde{\chi}_1^0$ decays, with the 100 % branching ratio assumption, both for purely left-handed states and for the states at the Z decoupling.

Table 22 shows the limit on the squark masses as a function of ΔM obtained with the non-degenerate analysis. The introduction of the systematics in the confidence level calculation has no effect on these numbers. Stop masses lower than 92 GeV/c^2 and sbottom masses lower than 87 GeV/c^2 are excluded if $\Delta M \geq 10$ GeV/c^2 for any squark mixing angle. These limits become 96 GeV/c^2 and 98 GeV/c^2 for purely left-handed squarks. For the stop, the analysis in the nearly-degenerate case gives a limit at 72 GeV/c^2 on the stop mass for $\Delta M \geq 2$ GeV/c^2, for any squark mixing angle and with the stop decaying promptly (see table 23). Moreover, this analysis confirms a stop mass lower limit of 92 GeV/c^2 for any stop mixing, for $\Delta M \geq 10$ GeV/c^2. Figure 32 shows the limits on the stop mass as a function of ΔM, including the range of very low ΔM values which are excluded by the analysis focussing on the nearly-degenerate case.

	Sbottom		Stop	
	$\theta_{\tilde{b}}$ =0	$\theta_{\tilde{b}} = 68°$	$\theta_{\tilde{t}}$ =0	$\theta_{\tilde{t}} = 56°$
$\Delta M \geq 7$ GeV/c^2	93	76	95	91
$\Delta M \geq 10$ GeV/c^2	98	87	96	92
$\Delta M \geq 15$ GeV/c^2	99	89	96	92

Table 22: Lower limits on squark masses as a function of ΔM (in GeV/c^2) from the squark analysis in the non-degenerate scenario.

7 Combined CMSSM exclusions and mass limits

7.1 The method

The method employed to set lower mass limits on the LSP mass and on the masses of other SUSY particles is to convert the negative results of the searches for charginos, neutralinos, sleptons and squarks into exclusion regions in the (M_2, μ) plane for different tan β values, and then to find the minimal allowed sparticle masses as a function of tan β.

Stop (nearly degenerate)		
	$\theta_{\tilde{t}}$ =0	$\theta_{\tilde{t}} = 56°$
$\Delta M \geq 2$ GeV/c^2	75	72
$\Delta M \geq 3$ GeV/c^2	80	78
$\Delta M \geq 4$ GeV/c^2	85	82
$\Delta M \geq 5$ GeV/c^2	91	87
$\Delta M \geq 7$ GeV/c^2	94	91
$\Delta M \geq 10$ GeV/c^2	96	93
$\Delta M \geq 15$ GeV/c^2	96	93

Table 23: Lower limits on stop masses as a function of ΔM (in GeV/c^2) in the nearly-degenerate scenario.

It is described in detail in [6, 7]. The Higgs boson search in the conservative maximal M_{h^0} scenario was used to exclude low values of $\tan\beta$ [12].

Unless stated otherwise, the limits presented in the following are valid for $M_2 \leq 1000$ GeV/c^2 and for the μ region in which the lightest neutralino is the LSP. The μ range depends on the values of $\tan\beta$ and m_0, and on the mixing parameters in the third family (A_τ, A_t, A_b). Unless stated otherwise, for high values of m_0 (above 500 GeV/c^2) the μ range between -2000 and 2000 GeV/c^2 was scanned, but the scan range was increased if any limit point was found to be close to the scan boundary.

7.1.1 Method of combining different searches

In the scan of the SUSY parameter space the efficiencies of the different searches, as obtained in the previous sections, were parameterised for the dominant channels, and used together with the information about the numbers of events selected in the data and the expected numbers of background events. The 95 % confidence level exclusion regions obtained with the different searches were then simply superimposed.

In the previous publications [6, 7] we have verified that our parameterizations lead to conservative results by comparing with a parallel approach, where these searches were combined with the very fast detector simulation program (SGV) together with SUSYGEN (see section 4), to simulate simultaneously all channels of chargino, neutralino, slepton and squark production and decay.

The typical scan step size in μ and M_2 was 1 GeV/c^2 except in the region of the LSP limit, where the step size was decreased to 0.5 GeV/c^2. The step size in m_0 was varying, the density of points being increased in regions of potentially difficult mass configurations. Special care was taken to set up the scan logic in such a way that no such configuration was overlooked. In particular, whenever two nearby scan points were excluded by different searches, the scan was performed with smaller steps between these points to check the continuity of the exclusion.

7.1.2 The influence of the m_0 value and of the mixing in the third family

The unification of sfermion masses to a common m_0 at the GUT scale allows sfermion masses at the Electroweak Scale to be calculated as functions of $\tan\beta$, M_2 and m_0. In

particular the masses of the sneutrino ($\tilde{\nu}$), the left-handed selectron and smuon ($\tilde{\mathrm{e}}_\mathrm{L}$,$\tilde{\mu}_L$), and the right-handed selectron and smuon ($\tilde{\mathrm{e}}_\mathrm{R}$, $\tilde{\mu}_R$) can be expressed as [7]:

1) $m_{\tilde{\nu}}{}^2 = m_0^2 + 0.77M_2^2 + 0.5m_\mathrm{Z}{}^2 \cos 2\beta$
2) $M_L^2 = m_0^2 + 0.77M_2^2 - 0.27m_\mathrm{Z}{}^2 \cos 2\beta$
3) $M_R^2 = m_0^2 + 0.22M_2^2 - 0.23m_\mathrm{Z}{}^2 \cos 2\beta$

In the high m_0 scenario, $m_0 = 1000$ GeV/c^2 was assumed, which implied sfermion masses of the same order. In this case only charginos, neutralinos and the Higgs boson can be produced at LEP [8] and limits arise from a combination of searches for these particles described in [12] and in previous sections of this paper.

For high m_0, the chargino pair-production cross-section is large and the chargino is excluded nearly up to the kinematic limit, provided $M_2 < 200$ GeV/c^2.

It may also be remarked that at low M_2, $\Delta\mathrm{M}{=}M_{\tilde{\chi}_1^\pm} - M_{\tilde{\chi}_1^0}$ is large, resulting in increased background from W^+W^- production. However, if $|\mu|$ is low as well, the chargino tends to decay via $\tilde{\chi}_1^\pm \to \tilde{\chi}_2^0 W^*$ to the next-to-lightest neutralino $\tilde{\chi}_2^0$, which then decays by $\tilde{\chi}_2^0 \to \tilde{\chi}_1^0\gamma$ or $\tilde{\chi}_2^0 \to \tilde{\chi}_1^0 \mathrm{Z}^*$. For setting the mass limits, it is therefore important that the chargino search includes topologies with photons stemming from the decays $\tilde{\chi}_1^\pm \to \tilde{\chi}_2^0 W^* \to \tilde{\chi}_1^0 \gamma W^*$, since the search for topologies with photons does not suffer from W^+W^- background and is effective for large ΔM (close to m_W).

Of the detectable neutralino production channels (*i.e.* excluding $\tilde{\chi}_1^0\tilde{\chi}_1^0$), the $\tilde{\chi}_1^0\tilde{\chi}_2^0$ and $\tilde{\chi}_1^0\tilde{\chi}_3^0$ channels are important for large regions in the parameter space, but in order to cover as much as possible one must also consider channels like $\tilde{\chi}_2^0\tilde{\chi}_3^0$ and $\tilde{\chi}_2^0\tilde{\chi}_4^0$, giving cascade decays with multiple jets or leptons in the final state. At high m_0 the production cross-section for all these neutralino production channels drops to very low values for $|\mu|$ above $\simeq$ 75 GeV/c^2. This is because the two lightest neutralinos then have large photino ($\tilde{\chi}_1^0$) and zino ($\tilde{\chi}_2^0$) components and their s-channel pair-production is therefore suppressed, while pair-production of heavier neutralinos is not kinematically accessible. Nevertheless, for $\tan\beta < 1.5$ and $M_2 > 60$ GeV/c^2 the neutralino exclusion reaches beyond the kinematic limit for chargino production at negative μ (see figure 33). This region of $\tan\beta$ is now excluded anyway by searches for the production for the lightest Higgs boson [12].

For medium m_0, 100 GeV/c^2 $\lessapprox$ m_0 $\lessapprox$ 1000 GeV/c^2, the $\tilde{\chi}_1^0\tilde{\chi}_2^0$ production cross-section in the gaugino-region ($|\mu| \gtrsim$ 75 GeV/c^2) grows quickly as m_0 falls, due to the rapidly rising contribution from the selectron t-channel exchange. Meanwhile the chargino production cross-section in the gaugino region drops slowly, but it remains high enough to allow chargino exclusion nearly up to the kinematical limit for $m_0 \gtrsim$ 200 GeV/c^2. For lower $m_0 \sim 100$ GeV/c^2, the chargino production cross-section in the gaugino region is close to its minimum, while the neutralino production cross-section is very much enhanced. Consequently the region of the (μ, M_2) parameter space excluded by searches for neutralino production at low m_0 is larger than the one excluded by the search for chargino and neutralino production at high m_0 as shown in [4, 6, 7].

[7] It is worth noting that for $\tan\beta \geq 1$ ($\tan\beta < 1$) we have $\cos 2\beta \leq 0$ ($\cos 2\beta > 0$), so the $\tilde{\nu}$ is never heavier (lighter) than the $\tilde{\mathrm{e}}_\mathrm{L}$.

[8] If $|\mu|$ and/or mixing terms for the third family sfermions are sufficiently high, they can be light for high m_0 as well, this case will be discussed further on

For low m_0, $m_0 \lesssim$ 100 GeV/c^2, and low M_2, $M_2 \lesssim$ 200 GeV/c^2, the situation is much more complicated because light sfermions affect not only the production cross-sections but also the decay patterns of charginos and neutralinos. They can also be searched for in direct pair-production. Exclusion regions at low m_0 arise from the combination of searches for chargino, neutralino and slepton production.

For low m_0 and M_2 the sneutrino is light, and for $M_{\tilde{\chi}_1^\pm} > m_{\tilde{\nu}}$ the chargino decay mode $\tilde{\chi}_1^\pm \to \tilde{\nu}\ell$ is dominant, leading to an experimentally undetectable final state if $M_{\tilde{\chi}_1^\pm} \simeq m_{\tilde{\nu}}$. In the gaugino region, for every value of M_2 and μ, an m_0 can be found such that $M_{\tilde{\chi}_1^\pm} \simeq m_{\tilde{\nu}}$, therefore the search for charginos cannot be used to exclude regions in the (μ,M_2) plane if very low m_0 values are allowed. The search for selectron production is used instead to put a limit on the sneutrino mass (and thus on the chargino mass), the selectron and the sneutrino masses being related by equations 1)-3). The selectron pair production cross-section is typically larger than the smuon pair production cross-section, due to the contribution of t-channel neutralino exchange. However, at $|\mu| \lesssim$ 200 GeV/c^2 the selectron production cross-section tends to be small and the exclusion arises mainly from the search for neutralino pair-production.

Mixing between the left-handed and right-handed sfermion states can be important for the third family sfermions and can lead to light $\tilde{\tau}_1$, $\tilde{\mathrm{b}}_1$ and $\tilde{\mathrm{t}}_1$. Mass splitting terms at the Electroweak Scale proportional to $m_\tau(A_\tau - \mu\tan\beta)$, $m_b(A_b - \mu\tan\beta)$, and $m_t(A_t - \mu/\tan\beta)$ were considered for $\tilde{\tau}$, $\tilde{\mathrm{b}}$, and $\tilde{\mathrm{t}}$ respectively. In the first instance A_τ=A_t=A_b=0 was assumed, then the dependence of the results on A_τ and A_t was studied. These terms lead to $\tilde{\tau}_1$, $\tilde{\mathrm{b}}_1$ or $\tilde{\mathrm{t}}_1$ being degenerate in mass with $\tilde{\chi}_1^0$ or being the LSP for large values of $|\mu|$. The results presented in this paper are limited to the range of the μ parameter where the lightest neutralino is the LSP.

7.2 Results

7.3 The LSP mass limit for high m_0

From charginos searches alone a limit of 37.8 GeV/c^2 on the lightest neutralino mass is obtained, valid for $\tan\beta \geq 1$ and a heavy sneutrino ($m_{\tilde{\nu}} > 300$ GeV/c^2). The limit is reached for $\tan\beta = 1$, $\mu = -64.5$ GeV/c^2, $\mathrm{M}_2 = 64.4$ GeV/c^2. This limit improves by ~ 1 GeV/c^2 due to the constraint from the search for neutralino production, thus from chargino and neutralino searches the LSP mass can be constrained to be $M_{\tilde{\chi}_1^0} > 38.7$ GeV/c^2 and the limit occurs at $\tan\beta$= 1.0. Figure 33 shows the region in the (μ,M_2) plane for $\tan\beta$=1 excluded by the chargino and neutralino searches, relevant for the LSP mass limit at $m_0 = 1000$ GeV/c^2. The lowest value of $M_{\tilde{\chi}_1^0}$ not excluded by chargino and neutralino searches occurs for $\tan\beta$=1, $\mu = -73$ GeV/c^2 and $M_2 = 66.0$ GeV/c^2. For these parameters, $\tilde{\chi}_4^0\tilde{\chi}_2^0$ production and chargino pair production are important.

Figure 34 gives the lower limit on $M_{\tilde{\chi}_1^0}$ as a function of $\tan\beta$. At $\tan\beta \gtrsim$ 1.2 the neutralino search no longer contributes, the LSP limit is given by the chargino search, and its value reaches about half the limit on the chargino mass at high $\tan\beta$, where the isomass contours of $\tilde{\chi}_1^\pm$ and $\tilde{\chi}_1^0$ in the (μ,M_2) plane become parallel. The rise of the LSP limit for small $\tan\beta$ can be explained by the change of the shape of these contours with $\tan\beta$ as illustrated in [6, 7]. It should be noted that, because the chargino and neutralino masses are invariant under the exchange $\tan\beta \leftrightarrow 1/\tan\beta$, the point $\tan\beta = 1$ is the real

minimum and the LSP limit for $\tan\beta < 1$ can be obtained by replacing $\tan\beta$ with $1/\tan\beta$ in figure 34.

For $M_A \leq 1000$ GeV/c^2, A_t-$\mu/\tan\beta$=$\sqrt{6}$ TeV/c^2 (maximal M_{h^0} scenario used in [12]), and $M_t = 174.3$ GeV/c^2, the $\tan\beta$ region $0.5 \geq \tan\beta \geq 2.36$ is excluded by the Higgs searches. Thus Higgs searches set a limit on $M_{\tilde{\chi}_1^0}$ (see figure 34) of $M_{\tilde{\chi}_1^0} > 49$ GeV/c^2 for $\tan\beta \geq 2.36$ and $M_{\tilde{\chi}_1^0} > 48.5$ GeV/c^2 for $\tan\beta < 0.5$.

Thus the lightest neutralino is constrained to have a mass:

$$M_{\tilde{\chi}_1^0} > 49.0 \text{ GeV}/c^2$$

for $m_0 = 1000$ GeV/c^2 and $M_2 \leq 1000$ GeV/c^2 and $\tan\beta \geq 1.0$. The limit occurs at the edge of the $\tan\beta$ exclusion given by searches for the Higgs boson. However, if $M_t = 179$ GeV/c^2, the $\tan\beta$ area excluded by searches for the Higgs boson shrinks to $0.6 \geq \tan\beta \geq 2.0$ and these limits worsen $M_{\tilde{\chi}_1^0} > 48.5$ GeV/c^2 for $\tan\beta \geq 2.0$ and $M_{\tilde{\chi}_1^0} > 47.0$ GeV/c^2 for $\tan\beta < 0.6$. Thus the above limit worsens by 2 GeV if $M_t = 179$ GeV/c^2 and the $\tan\beta < 1.0$ region is included.

7.4 The LSP mass limit for any m_0

Figure 34 also gives the lower limit on $M_{\tilde{\chi}_1^0}$ as a function of $\tan\beta$ for any m_0. The "any m_0" limit resulting from chargino, neutralino and slepton searches follows the high m_0 limit up to $\tan\beta$=1.4; then it increases slower due to the opening of the possibility of the chargino-sneutrino degeneracy, reaching 46.0 GeV/c^2 at $\tan\beta \geq 2.36$ (edge of the region excluded by Higgs boson searches); finally, as discussed in more detail below, it falls to its lowest value, 36.7 GeV/c^2, at $\tan\beta \geq 5$, due to small $M_{\tilde{\tau}_1}$-$M_{\tilde{\chi}_1^0}$, if mixing in the stau sector is of the form $A_\tau - \mu\tan\beta$, and $A_\tau = 0$. This limit is set by searches for $\tilde{\chi}_1^0\tilde{\chi}_2^0$ production with $\tilde{\chi}_2^0 \to \tilde{\tau}_1\tilde{\chi}_1^0$. Preliminary studies show that if the searches for $\tilde{\chi}_2^0\tilde{\chi}_2^0$ as described in 5.4.2 and 6.3 are used the limit grows to 43 GeV/c^2 for $A_t = A_b = A_\tau = 0$.

Thus

$$M_{\tilde{\chi}_1^0} > 46.0 \text{ GeV}/c^2$$

independent of m_0, for $\tan\beta \geq 1$ if there is no mixing in the third family ($A_\tau = \mu\tan\beta$, $A_b = \mu\tan\beta$, $A_t = \mu/\tan\beta$), or if the mixing parameters leading to $M_{\tilde{\tau}_1} - M_{\tilde{\chi}_1^0} < 5$ GeV/c^2 are avoided. The Higgs boson search in the conservative maximal M_{h^0} scenario was used to exclude $0.5 \leq \tan\beta \leq 2.36$.

LSP mass limits obtained with various assumptions are summarized in table 24.

7.4.1 The dependence of the LSP limit on the mixing in the third family.

Mixing in the third family affects in a complicated way exclusion regions obtained from Higgs, chargino, neutralino and squark searches, and a consistent discussion of the mixing is difficult.

For example the maximal M_{h^0} scenario used to set $\tan\beta$ limits from Higgs searches implies A_t-$\mu/\tan\beta$=$\sqrt{6}$ TeV/c^2, thus a different A_t for every μ. Such a scenario implies as well that low m_0 values are forbidden for M_2 sufficiently low to be of interest from the point of view of the LSP mass limit. Thus to be consistent we should consider only the

high m_0 scenario for the LSP limit (thus higher limit), when we use $\tan\beta$ limits from the maximal M_{h^0} scenario.

In the no-mixing scenario ($A_\tau = \mu\tan\beta$, $A_b = \mu\tan\beta$, $A_t = \mu/\tan\beta$), the LSP limit occurs in the chargino-sneutrino degeneracy region, at $\tan\beta > 1.5$, where both the chargino and sneutrino mass limits are given by the selectron exclusion (see section 7.5). If there is no mixing in the stop sector, the $\tan\beta$ region excluded from the Higgs searches grows to $\tan\beta \leq 9.4$, compared to $0.5 \leq \tan\beta \leq 2.36$ for the maximal M_{h^0} scenario. However, there is no improvement of the LSP limit as compared to $M_{\tilde{\chi}^0_1} > 46.0$ GeV/c^2 given above, as the $\tan\beta$ dependence of the limit "flattens out" at high $\tan\beta$ (see figure 34).

As discussed in our previous papers [6, 7], mixing in the stau sector can lead to a configuration where $M_{\tilde{\tau}_1}$-$M_{\tilde{\chi}^0_1}$ is small enough to make the $\tilde{\tau}_1$ undetectable and cause a blind spot both in $\tilde{\tau}_1$ and chargino exclusion. For $A_t{=}A_\tau{=}A_b{=}0$ with the present data, the LSP mass limit occurs a) at high enough M_2 that already for $\tan\beta \geq 3$ both $M_{\tilde{\mathrm{b}}_1}$ and $M_{\tilde{\mathrm{t}}_1}$ are pushed above $M_{\tilde{\tau}_1}$ [9], and $\tilde{\tau}_1$ can become degenerate in mass with $\tilde{\chi}^0_1$, and b) at high enough m_0 that selectron and sneutrino pair-production are not allowed by kinematics.

For the above mixing assumptions, the mass of the lightest Higgs boson corresponding to the LSP limit point varies between 109 and 120 GeV/c^2, depending on the $\tan\beta$ region. However, when the stau is light the lightest Higgs boson decays predominantly to $\tilde{\tau}_1\,\bar{\tilde{\tau}}_1$, thus "invisibly". The mass limit $M_h > 113.1$ GeV/c^2 set for an invisibly decaying Higgs boson [12] can be used to exclude some of these points, but it is enough to change slightly the mixing in the stop sector (A_t) to push the Higgs mass above 113.1 GeV/c^2.

For such a mixing configuration and for $\tan\beta \gtrsim 3$, the LSP limit is therefore set by the searches for stop and sbottom and those for $\tilde{\chi}^0_1\tilde{\chi}^0_2$ production with $\tilde{\chi}^0_2 \to \tilde{\tau}_1\tau$, and it falls to $M_{\tilde{\chi}^0_1} > 36.7$ GeV/c^2 (see dot-dashed line in figure 34). However, preliminary studies show that including searches for $\tilde{\chi}^0_2\tilde{\chi}^0_2$ with $\tilde{\chi}^0_2 \to \tilde{\tau}_1\tau$ (see sections 5.4.2 and 6.3) allows to exclude $M_{\tilde{\chi}^0_1} < 43$ GeV/c^2 for $A_t{=}A_\tau{=}A_b{=}0$.

As noted in the previous paper [6, 7], it is the appearance of the light sbottom and stop which protects the stau from being degenerate in mass with the LSP for very high m_0 values, where the $\tilde{\chi}^0_1\tilde{\chi}^0_2$ production cross-section is small. This is illustrated on figure 35 where the stop, sbottom, and stau masses at the highest allowed $|\mu|$ value at the lowest non-excluded M_2 are plotted. At high $\tan\beta$, the highest $|\mu|$ value occurs when the sbottom and stop masses have their lowest non-excluded (see section 6.5) values. In a pathological model where there is no mixing in the sbottom or stop sector ($A_b = \mu\tan\beta$, $A_t = \mu/\tan\beta$), but only in the stau sector, one can make $\tilde{\tau}_1$ degenerate with $M_{\tilde{\chi}^0_1}$ even at high values of m_0 and $|\mu|$ so that the $\tilde{\chi}^0_1\tilde{\chi}^0_2$ production cross-section at LEP is very small, and the production of the Higgs boson and other sfermions is not accessible kinematically.

The dependence of the LSP limit on the mixing in the stau sector and the stop sector was studied, while keeping $A_b{=}0$. For A_τ large and positive, $\simeq +1000$ GeV/c^2, for $\tan\beta \gtrsim 8$ the limit falls by ~ 1 GeV/c^2 because, with the larger splitting in the stau sector, the stau-neutralino mass degeneracy occurs for a higher m_0 value, where the neutralino production cross-section is lower. The limit reaches the no mass splitting limit

[9] The "mixing -independent" (diagonal) terms of the mass matrices grow faster with M_2 for squarks than for sleptons, and they have different dependence on $\tan\beta$. For example, for $A_t{=}A_\tau{=}A_b{=}0$, $\mu{=}0$, and $\tan\beta{=}1$, both the $\tilde{\mathrm{t}}_1$ and $\tilde{\mathrm{b}}_1$ are heavier than the $\tilde{\tau}_1$; but they become lighter than the $\tilde{\tau}_1$ for large $|\mu|$ values. The mass hierarchy between $\tilde{\tau}_1$, $\tilde{\mathrm{b}}_1$, and $\tilde{\mathrm{t}}_1$ depends on M_2, $\tan\beta$, μ, and m_0.

if A_τ is close to $\mu\tan\beta$.

If in turn A_t was varied while keeping A_b=A_τ=0, the $\tan\beta$ region where $\tilde{\tau}_1$ was allowed to be lighter than $\tilde{t}_1$ and thus degenerate with neutralino moved to higher (lower) $\tan\beta$ for $A_t > 0$ ($A_t < 0$).

7.5 $\tilde{\chi}_1^\pm$ mass limits for any m_0

Figure 36 shows the chargino mass limit as a function of $\tan\beta$ for $M_2 < 200$ GeV/c^2. The lowest non-excluded chargino mass is found at MSSM points very close to those giving the LSP mass limit, and the arguments presented in section 7.4 also apply to explain the dependence of the chargino mass limit on $\tan\beta$. For $\tan\beta \lesssim 1.4$ the limit occurs at high m_0 values. For $1.4 \lesssim \tan\beta \lesssim 3$ and $M_2 < 200$ GeV/c^2, the limit occurs at low m_0 in the chargino-sneutrino degeneracy region. It falls at $\tan\beta \gtrsim 4$ because of the small ΔM $= M_{\tilde{\tau}} - M_{\tilde{\chi}_1^0}$.

The lightest chargino is constrained to have a mass:

$$M_{\tilde{\chi}_1^\pm} > 95 \text{ GeV}/c^2.$$

independent of m_0, for $\tan\beta \leq 40$, $M_2 \leq 1000$ GeV/c^2, if either is no mixing in the third family ($A_\tau = \mu\tan\beta$, $A_b = \mu\tan\beta$, $A_t = \mu/\tan\beta$) or the mixing parameters leading to $M_{\tilde{\tau}_1} - M_{\tilde{\chi}_1^0} < 5$ GeV/c^2 are avoided.

If mixing in the stau sector is of the form $A_\tau - \mu\tan\beta$, and $A_\tau = 0$, the limit falls to 70.0 GeV/c^2, at $\tan\beta \geq 3$, due to small $M_{\tilde{\tau}_1}$-$M_{\tilde{\chi}_1^0}$. Preliminary studies show that if searches for $\tilde{\chi}_2^0\tilde{\chi}_2^0$ as described in 5.4.2 and 6.3 are used the limit grows to 85 GeV/c^2 for $A_t = A_b = A_\tau = 0$.

The chargino mass limits for high M_2 values where the chargino can be degenerate in mass with the LSP presented in 6.2.2, are close to 75 GeV/c^2.

Chargino mass limits obtained with various assumptions are summarized in table 24.

7.6 $\tilde{\nu}$ and $\tilde{\mathrm{e}}_\mathrm{R}$ mass limits for any m_0

The sneutrino and the $\tilde{\mathrm{e}}_\mathrm{R}$ mass limits are:

$$m_{\tilde{\nu}} > 95 \text{ GeV}/c^2 \text{ and } M_{\tilde{\mathrm{e}}_\mathrm{R}} > 95 \text{ GeV}/c^2.$$

These limits, shown in figure 36, were obtained assuming no mass splitting in the third sfermion family ($A_\tau = \mu\tan\beta$), implying $M_{\tilde{\mathrm{e}}_\mathrm{R}} = M_{\tilde{\mathcal{T}}_R} = M_{\tilde{\tau}_1} = M_{\tilde{\mu}_\mathrm{R}}$, as this gives the lowest values.

These limits result from the combination of slepton and neutralino searches. The selectron mass limit (see figure 36, dotted curve) is valid for -1000 GeV/$c^2 \leq \mu \leq 1000$ GeV/c^2 and $1 \leq \tan\beta \leq 40$ provided that $M_{\tilde{\mathrm{e}}_\mathrm{R}} - M_{\tilde{\chi}_1^0} > 10$ GeV/c^2, and it allows a limit to be set on the sneutrino mass as shown in figure 36 (dashed curve). The sneutrino mass limit is expected to rise for $\tan\beta < 1$, the sneutrino being heavier than the $\tilde{\mathrm{e}}_\mathrm{R}$ for small $\tan\beta$. If $M_{\tilde{\mathrm{e}}_\mathrm{R}} - M_{\tilde{\chi}_1^0} < 10$ GeV/c^2, the most unfavourable situation appears when $\tilde{\chi}_1^+\tilde{\chi}_1^-$ and $\tilde{\chi}_2^0\ \tilde{\chi}_1^0$ production are kinematically inaccessible and the splitting between $M_{\tilde{\mathrm{e}}_\mathrm{R}}$ and $M_{\tilde{\mathrm{e}}_\mathrm{L}}$ is sufficiently large to make $\tilde{\mathrm{e}}_\mathrm{R}\tilde{\mathrm{e}}_\mathrm{L}$ production inaccessible as well. In this case the

lower limit on $M_{\tilde{e}_R}$ is about 80 GeV/c^2; but the limit on the sneutrino mass does not deteriorate, as $m_{\tilde{\nu}}$ is high. The sneutrino and the $\tilde{e}_R$ mass limits occur at points where the chargino production is not kinematically accessible and $M_{\tilde{\chi}_1^0}$ is high. The selectron mass limit for $\tan\beta = 1.5$ and $\mu = -200$ GeV/c^2 was shown in section 6.4.1.

Slepton mass limits obtained with different assumptions are summarized in table 24.

7.7 MSSM parameter space exclusion

Limits on Higgs, chargino, neutralino, slepton and squark production used in the previous sections to set a mass limit on the LSP and other particles can be also used to exclude regions in a parameter space of the CMSSM. The exclusion regions in the (μ, M_2) plane for $\tan\beta = 35$ and several assumptions about m_0 and mixing in the third family are shown in figure 37.

8 Summary

Searches for charginos, neutralinos, sleptons and squarks in e^+e^- collisions at centre-of-mass energies up to 208 GeV were performed with the DELPHI detector at LEP. No evidence for a signal was found in any of the channels and 95 % CL upper limits on the production cross-sections were derived.

Under assumptions that depend on the channel, such results were translated into lower limits on the masses of SUSY particles. In particular, in the framework of constrained SUGRA-broken MSSM scenarios (section 2) regions of the parameter space can be excluded and these exclusions can be translated into limits on the masses of SUSY particles. The combination of the results of the different search channels is crucial to ensure a complete coverage of the parameter space.

A summary of the limits obtained on the masses of SUSY particles is presented in table 24. The results presented extend previous exclusions set by DELPHI (see [2] to [10]) and are consistent with those obtained by the other LEP experiments [39].

Particle	Validity conditions	Mass imit
$\tilde{e}_R$	tanβ=1.5, μ=-200, ΔM>5	99 GeV/c^2
	CMSSM, ΔM>10	95.0 GeV/c^2
$\tilde{\mu}_R$	BR($\tilde{\mu}\rightarrow \mu\tilde{\chi}^0$)=1 , ΔM>5	85 GeV/c^2
	CMSSM, ΔM>10	95.0 GeV/c^2
$\tilde{\tau}_R$	ΔM>6, no mixing	82.5 GeV/c^2
$\tilde{\tau}_{min}$	ΔM>6, minimal cross-section	83.6 GeV/c^2
$\tilde{\nu}$	ΔM>10	95.0 GeV/c^2
$\tilde{b}$	ΔM>10, BR($\tilde{b}\rightarrow$ b $\tilde{\chi}^0$)=1, no mixing	98 GeV/c^2
	ΔM>10, BR($\tilde{b}\rightarrow$ b $\tilde{\chi}^0$)=1, minimal cross-section	87 GeV/c^2
$\tilde{b}$	ΔM>10, BR($\tilde{t}\rightarrow$ c $\tilde{\chi}^0$)=1, no mixing	96 GeV/c^2
	ΔM>2, BR($\tilde{b}\rightarrow$ c $\tilde{\chi}^0$)=1, no mixing	75 GeV/c^2
	ΔM>10, BR($\tilde{b}\rightarrow$ c $\tilde{\chi}^0$)=1, minimal cross-section	92 GeV/c^2
	ΔM>2, BR($\tilde{b}\rightarrow$ c $\tilde{\chi}^0$)=1, minimal cross-section	72 GeV/c^2
$\tilde{\chi}^\pm$	$m_{\tilde{\nu}}$> 300, ΔM>10, $M_1 = \sim 0.5 M_2$,	102.5 GeV/c^2
	m$_{\tilde{f}} > m_{\tilde{\chi^\pm}}$, ΔM>3	97.3 GeV/c^2
	$M_1 = \sim 0.5 M_2$, any ΔM, m$_{\tilde{f}} > m_{\tilde{\chi^\pm}}$	75.0 GeV/c^2
	no gaugino mass unification, $m_{\tilde{\nu}}$> 300, $\|\mu\| \geq$ M$_2$	70.0 GeV/c^2
	CMSSM, ΔM>3, any m$_0$, no mixing or ΔM($\tilde{\tau}$-$\tilde{\chi}^0$)>6	95.0 GeV/c^2
	CMSSM, any m$_0$, any M$_2$, tanβ <40, mixing A$_\tau$=A$_b$=A$_t$=0	70.0 GeV/c^2 *
$\tilde{\chi}^0$	CMSSM, high m$_0$, tanβ >1, maximal mixing in $\tilde{t}$ sector	49(47) GeV/c^2
	CMSSM, any m$_0$, tanβ <40 no mixing or ΔM($\tilde{\tau}$-$\tilde{\chi}^0$)>6	46 GeV/c^2
	CMSSM, any m$_0$, tanβ <40, mixing A$_\tau$=A$_b$=A$_t$ = 0	36.7 GeV/c^2 *

Table 24: Summary of mass limits for supersymmetric particles and their validity conditions. In each line of the table ΔM is the mass difference between the corresponding sparticle and the LSP. All masses and ΔM values are in GeV/c^2. The chargino (neutralino) mass limit marked with * improves to 85 GeV/c^2 (43 GeV/c^2) if the searches for staus in $\tilde{\chi}^0_2\tilde{\chi}^0_2$ (see sections 5.4.2 and 6.3) are used.

9 Acknowledgements

We are greatly indebted to our technical collaborators, to the members of the CERN-SL Division for the excellent performance of the LEP collider, and to the funding agencies for their support in building and operating the DELPHI detector.
We acknowledge in particular the support of
Austrian Federal Ministry of Science and Traffics, GZ 616.364/2-III/2a/98,
FNRS–FWO, Belgium,
FINEP, CNPq, CAPES, FUJB and FAPERJ, Brazil,
Czech Ministry of Industry and Trade, GA CR 202/96/0450 and GA AVCR A1010521,
Danish Natural Research Council,
Commission of the European Communities (DG XII),
Direction des Sciences de la Matière, CEA, France,
Bundesministerium für Bildung, Wissenschaft, Forschung und Technologie, Germany,
General Secretariat for Research and Technology, Greece,
National Science Foundation (NWO) and Foundation for Research on Matter (FOM), The Netherlands,
Norwegian Research Council,
State Committee for Scientific Research, Poland, 2P03B06015, 2P03B1116 and SPUB/P03/178/98,
JNICT–Junta Nacional de Investigação Científica e Tecnológica, Portugal,
Vedecka grantova agentura MS SR, Slovakia, Nr. 95/5195/134,
Ministry of Science and Technology of the Republic of Slovenia,
CICYT, Spain, AEN96–1661 and AEN96-1681,
The Swedish Natural Science Research Council,
Particle Physics and Astronomy Research Council, UK,
Department of Energy, USA, DE–FG02–94ER40817.

References

[1] P. Fayet and S. Ferrara, Phys. Rep. **32** (77) 249;
H.P. Nilles, Phys. Rep. **110** (84) 1;
H.E. Haber and G.L. Kane, Phys. Rep. **117** (85) 75.

[2] DELPHI Coll., P. Abreu et al., Phys. Lett. **B479** (2000) 118;
T. Alderweireld, I. Gil, P. Rebecchi, *Review of the chargino search in DELPHI. Latest results at* $E_{\rm cm}$ *= 189 GeV*, DELPHI note 99-177 PHYS 843 (1999);
DELPHI Coll., P. Abreu et al., Phys. Lett. **B446** (1999) 75.

[3] DELPHI Coll., P. Abreu et al., Phys. Lett. **B485** (2000) 65;
DELPHI Coll., P. Abreu et al., E. Phys. J. **C11** (1999) 1.

[4] DELPHI Coll., P. Abreu et al., E. Phys. J., ISSN 1434-6044, 20001.

[5] T. Alderweireld, P. Andersson, M. Espirito Santo, I. Gil, K. Hultqvist, A. Lipniacka, M. Margoni, F. Mazzucato, P. Rebecchi, *Search for charginos and neutralinos in*

e^+e^- *interaction at* $\sqrt{s}$ *= 192-196-200-202 GeV*, DELPHI note 2000-072 CONF 371, contributed paper for Osaka ICHEP 2000.

[6] DELPHI Coll., P. Abreu et al., Phys. Lett. **B489** (2000) 38.

[7] M. Espirito Santo, K. Hultqvist, P. Johansson, A. Lipniacka, F. Mazzucato, *Limits on the masses of supersymmetric particles at* $\sqrt{s}$ *up to 202 GeV*, DELPHI note 2000-087 CONF 386, contributed paper for Osaka ICHEP 2000.

[8] DELPHI Coll., P. Abreu *et al.*, E. Phys. J. **C19** (2001) 29.

[9] DELPHI Coll., P. Abreu *et al.*, Phys. Lett. **B496** (2000) 59.

[10] P. Verdier, J. Abdallah, M. Berggren, W. Da Silva, F. Kapusta, A. Savoy Navarro and M. Besançon, *Search for supersymmetric partners of top and bottom quarks at* $\sqrt{s}$ *=192-202 GeV*, DELPHI note 2000-090 CONF 389, contributed paper for Osaka ICHEP 2000.

[11] R. Alemany, et al., *Update of the search for supersymmetric particles in the light gravitino scenarios at* $\sqrt{s}$ *from 204 to 208 GeV*, DELPHI 2001-012 CONF 453 (March 2001), contributed to Moriond 2001;
DELPHI Coll., P. Abreu et al., Phys. Lett. **B503** (2001) 34.

[12] DELPHI Coll., P. Abreu et al.,Phys. Lett. **B499** (2001) 23;
DELPHI Coll., *Search for neutral supersymmetric Higgs bosons in* e^+e^- *collisions up to* $\sqrt{s} = 209$ *GeV*, DELPHI note 2001-017 CONF 458 (March 2001), contributed to Moriond 2001.

[13] C.H. Chen, M. Drees, J.F. Gunion, Phys. Rev. **D55** (1997) 330, erratum/addendum *ibid.* **D60**:039901 (1999).

[14] DELPHI Coll., P. Aarnio *et al.*, Nucl. Instr. and Meth. **303** (91) 233;
DELPHI Coll., P. Abreu *et al.*, Nucl. Instr. and Meth. **378** (96) 57.

[15] P. Rebecchi, *Optimisation the l'herméticité du détecteur DELPHI pour la recherche de particules supersymétriques à LEP2*, Ph.D. thesis, LAL 96-30 (May 1996), Université Paris XI Orsay, CERN THESIS-96-003.

[16] T. Sjöstrand, Comp. Phys. Comm. **39** (86) 347;
T. Sjöstrand, `PYTHIA 5.6` *and* `JETSET 7.3`, CERN-TH/6488-92.

[17] J.E. Campagne and R. Zitoun, Z. Phys. **C43** (1989) 469.

[18] S. Jadach, B.F.L. Ward and Z. Was, Comp. Phys. Comm. **79** (94) 503.

[19] S. Jadach, W. Placzek and B.F.L. Ward, Phys. Lett. **B390** (97) 298.

[20] F.A. Berends, R. Pittau, R. Kleiss, Comp. Phys. Comm. **85** (95) 437.

[21] J.Fujimoto *et al.*, Comp. Phys. Comm. **100** (97) 128

[22] S. Nova, A. Olshevski, and T. Todorov, *A Monte Carlo event generator for two photon physics*, DELPHI note 90-35 (1990).

[23] R. Engel, Z. Phys. **C66** (95) 203;
R. Engel and J. Ranft, Phys. Rev. **D54** (96) 4244.

[24] F.A. Berends, P.H. Daverveldt, R. Kleiss, Comp. Phys. Comm. **40** (86) 271, Comp. Phys. Comm. **40** (86) 285, Comp. Phys. Comm. **40** (86) 309.

[25] S.Katsanevas and P.Morawitz, Comp. Phys. Comm. **112** (98) 227.

[26] G. Altarelli *et al.*, *"Physics at LEP2"*, Yellow Report CERN 96-01, vol. 2.

[27] DELPHI Coll., Z. Phys. **C73** (96) 11.

[28] S. Catani *et al.*, Phys. Lett. **B269** (1991) 432.

[29] F. Cossutti, A. Tonazzo, F. Mazzucato, *REMCLU : a package for the Reconstruction of Electromagnetic CLUsters at LEP200*, DELPHI note 2000-164 PROG 242 (2000).

[30] DELPHI Coll., P. Abreu *et al.*, Z. Phys. **C70** (1996) 531;
G. Borisov, C. Mariotti, Nucl. Instr. and Meth. **372** (1996) 181;

[31] T.W. Anderson, An Introduction to multivariate analysis, New York Wiley, 1958.

[32] A. Zell *et al.*, "SNNS user manual : Version 4.1", Report N 6/95.

[33] A.V. Oppenheim and R.W. Schafer, Discrete-time signal processing, Prentice-Hall, 1989

[34] Particle Data Group, R.M. Barnett *et al.*, Phys. Rev. **D54** (1996) .

[35] V.F. Obraztsov, Nucl. Instr. and Meth. **316** (92) 388;
V.F. Obraztsov, Nucl. Instr. and Meth. **399** (97) 500.

[36] F. James *et al.*, *1st Workshop on Confidence Limits*, Yellow report CERN 2000-005, (May 2000);
A. Read, note DELPHI 97-158 PHYS 737.

[37] DELPHI Coll., P. Abreu *et al.*, Z. Phys. **C74** (97) 577

[38] S. Jadach *et al.*, *LEP2 Monte Carlo Workshop : Report of the Working Groups on Precision Calculations for LEP2 Physics*, Yellow Report CERN 2000-009, (September 200);
T. Alderweireld, S. Todorovova et P. Verdier, *Study of the hadronic $\gamma\gamma$ interactions at $\sqrt{s}$ =200GeV*, Note DELPHI 2000-163 PHYS 878.

[39] Results from the other LEP experiments submitted to this conference:
Aleph Coll., *Search for Charginos and Neutralinos in $e+e-$ Collisions at $\sqrt{s}$ up to 208 GeV and Mass Limit for the Lightest Neutralino*, ALEPH 2001-009, February 2001;
L3 Coll., *Search for Supersymmetry in $e+e-$ collisions at $\sqrt{s}$= 202-208 GeV*, L3 note 2644, February 2001;
Opal Coll., *New Particle Searches in e^+e^- Collisions at $\sqrt{s}$ = 200-209 GeV*, Opal Physics note PN470, February 2001.

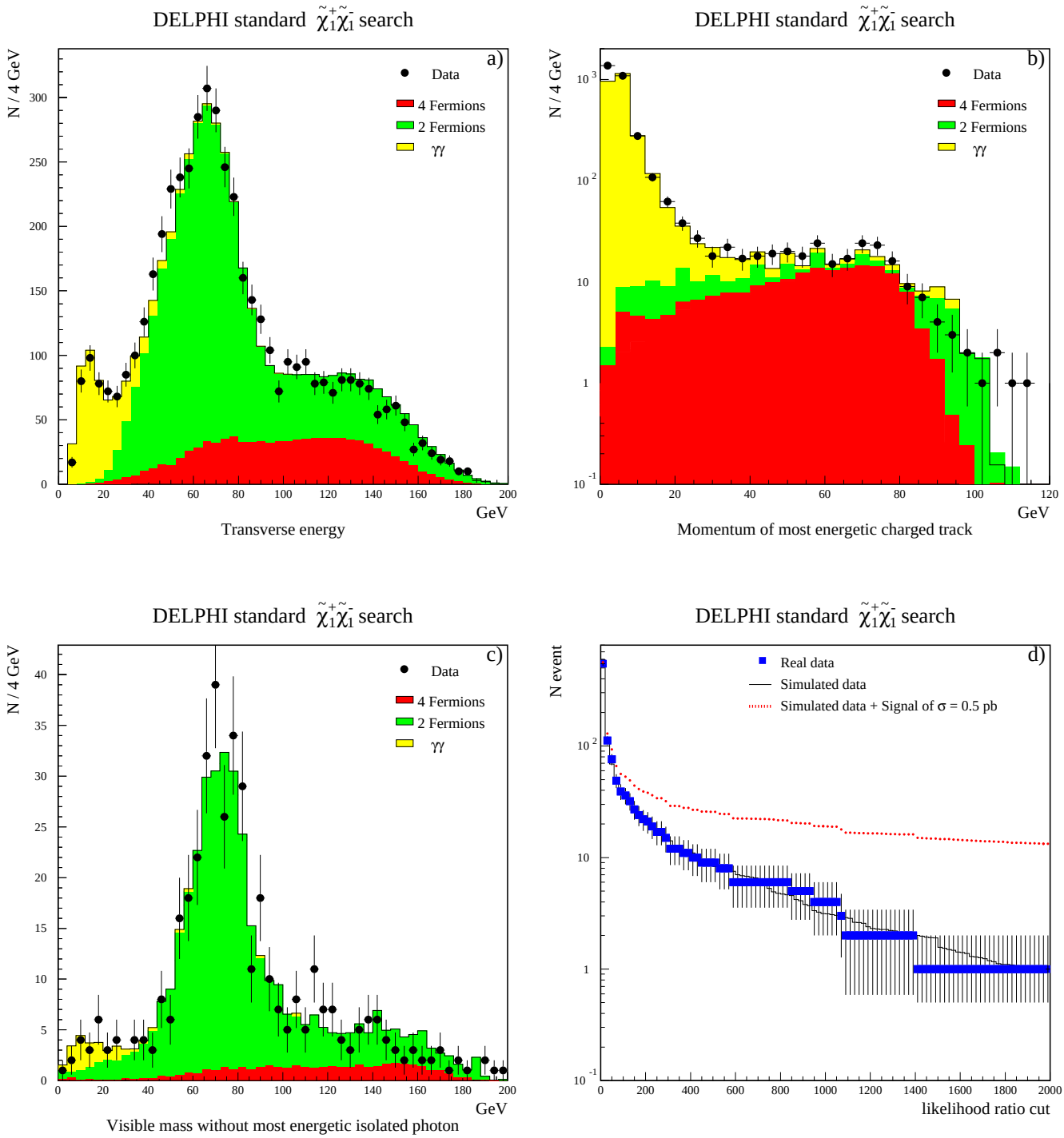

Figure 1: a), b) and c) show comparisons between real data (dots) and simulated background events (histogram) for the *jets*, $\ell\ell$ and *rad* topologies respectively, using a logical OR of the 6 preselection cut functions of the corresponding topology. d) shows the number of events selected by the standard chargino analysis as a function of the $\mathcal{L}_{R_{CUT}}$ cut in the $jj\ell$ topology for $25 \leq \Delta\mathrm{M} < 35$ GeV/c^2. The squares are the data and the solid line is the background simulation. The dotted curve shows a possible signal, $M_{\tilde{\chi}_1^\pm}$=102 GeV/c^2 $M_{\tilde{\chi}_1^0}$=72 GeV/c^2, of 0.5 pb added to the background. In all cases the data collected in the year 2000 are shown.

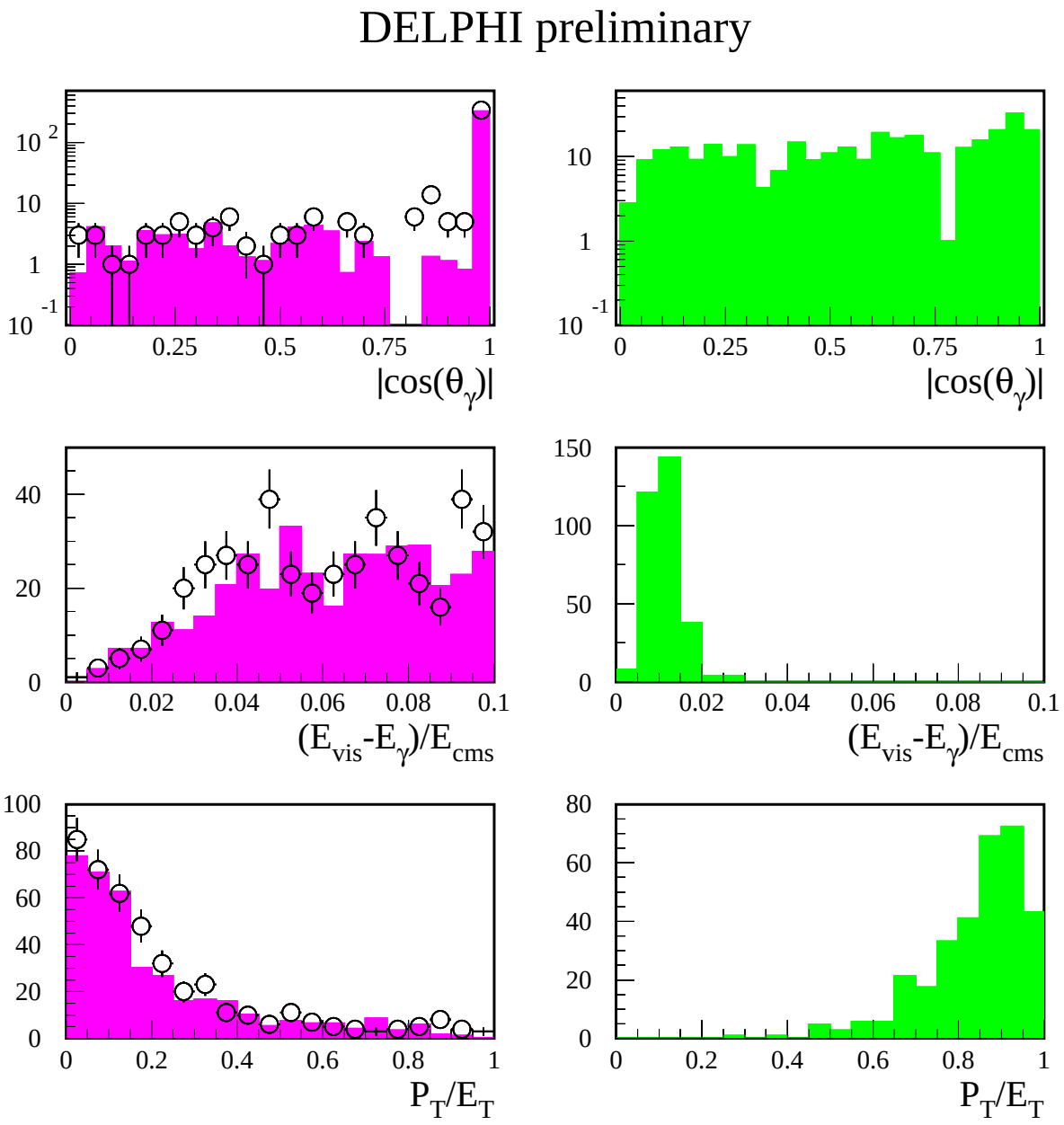

Figure 2: Some of the variables used in the selection for mass-degenerate charginos with an ISR photon tag. In the plots on the left the data (dots) are compared with the SM expectations. On the right, as an example, the corresponding distributions (with arbitrary normalization) are shown for the signal with $M(\tilde{\chi}_1^+) = 80$ GeV/c^2 and $\Delta M = 1$ GeV/c^2.

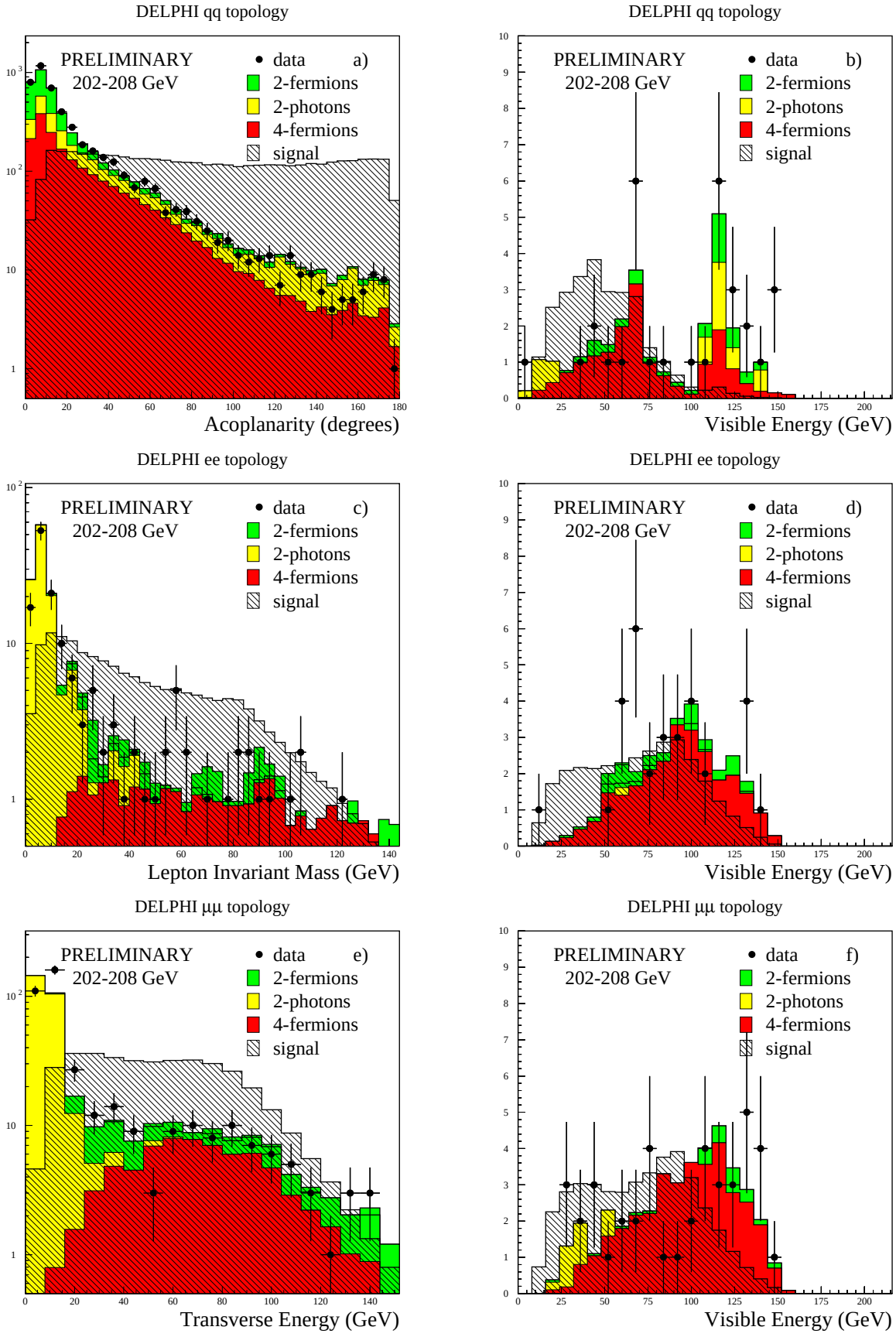

Figure 3: On the left the comparison between the real and simulated data is shown at preselection level for different variables for the $q\bar{q}$, ee, and $\mu\mu$ topologies in the neutralino search. On the right the visible energy distribution is shown for the events selected at the final stage, after the likelihood selection.

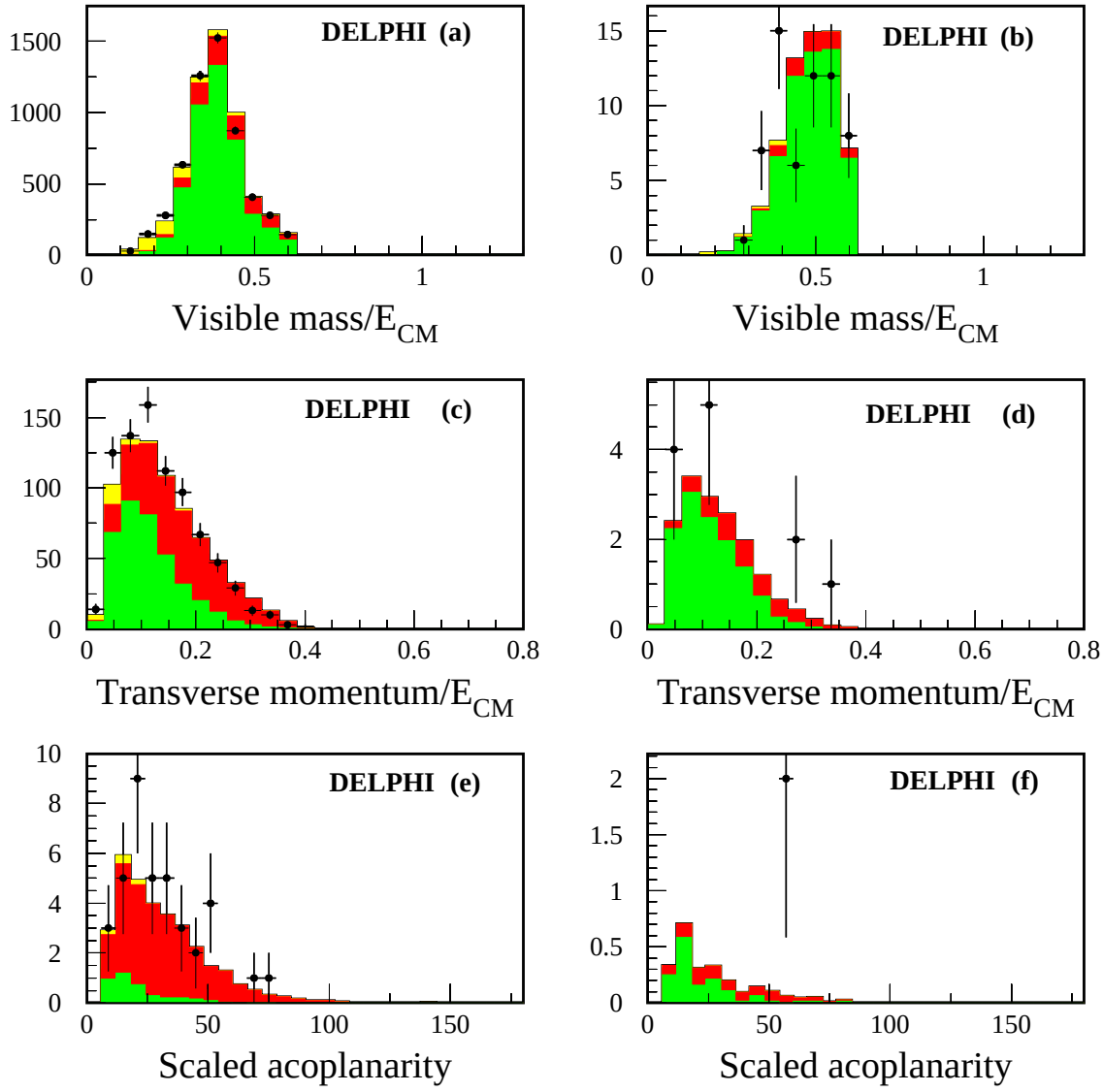

Figure 4: Comparison of real and simulated data for the multijet selection without gammas (left) and with gammas (right) at, from top to bottom, the preselection, intermediate, and final selection stages. The expected background (filled histogram) is divided into four-fermion (dark shading), two-fermion (intermediate shading), and two-photon processes (light shading).

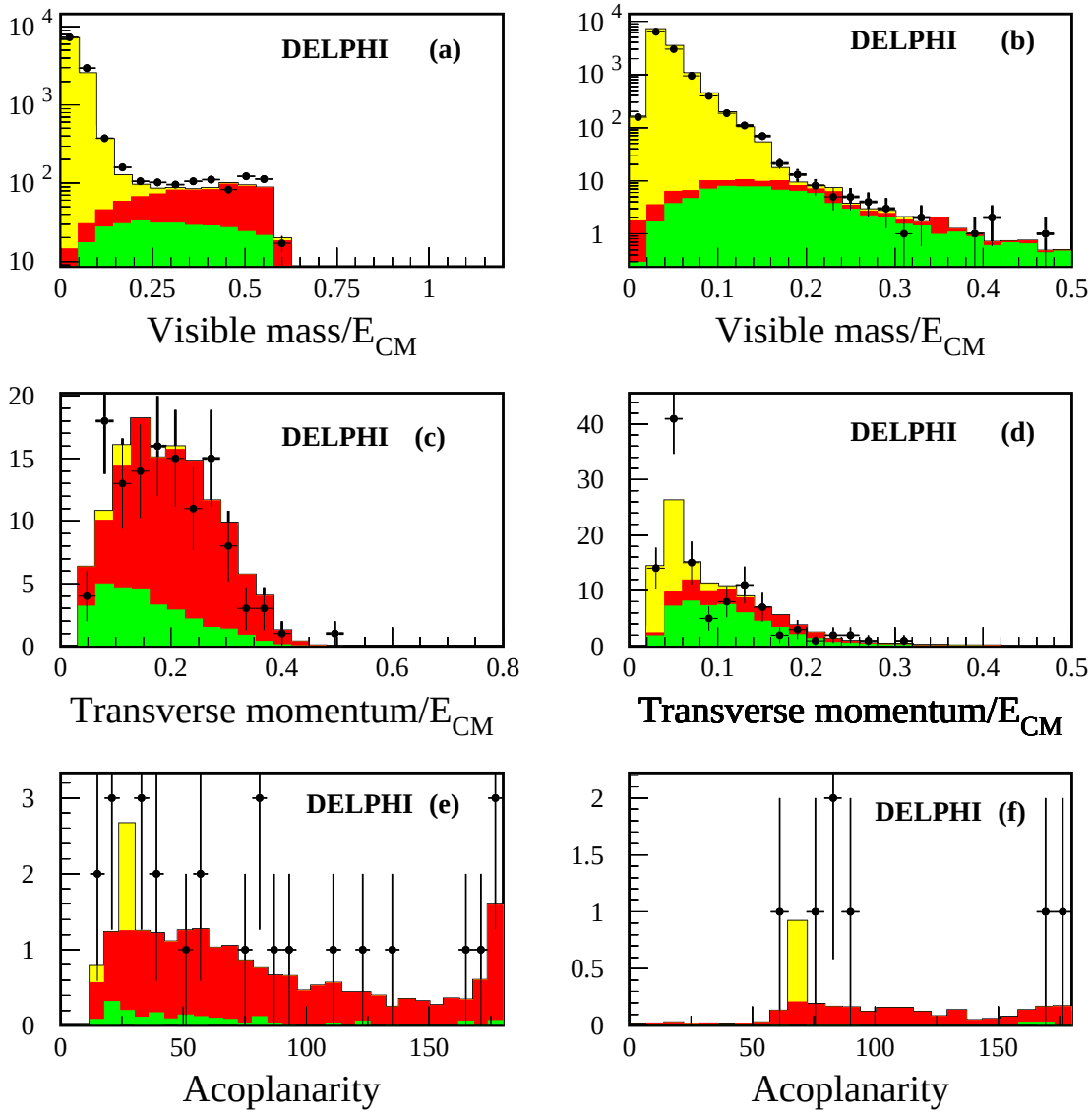

Figure 5: Comparison of real and simulated data for the multilepton search (left) and asymmetric tau search (right) at, from top to bottom, the preselection, intermediate, and final selection stages. The expected background (filled histogram) is divided into four-fermion (dark shading), two-fermion (intermediate shading), and two-photon processes (light shading).

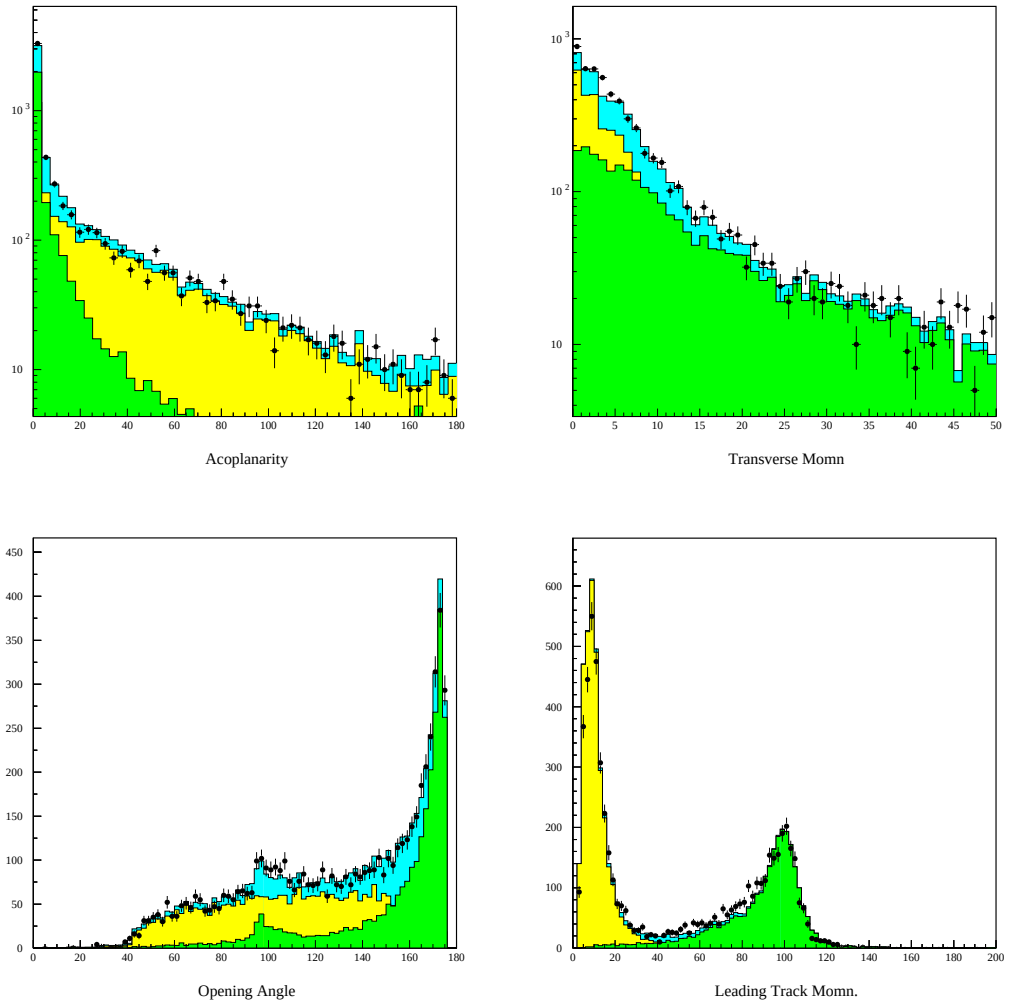

Figure 6: Comparison of data and simulation in the selectron channel at preselection level. The dots with error bars show the data, shaded histograms show the simulation.

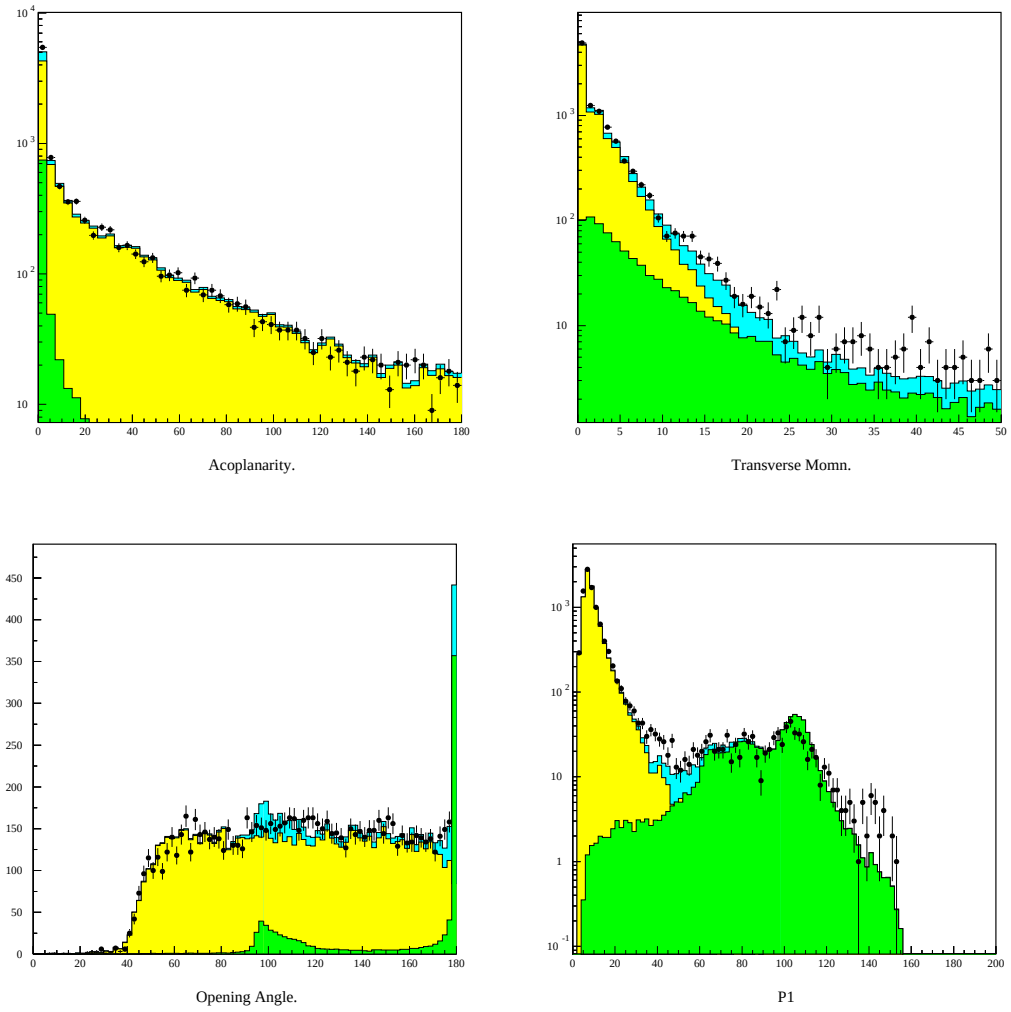

Figure 7: Comparison of data and simulation in the smuon channel at preselection level. The dots with error bars show the data, shaded histograms show the simulation.

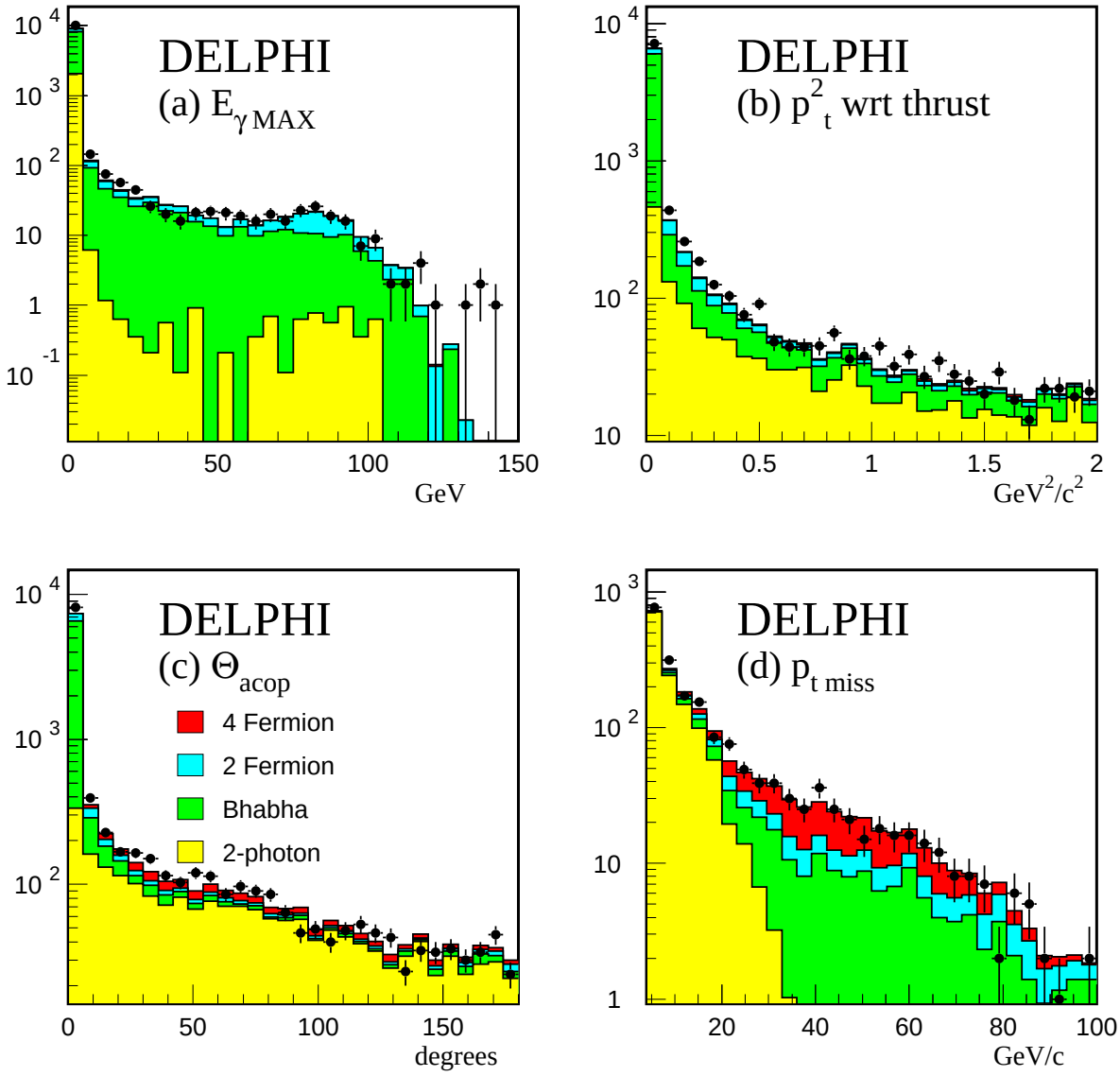

Figure 8: A pre-selection comparison of data and simulation in the stau analysis. The plots show: (a) energy of the most energetic isolated photon, (b) the square of the transverse momentum with respect to the thrust axis, (c) the acoplanarity, (d) the missing transverse momentum. The dots with error bars show the data, while the simulation is shown shaded.

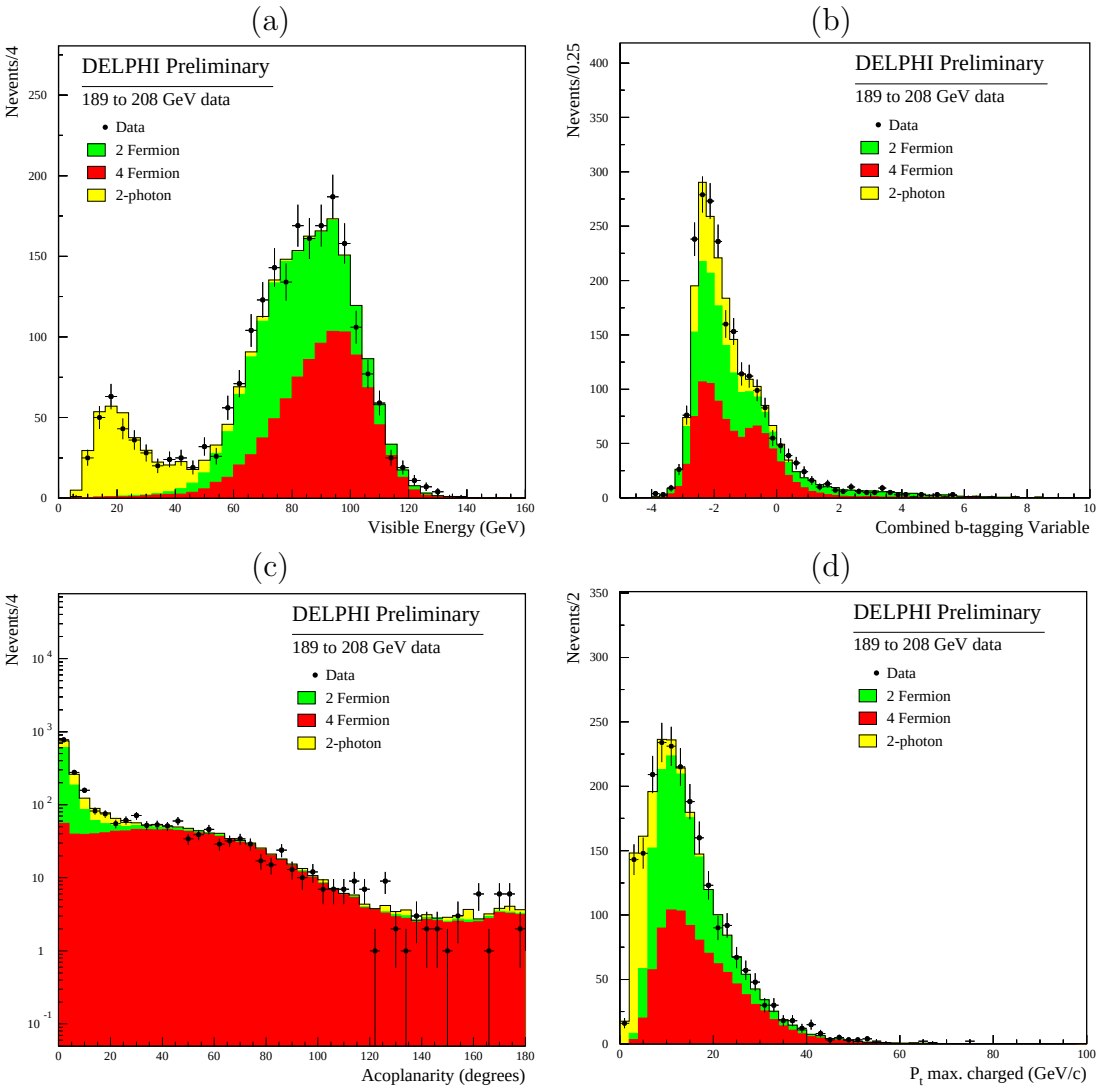

Figure 9: Comparison of data and simulation at the pre-selection level in the non-degenerate squark analysis. Plots include all DELPHI data from 189 to 208 GeV: (a) visible energy, (b) combined b-tagging variable, (c) acoplanarity, (d) maximal transverse momentum of a charged particle.

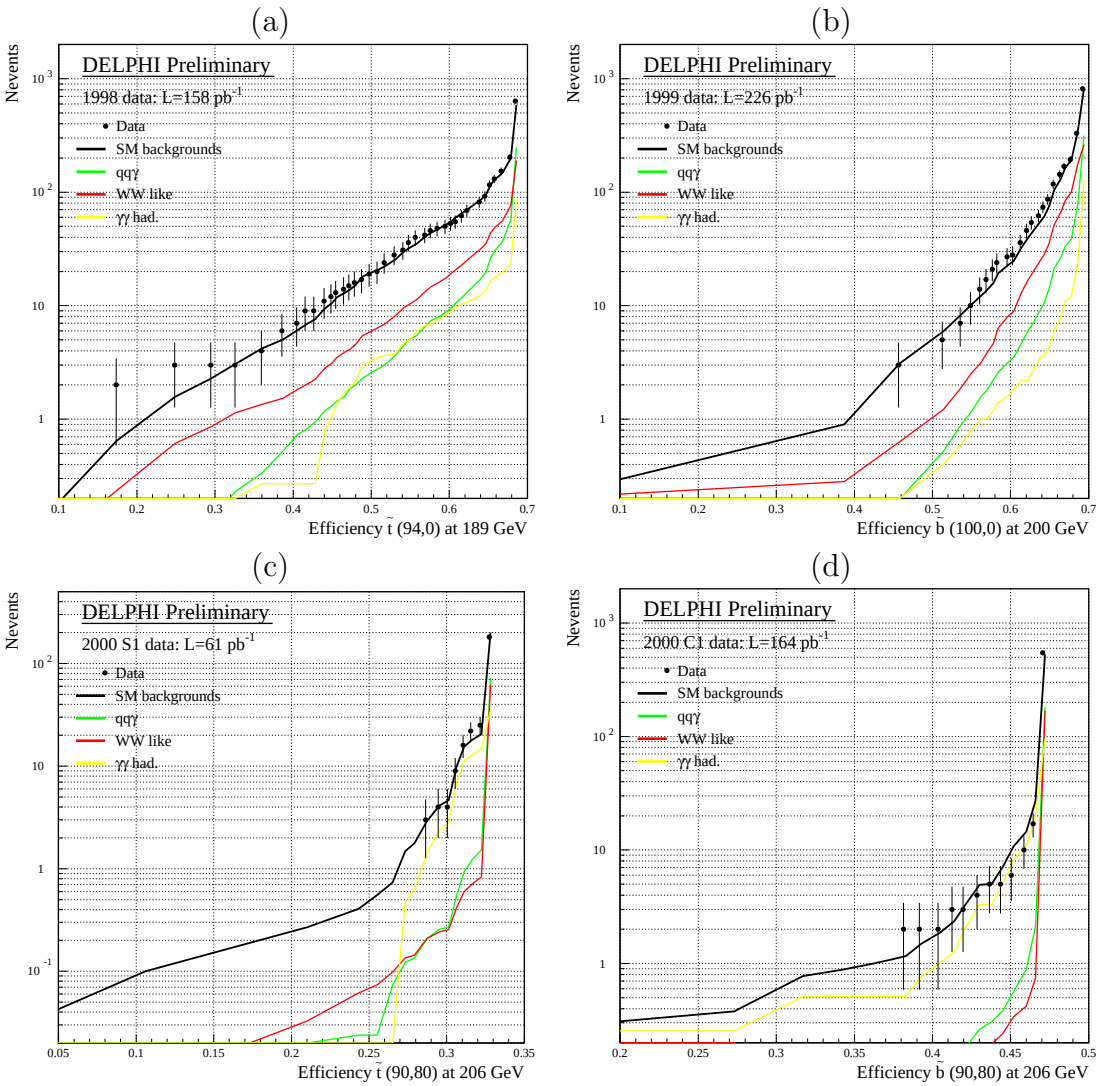

Figure 10: Number of events as a function of the signal detection efficiencies in the non-degenerate squark analysis: (a) 1998 data at 189 GeV: stop analysis for $\Delta M > 20$ GeV/c^2, (b) 1999 data from 192 to 202 GeV: sbottom analysis for $\Delta M > 20$ GeV/c^2, (c) 2000 data with TPC sector 6 off: stop analysis for $5 \leq \Delta M \leq 20$ GeV/c^2, (d) 2000 data: sbottom analysis for $5 \leq \Delta M \leq 20$ GeV/c^2.

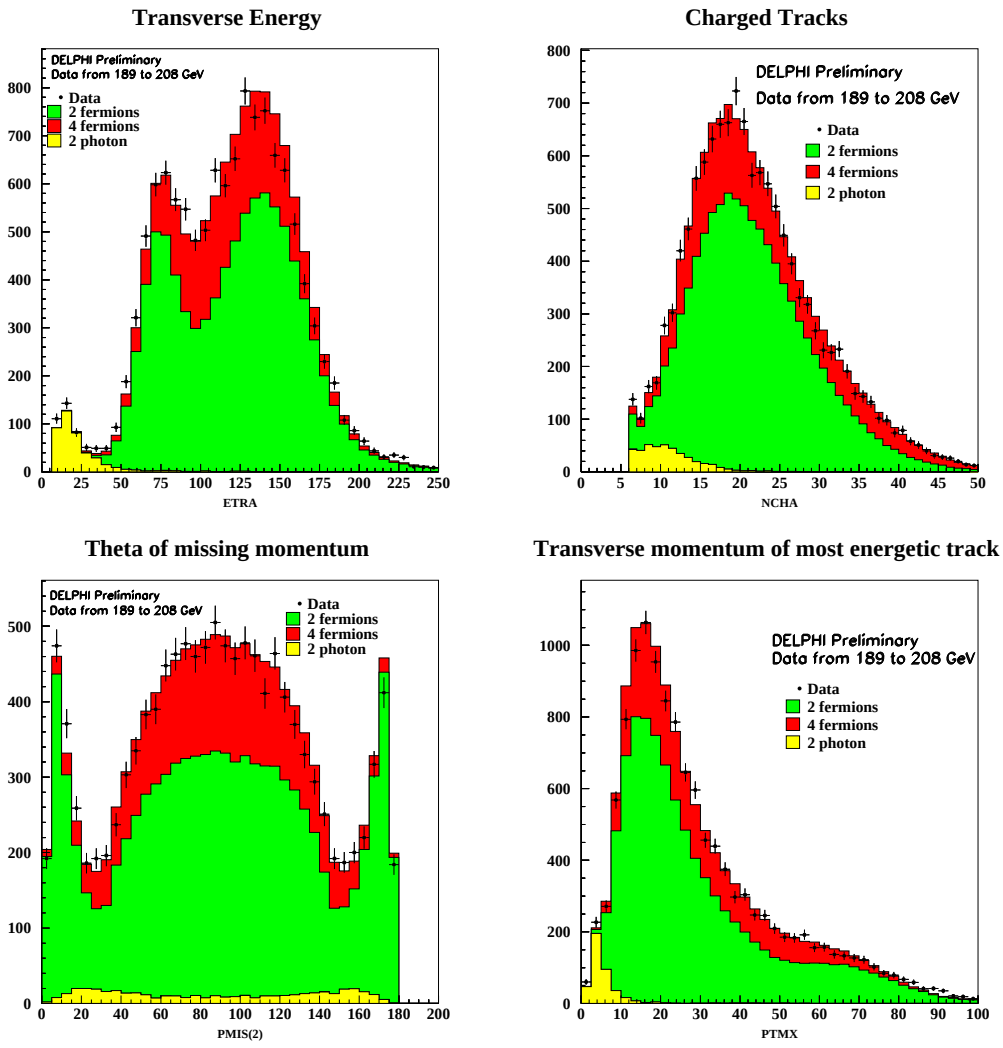

Figure 11: Comparison of data and simulation at the pre-selection level in the degenerate squark analysis. The distributions of the total transverse energy, total number of charged tracks, angle between the missing momentum and the beam axis, and the transverse momentum of the leading particle are shown for all DELPHI data from 189 to 208 GeV.

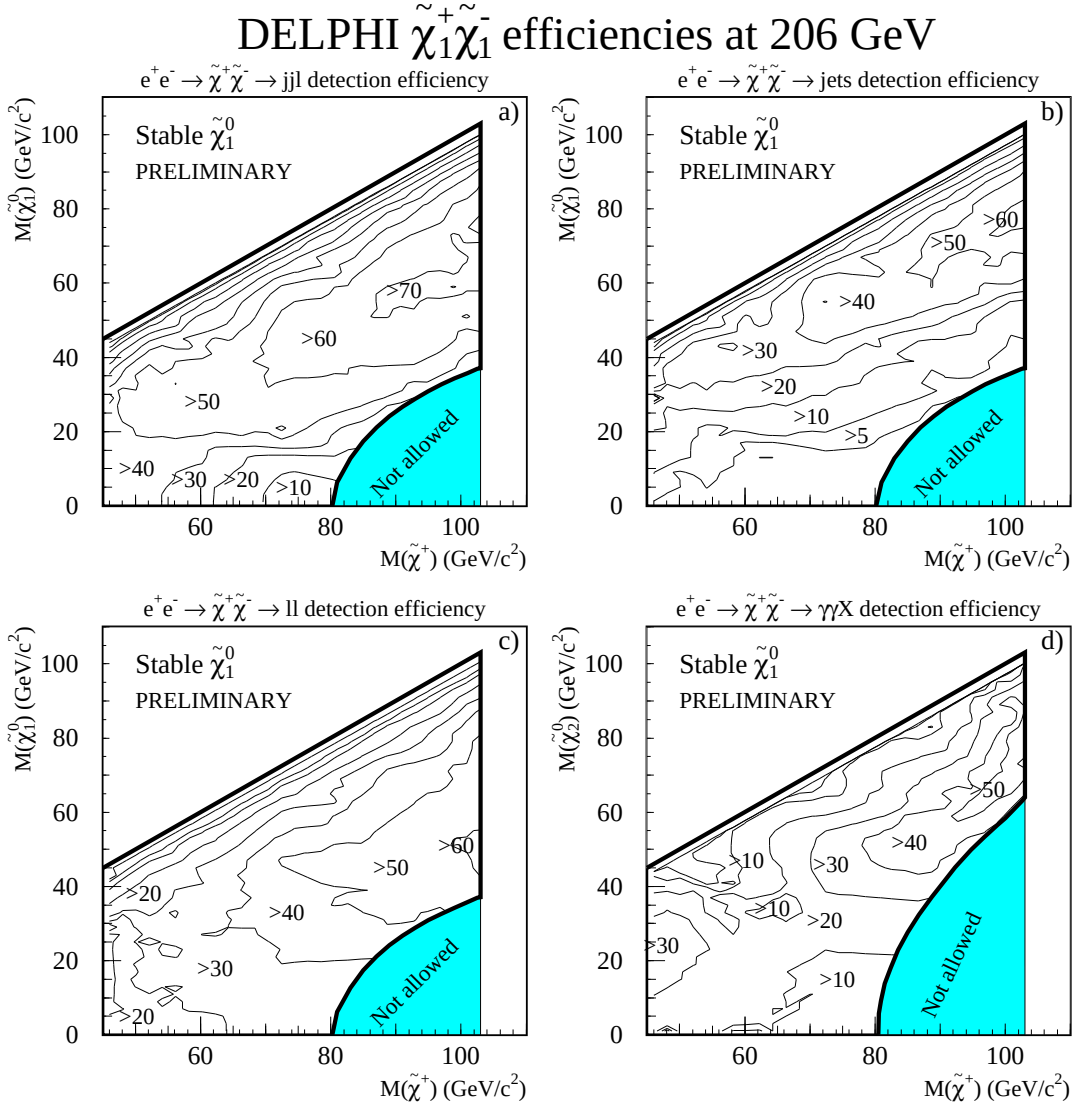

Figure 12: Chargino pair production detection efficiencies (%) for the four decay channels a) $jj\ell$, b) *jets*, c) $\ell\ell$ and d) *rad*, at 206.0 GeV in the $(M_{\tilde{\chi}^\pm}, M_{\tilde{\chi}^0})$ plane. A stable $\tilde{\chi}_1^0$ is assumed. The shaded areas are disallowed in the MSSM scheme.

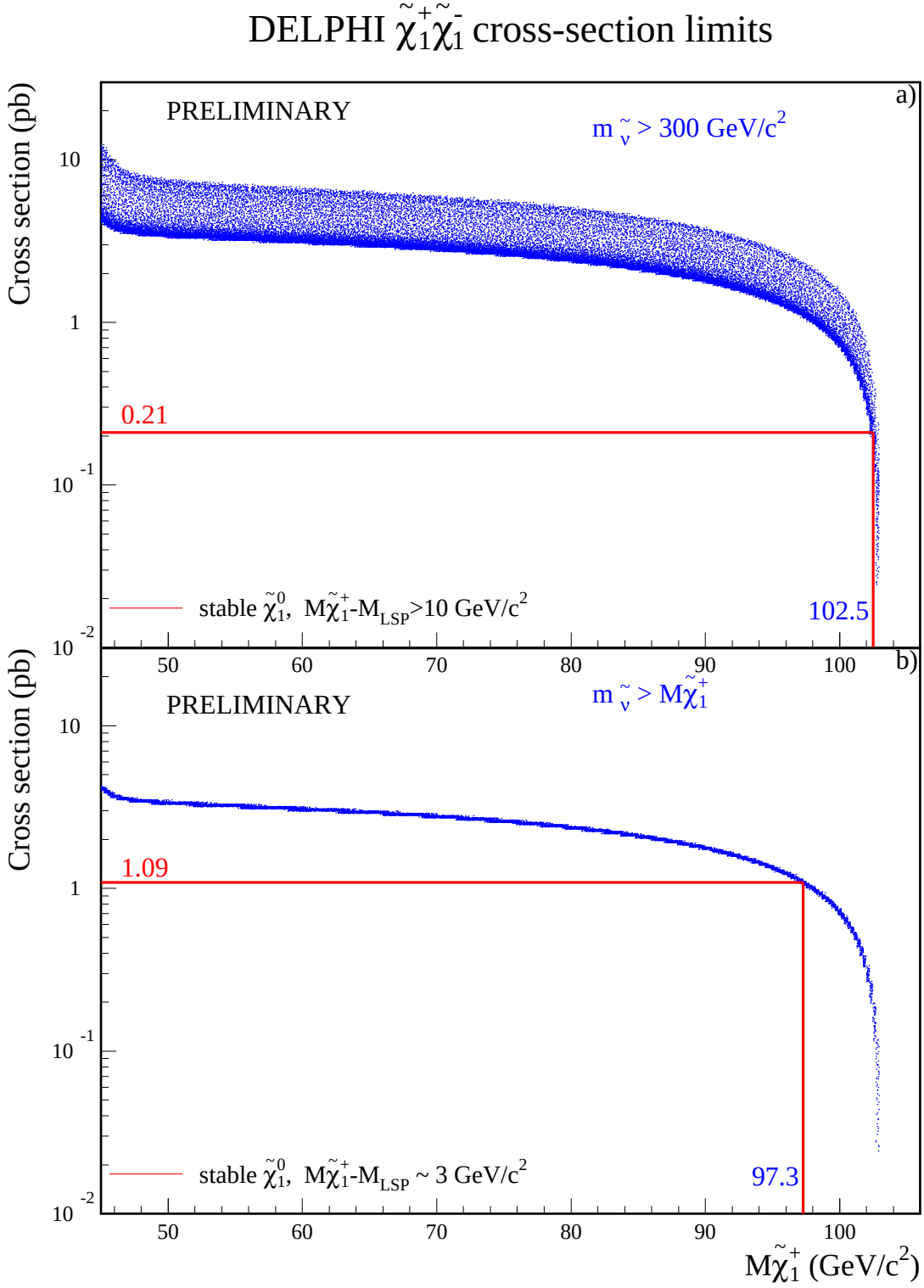

Figure 13: Expected cross-sections in pb at 205.9 GeV (dots) versus the chargino mass in a) for ΔM> 10 GeV/c^2 and b) for ΔM$\sim$ 3 GeV/c^2. The spread in the dots originates from the random scan over the parameters μ and M_2. A heavy sneutrino ($m_{\tilde{\nu}}$> 300 GeV/c^2) has been assumed in a) and $m_{\tilde{\nu}} > M_{\tilde{\chi}_1^\pm}$ in b). The minimal cross-sections below the mass limits are indicated by the horizontal lines.

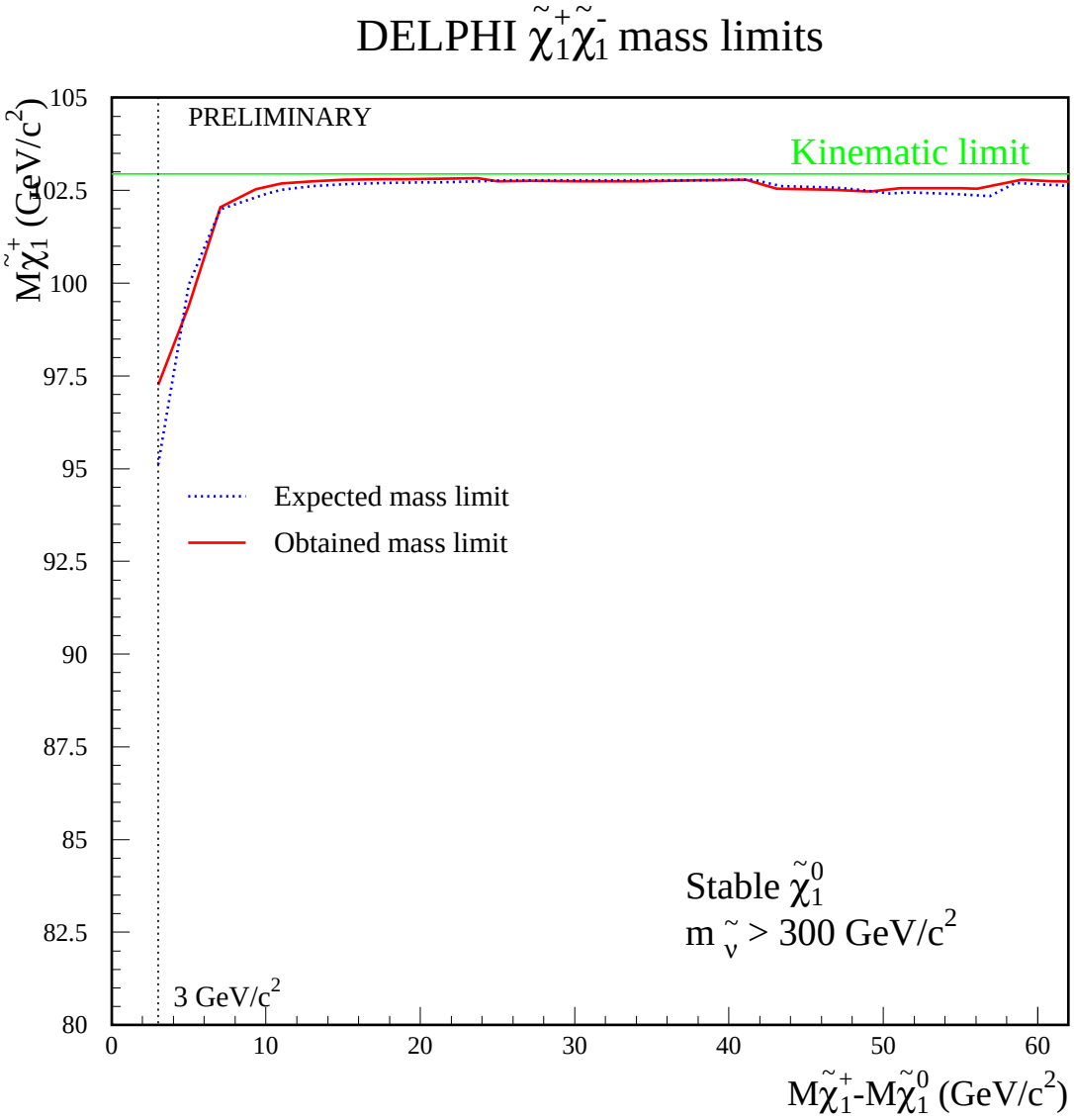

Figure 14: The chargino mass limit as function of the ΔM value under the assumption of a heavy sneutrino. The limit applies to the case of a stable $\tilde{\chi}_1^0$. The straight horizontal line shows the kinematic limit.

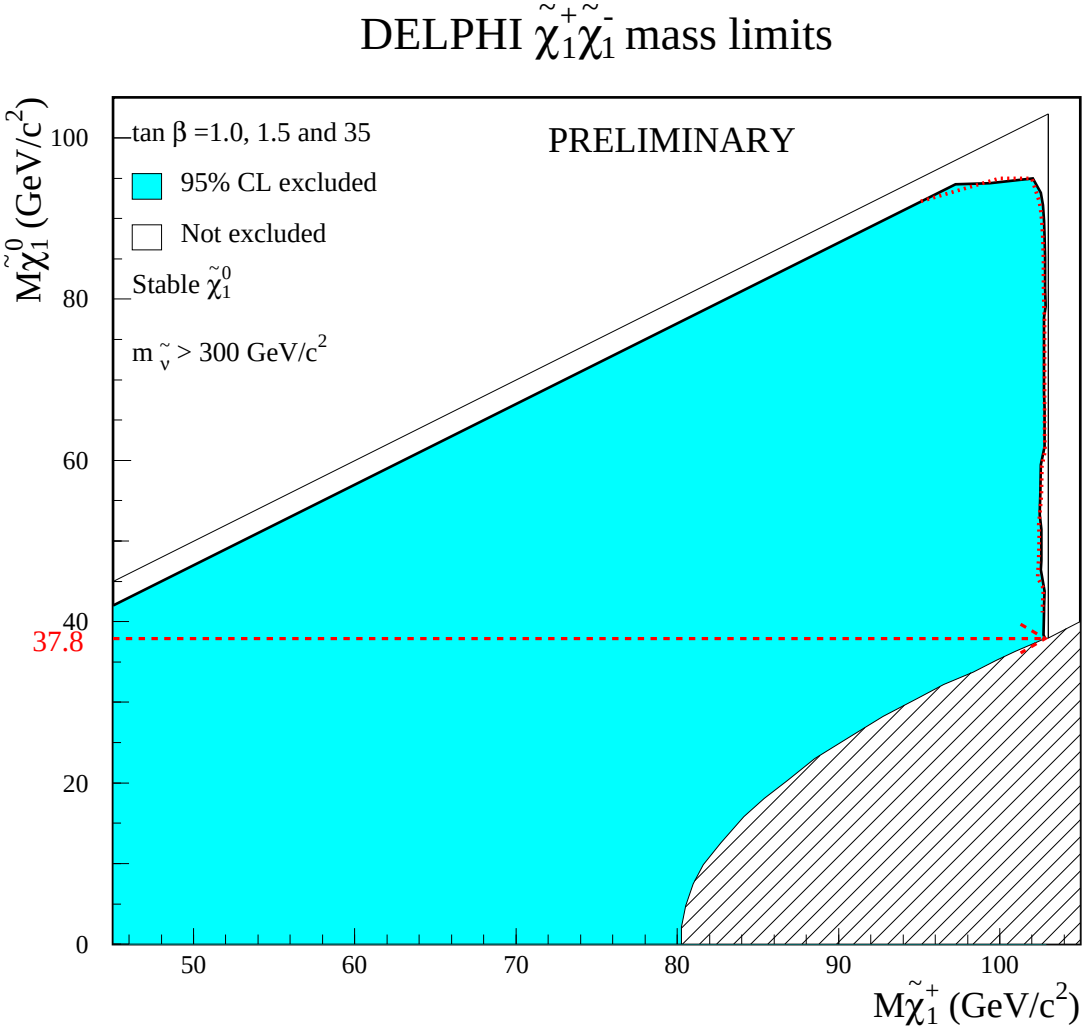

Figure 15: Region excluded at 95% confidence level in the plane of the mass of the lightest neutralino versus that of the lightest chargino under the assumption of a heavy sneutrino, for $\tan\beta = 1.0$, 1.5 and 35. The thin lines show the kinematic limits in the production and the decay. The dotted line (partly hidden by the shading) shows the expected exclusion limit. The dashed region is not allowed in the MSSM. The limit applies in the case of a stable $\tilde{\chi}_1^0$. The mass limit on the lightest neutralino is indicated by the horizontal dashed line.

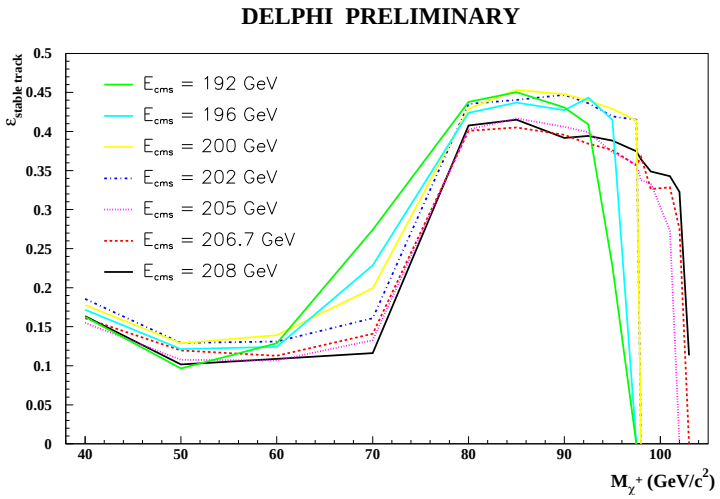

Figure 16: Efficiency for selecting a single almost stable chargino, as function of its mass, at the reference centre-of-mass energies collected by DELPHI in the years 1999 and 2000.

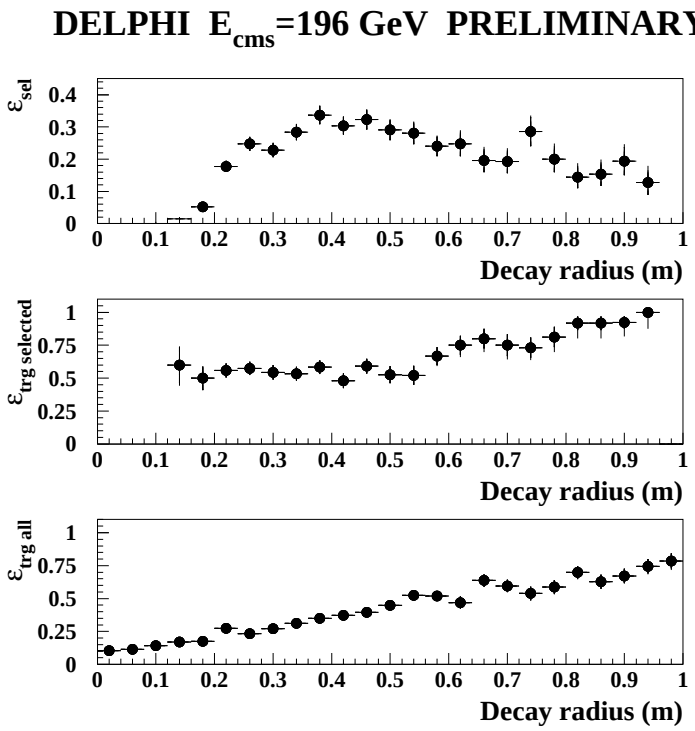

Figure 17: On top: efficiency for selecting a single 75 GeV/c^2 chargino in the search for displaced decay vertices (kinks) at the centre-of-mass energy of 196 GeV, as function of its decay radius. In the middle: trigger efficiency for the selected charginos. Below: trigger efficiency for all 75 GeV/c^2 charginos, whether or not they were selected.

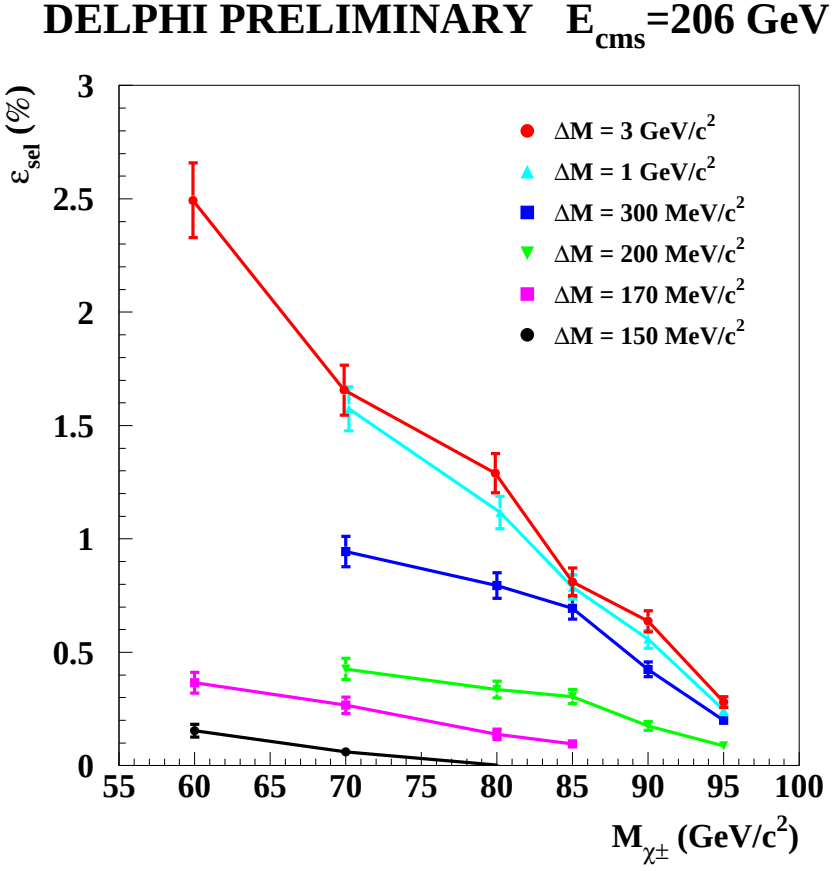

Figure 18: Selection times trigger efficiency in the search for nearly mass degenarate charginos in the search with the ISR photon. The efficiency for higgsinos at $\sqrt{s} = 206$ GeV at the different chargino masses and ΔM fully simulated is given as an example.

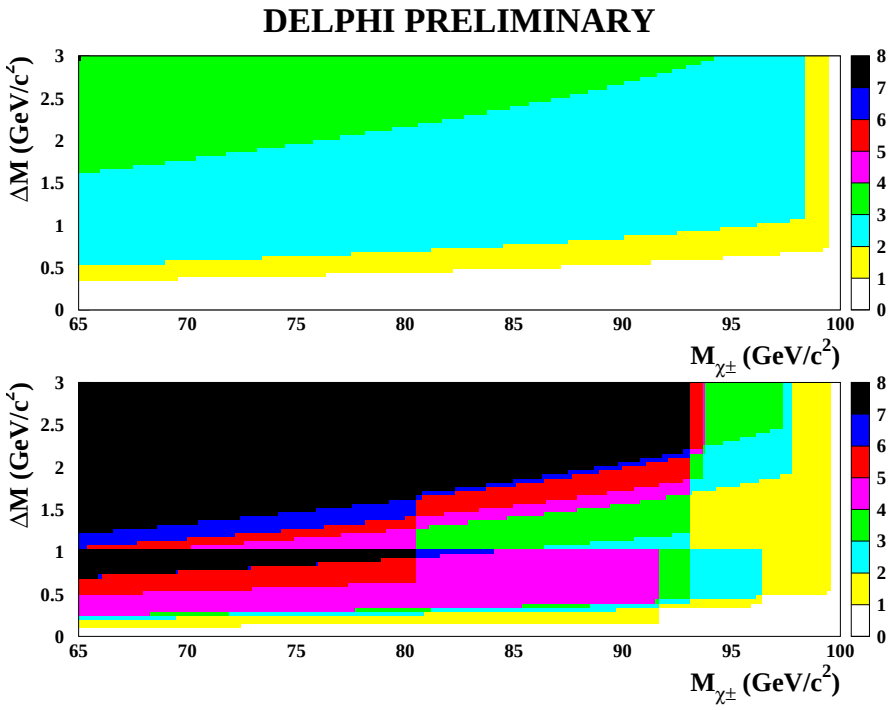

Figure 19: Expected number of background events (top) and number of selected events in the real data (bottom) after the final selection, for the year 2000 data with the TPC fully operational, as function of the points of the plane $(M_{\tilde{\chi}_1^+}, \Delta\mathrm{M})$ considered in the chargino search with the ISR photon.

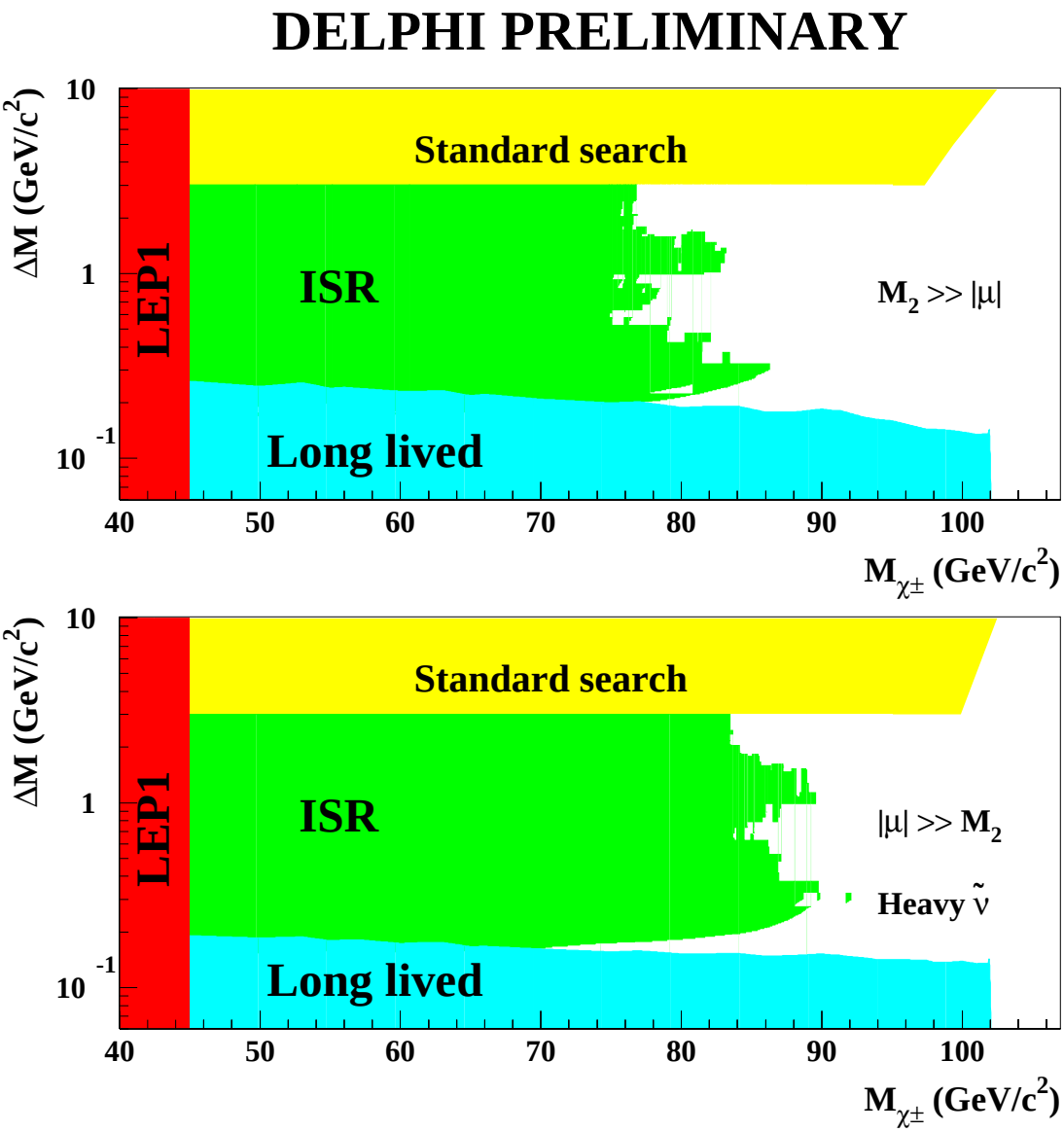

Figure 20: Regions in the plane $(M_{\tilde{\chi}_1^+}, \Delta\mathrm{M})$ excluded by DELPHI at the 95% CL using: the standard search for high ΔM charginos; the search for soft particles accompanied by ISR; and the search for long-lived charginos. The two scenarios are (a) the one in which the lightest chargino is a higgsino and (b) the one in which the lightest chargino is a gaugino. For the second scenario, the limits are valid in the heavy sfermion approximation, while for the higgsino scenario it is sufficient that $M_{\tilde{f}} > M_{\tilde{\chi}_1^+}$.

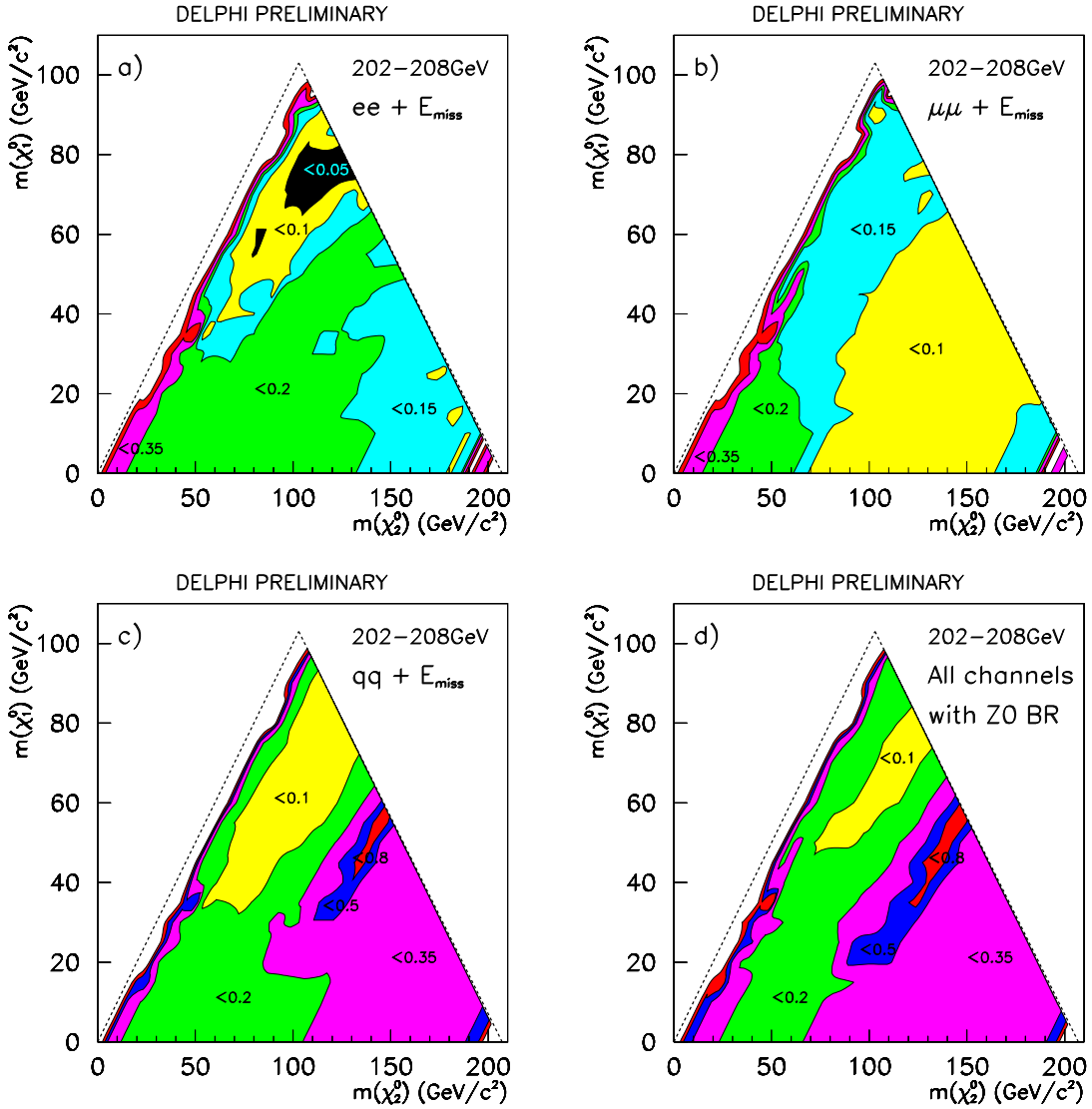

Figure 21: Contour plots of the upper limits obtained on the cross-sections at the 95% confidence level for $\tilde{\chi}^0_1\tilde{\chi}^0_2$ production at $\sqrt{s}$ = 202 GeV. The data at all energies were used, assuming the cross-section energy dependence expected at a chosen high m_0 point in the higgsino region where the neutralino searches play an important role (m_0=1 TeV/c^2, μ=-60 GeV/c^2, M_2=200 GeV/c^2). In each plot, the different shadings correspond to regions where the cross-section limit in picobarns is below the indicated number. For figures a), b), c), $\tilde{\chi}^0_2$ decays into $\tilde{\chi}^0_1$ and a) e^+e^-, b) $\mu^+\mu^-$, and c) $q\bar{q}$, while in d) the branching ratio of the Z was assumed, including invisible states. The dotted lines indicate the kinematic limit and the defining relation $M_{\tilde{\chi}^0_2} > M_{\tilde{\chi}^0_1}$.

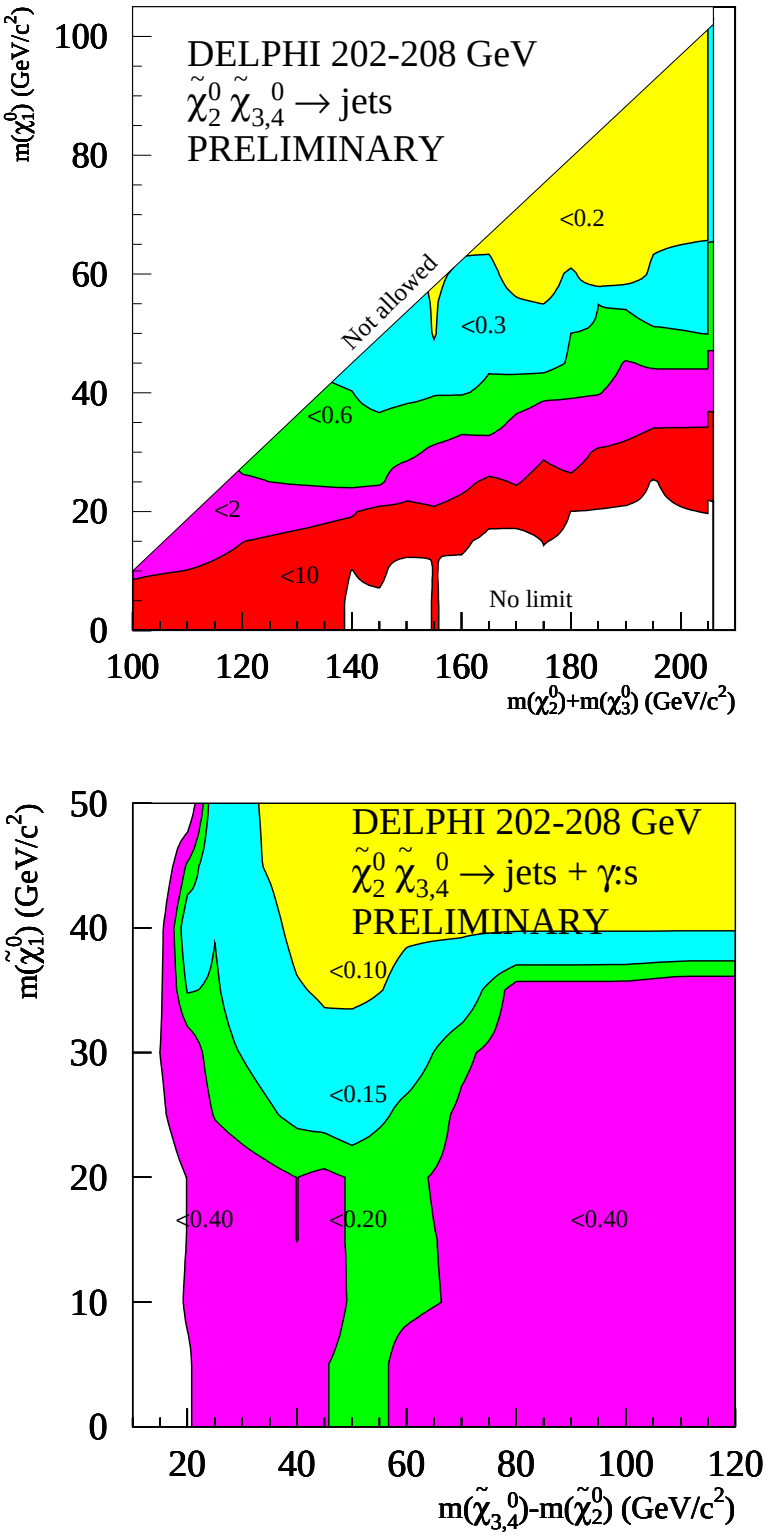

Figure 22: Upper limits on the cross-sections at the 95% confidence level for $\tilde{\chi}_2^0\tilde{\chi}_i^0$ production with $\tilde{\chi}_i^0 \rightarrow \tilde{\chi}_2^0 \mathrm{q}\bar{\mathrm{q}}$ (i=3,4) at $\sqrt{s}$ up to 202 GeV. The different shadings correspond to regions where the cross-section limit in picobarns is below the indicated number. The $\tilde{\chi}_2^0$ was assumed to decay 100 % into $\tilde{\chi}_1^0 \mathrm{q}\bar{\mathrm{q}}$ in a), and into $\tilde{\chi}_1^0\gamma$ in b). The limits in a) are based on the acoplanar jets and multijets selections, while those in b) derive from the search for multijets with photons.

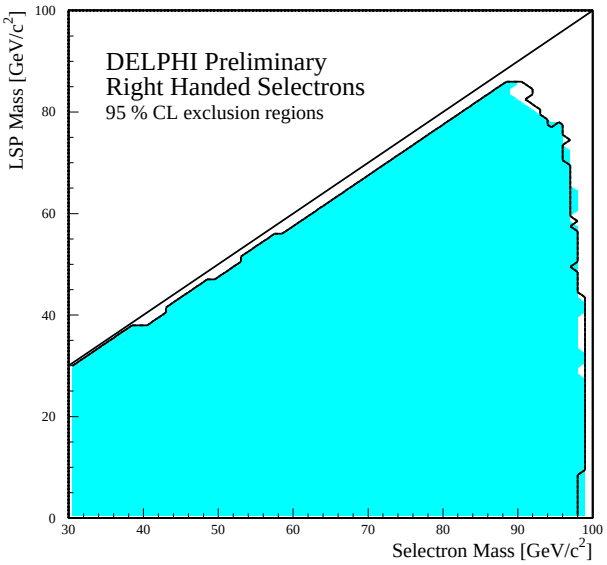

Figure 23: 95% CL exclusion region in the ($M_{\tilde{e}_R}$ M_{LSP}) plane. The shaded region shows the obtained exclusion limit, and the solid line shows the expected limit treating simulated background as data.

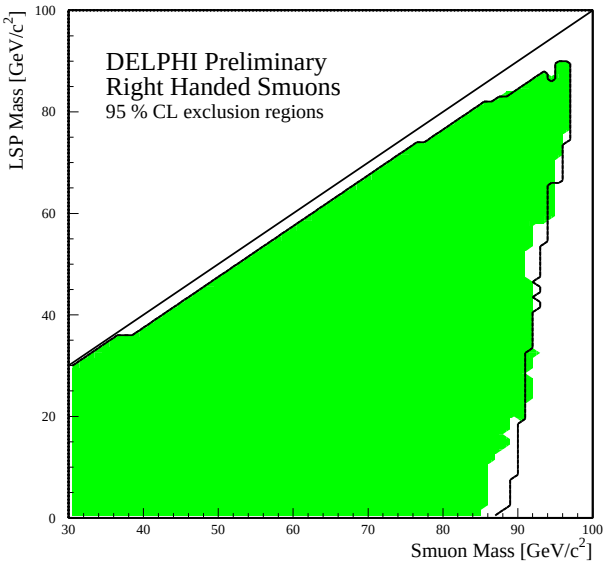

Figure 24: 95% CL exclusion region in the ($M_{\tilde{\mu}_R}$ M_{LSP}) plane. The shaded region shows the obtained exclusion limit, and the solid line shows the expected limit treating simulated background as data.

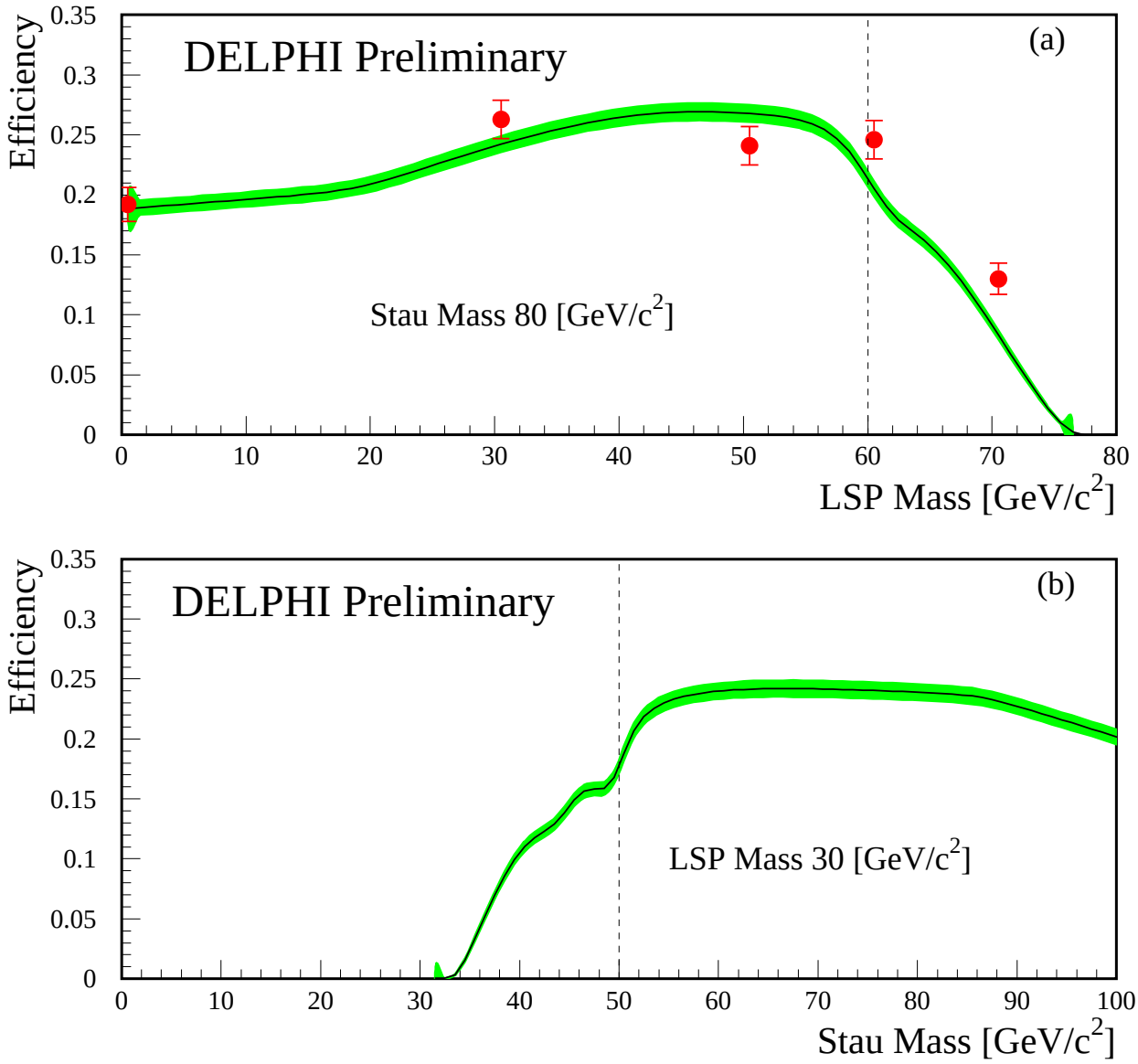

Figure 25: The selection efficiency in the stau analysis. The plots show: (a) Efficiency as a function of M_{LSP} at $M_{\tilde{\tau}}$= 80 GeV/c^2. The line shows the result of the fast simulation, and the points with error bars show the result of the full simulation. The shaded area indicates the statistical uncertainty of the estimate, and the vertical line shows the position of the transition between the two ΔM-regions. (b) Efficiency as a function of $M_{\tilde{\tau}}$ at $M_{LSP} = 30$ GeV/c^2. The line shows the result of the fast simulation, and the shaded area indicates the statistical uncertainty of the estimate, and the vertical line shows the position of the transition between the two ΔM-regions.

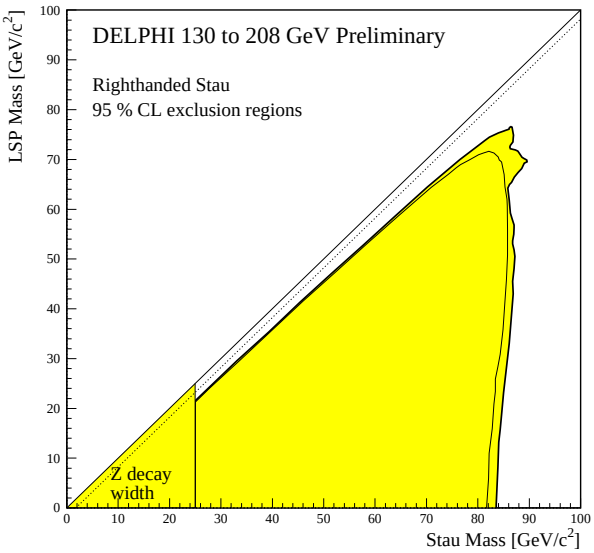

Figure 26: 95% CL exclusion region in the ($M_{\tilde{\tau}_R}$, M_{LSP}) plane. The shaded region shows the obtained exclusion limit, and the thin solid line shows the limit expected for no signal events.

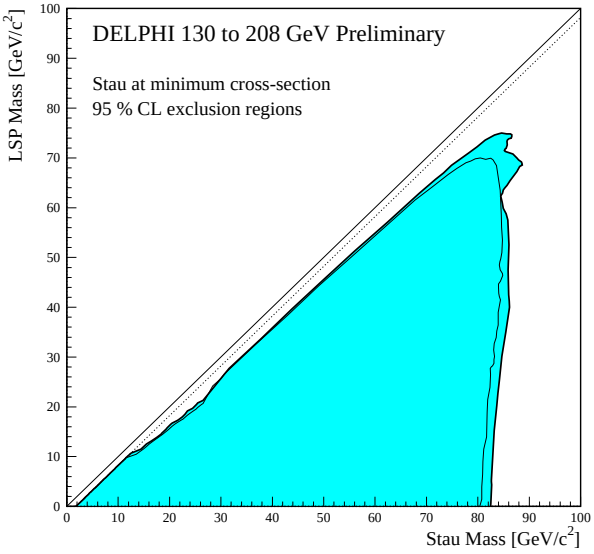

Figure 27: 95% CL exclusion region in the ($M_{\tilde{\tau}}$, M_{LSP}) plane obtained for the minimal $\tilde{\tau}\tilde{\text{p}}$air-production cross-section. The shaded region shows the obtained exclusion limit, and the thin solid line shows the limit expected for no signal events.

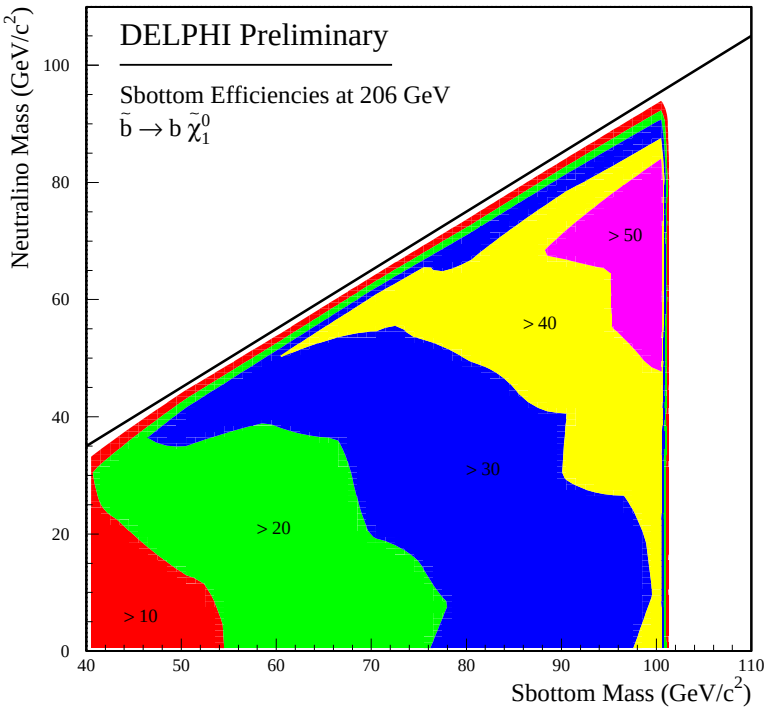

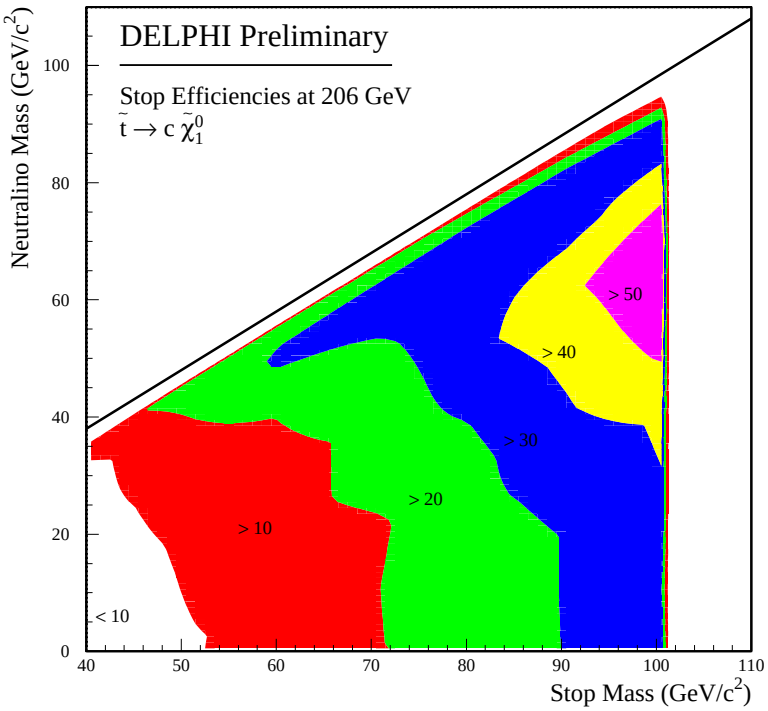

Figure 28: Squark signal detection efficiencies in the plane $(M_{\tilde{q}_1}, M_{\tilde{\chi}_1^0})$ in the non-degenerate scenario.

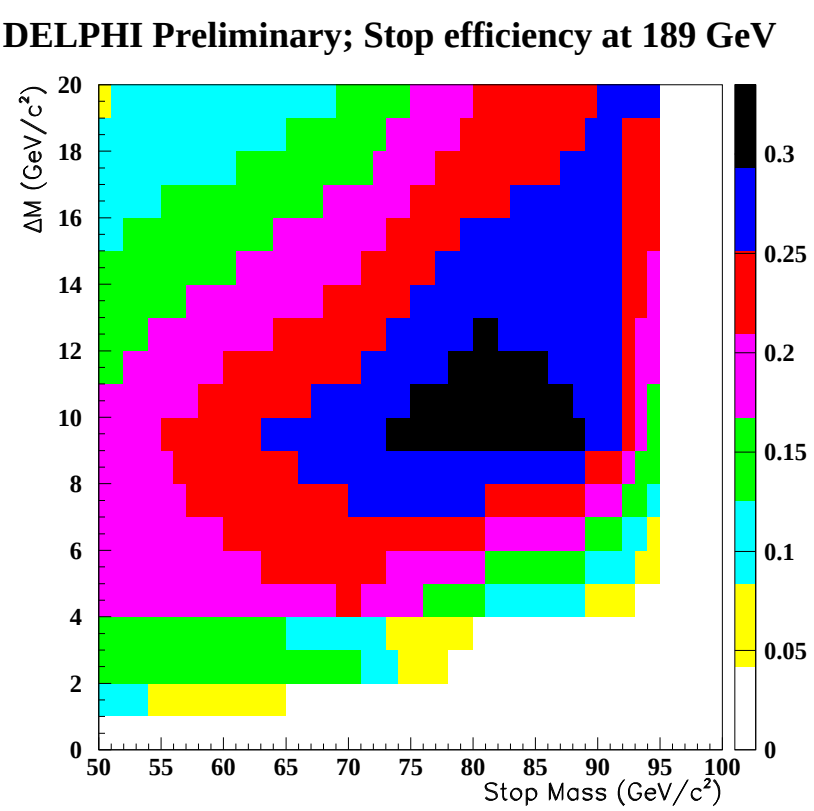

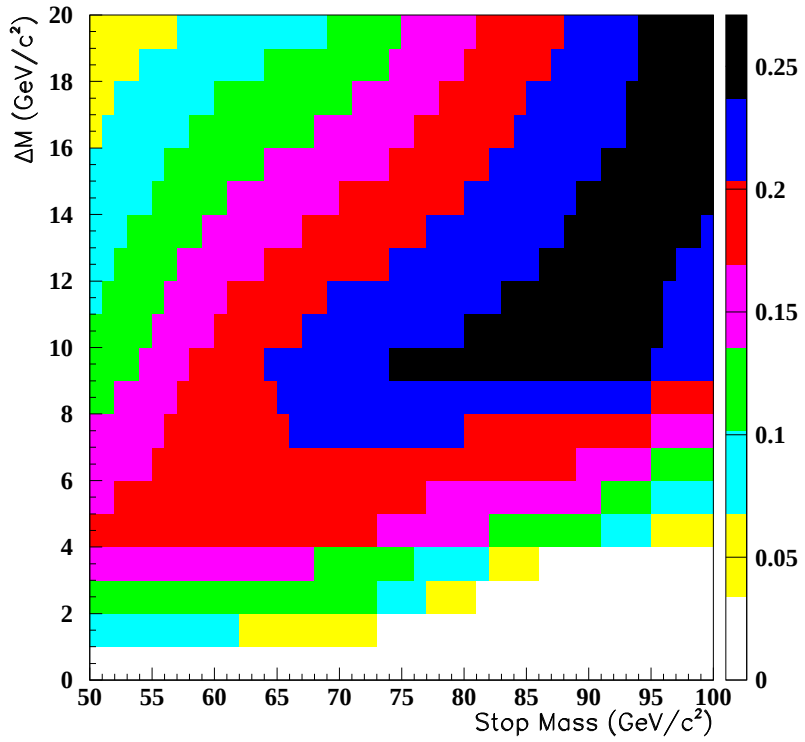

Figure 29: Signal efficiency of the stop search in the degenerate scenario in the plane ($M_{\tilde{t}_1}$, $\Delta M = M_{\tilde{t}_1} - M_{\tilde{\chi}_1^0}$), for $\sqrt{s}$=189 and 206 GeV.

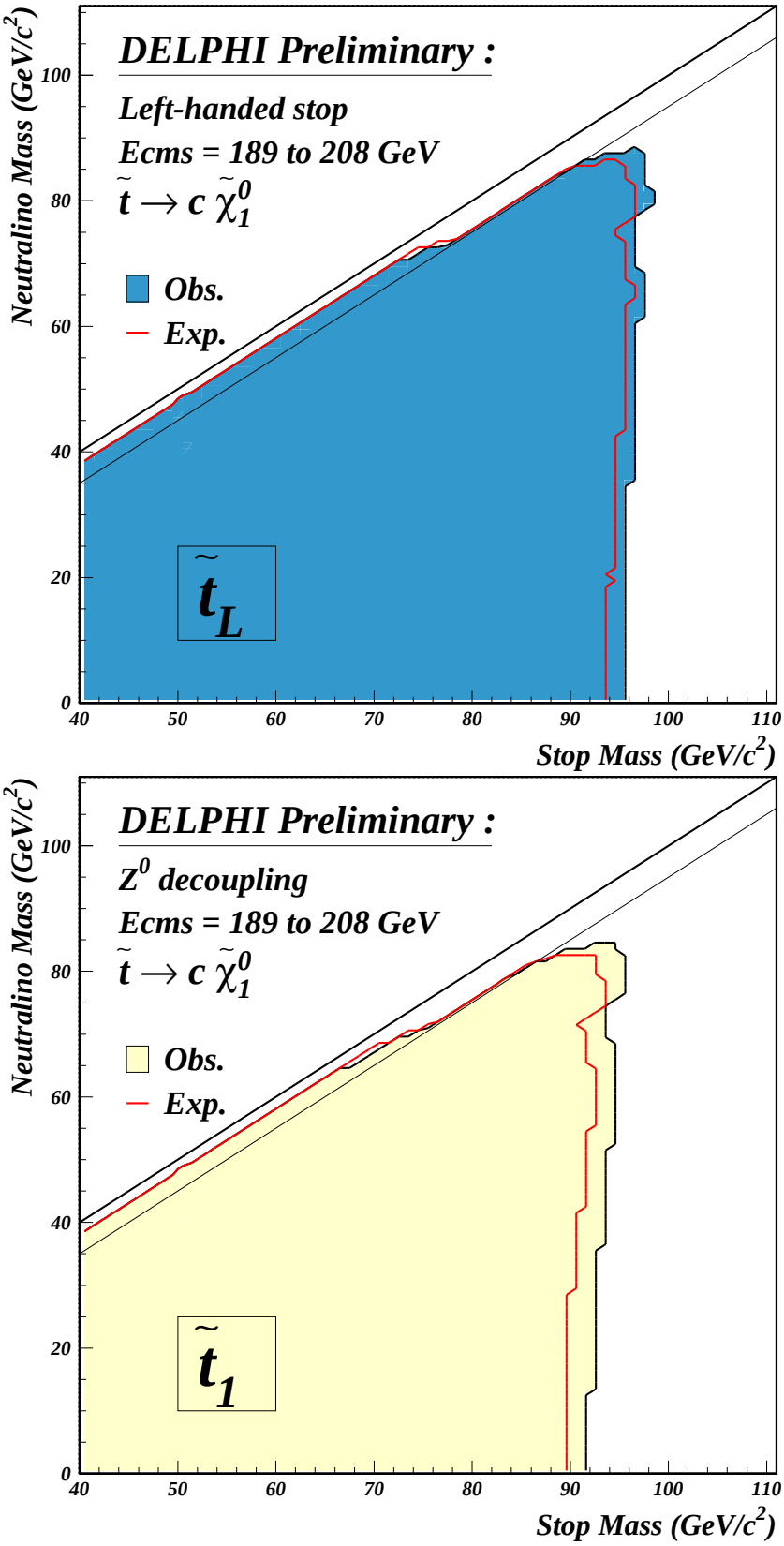

Figure 30: Excluded regions at 95 % confidence level for the stop search in the plane ($M_{\tilde{t}_1}$,$M_{\tilde{\chi}_1^0}$) for purely left handed stops (top) and for the states at the Z^0 decoupling (bottom). The shaded region shows the observed excluded region and the line corresponds to the expected exclusion.

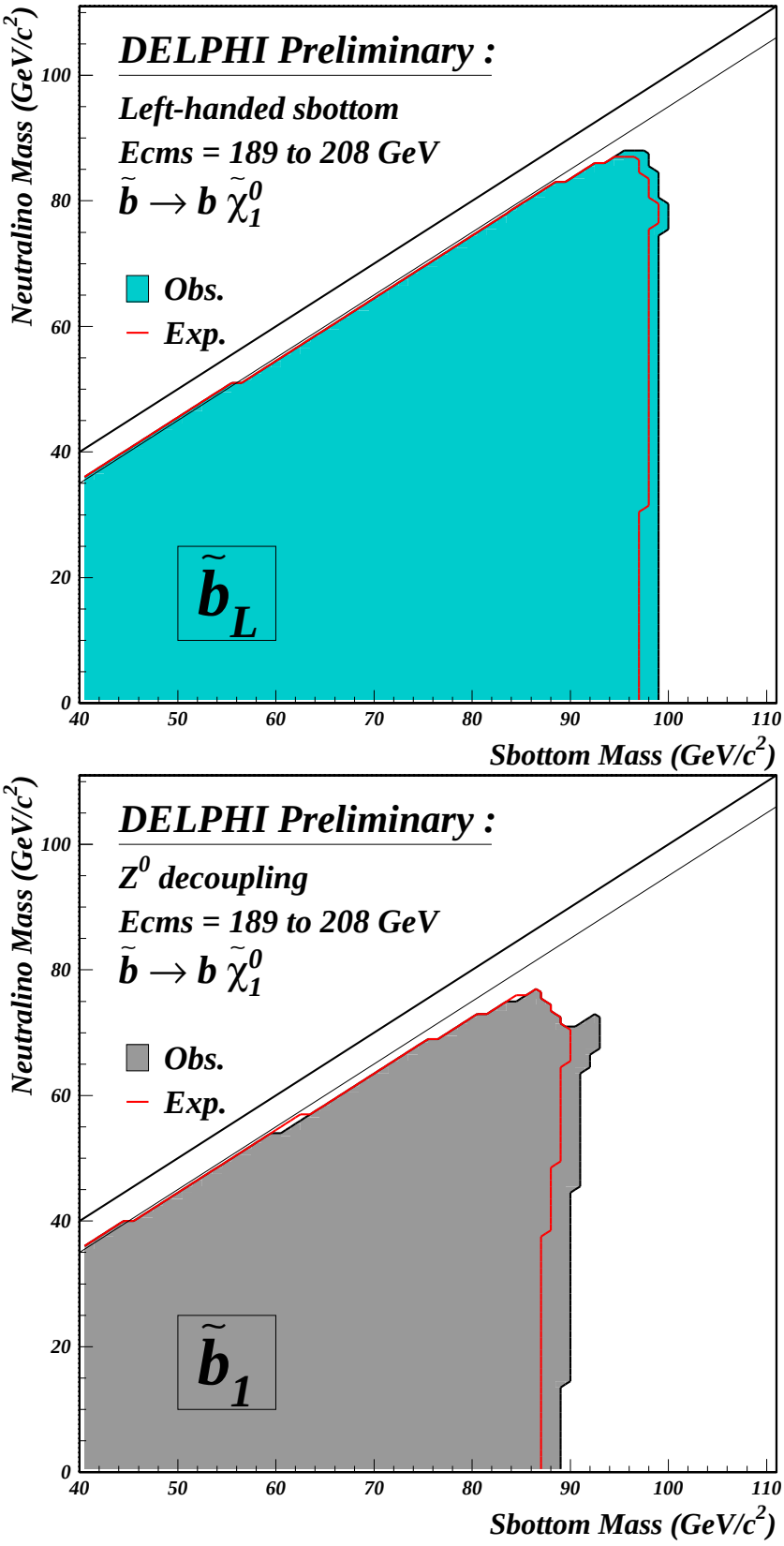

Figure 31: Excluded regions at 95 % confidence level for the sbottom search in the plane ($M_{\tilde{b}_1}$,$M_{\tilde{\chi}_1^0}$) for purely left handed sbottoms (top) and for the states at the Z^0 decoupling (bottom). The shaded region shows the observed excluded region and the line corresponds to the expected exclusion.

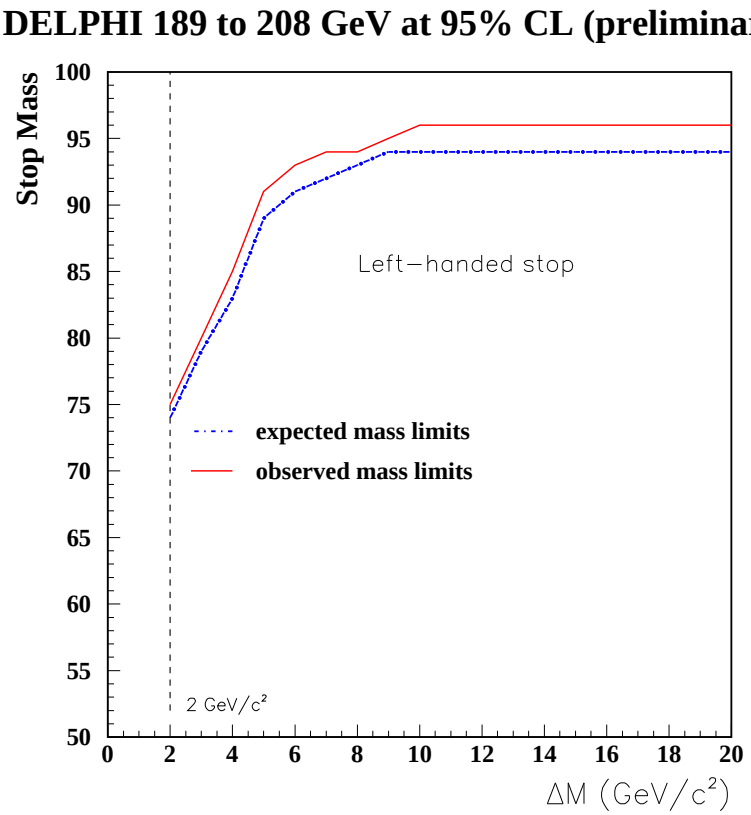

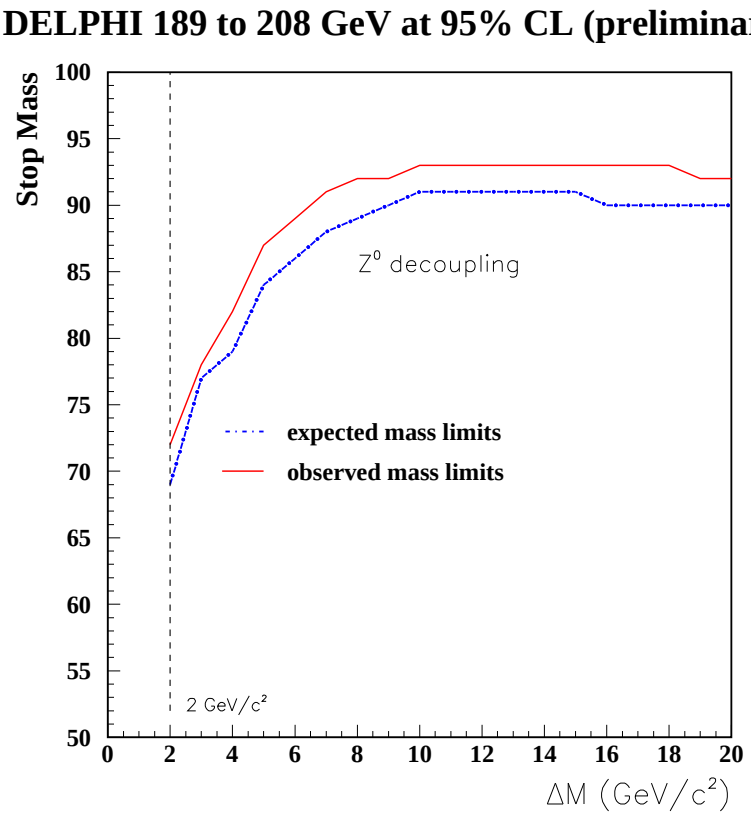

Figure 32: Stop mass limit as a function of ΔMfor a purely left-handed stop and for the stop mixing angle which minimises the cross-section.

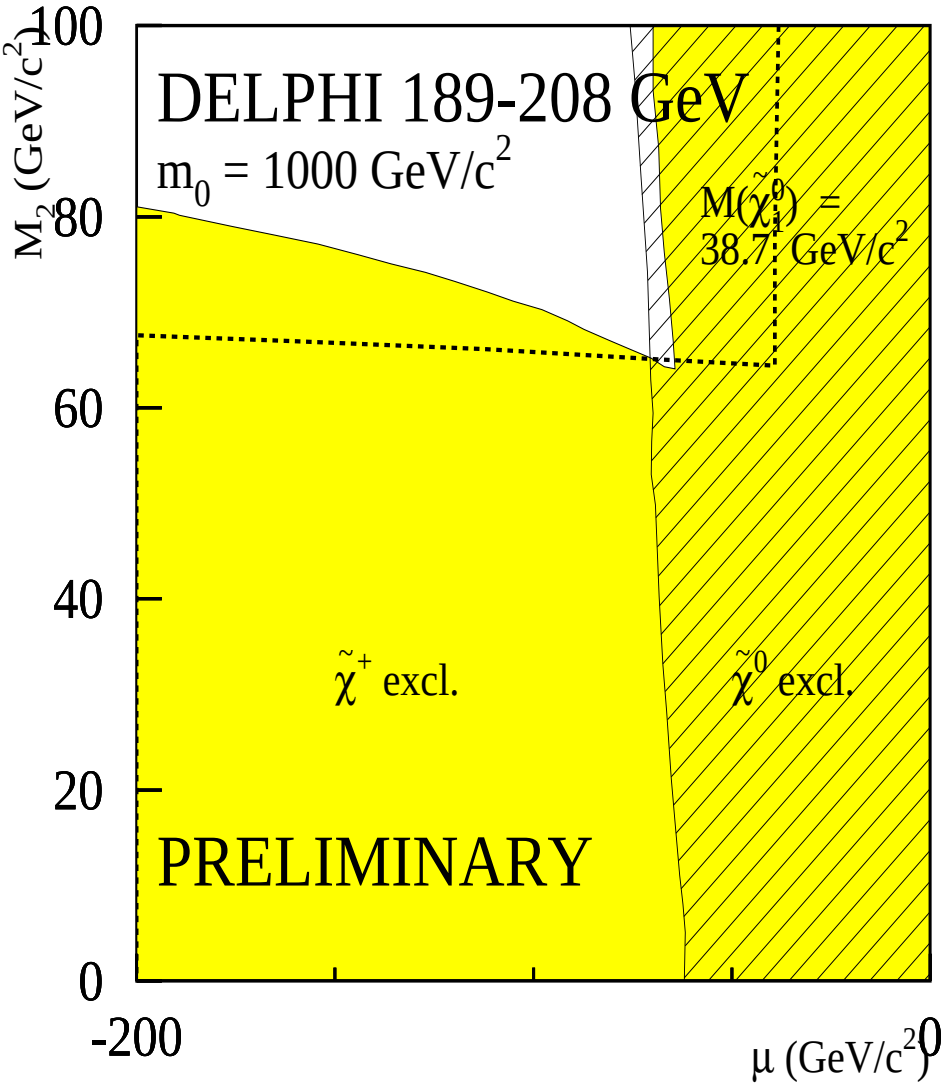

Figure 33: Excluded regions in the (μ,M_2) plane for $\tan\beta = 1$ for $m_0 = 1000$ GeV/c^2 The shaded areas show regions excluded by searches for charginos and the hatched areas show regions excluded by searches for neutralinos. The thick dashed curve shows the isomass contour for $M_{\tilde{\chi}_1^0} = 38.7$ GeV/c^2, the lower limit on the LSP mass obtained at $\tan\beta$=1. The chargino exclusion is close to the isomass contour for $M_{\tilde{\chi}_1^\pm}$ at the kinematic limit. From chargino searches alone the lower limit on $M_{\tilde{\chi}_1^0}$ is $M_{\tilde{\chi}_1^0} = 37.8$ GeV/c^2.

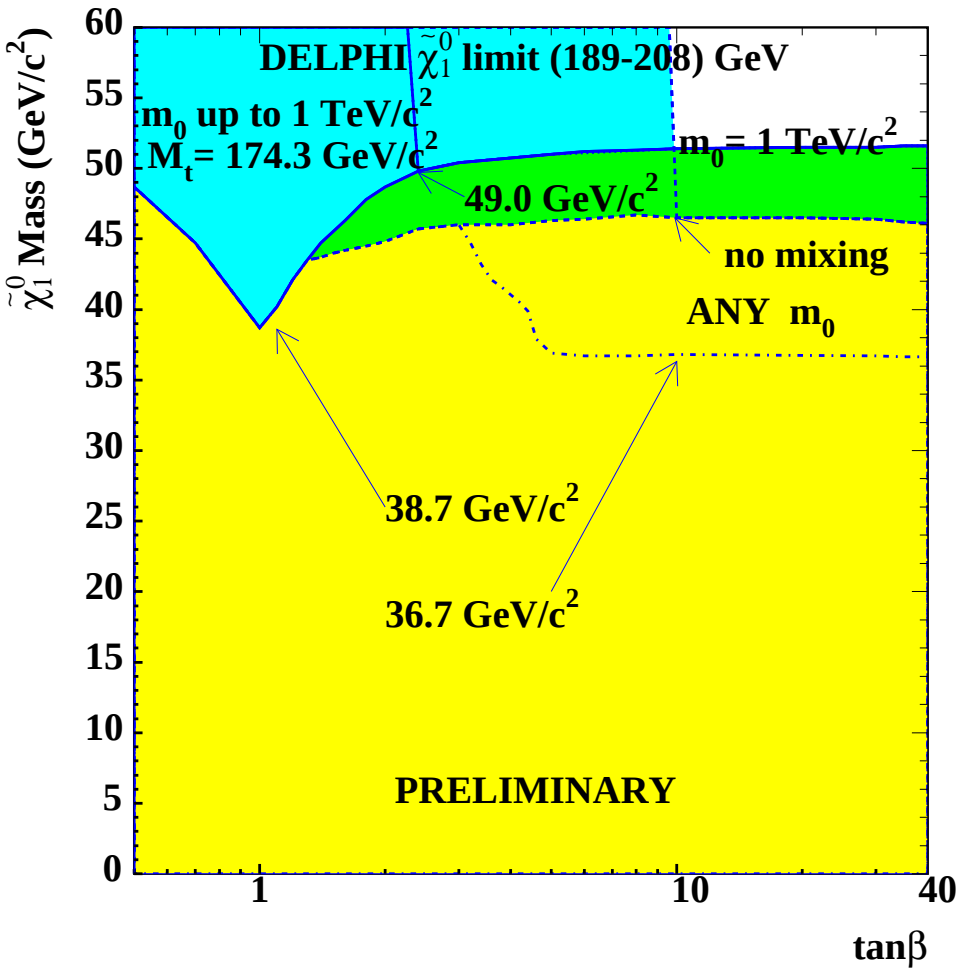

Figure 34: The lower limit at 95 % confidence level on the mass of the lightest neutralino, $\tilde{\chi}_1^0$, as a function of $\tan\beta$ assuming a stable $\tilde{\chi}_1^0$. The solid curve shows the limit obtained for m_0 =1000 GeV/c^2, the dashed curve shows the limit obtained allowing for any m_0 assuming that there is no mixing in the third family ($A_\tau = \mu\tan\beta$, $A_b = \mu\tan\beta$, $A_t = \mu/\tan\beta$), and the dash-dotted curve shows the limit obtained for any m_0 allowing for the mixing with A_τ=A_b=A_t=0. This limit would improve to 43 GeV/c^2 if dedicated searches for staus originating from $\tilde{\chi}_2^0\tilde{\chi}_2^0$ production were used. The steep solid (dashed) curve shows the effect of the searches for the Higgs boson for the maximal M_{h^0} scenario (no mixing scenario), $m_0 \leq 1000$ GeV/c^2 and M_t= 174.3 GeV/c^2, which amounts to excluding the region of $\tan\beta < 2.36(9.7)$

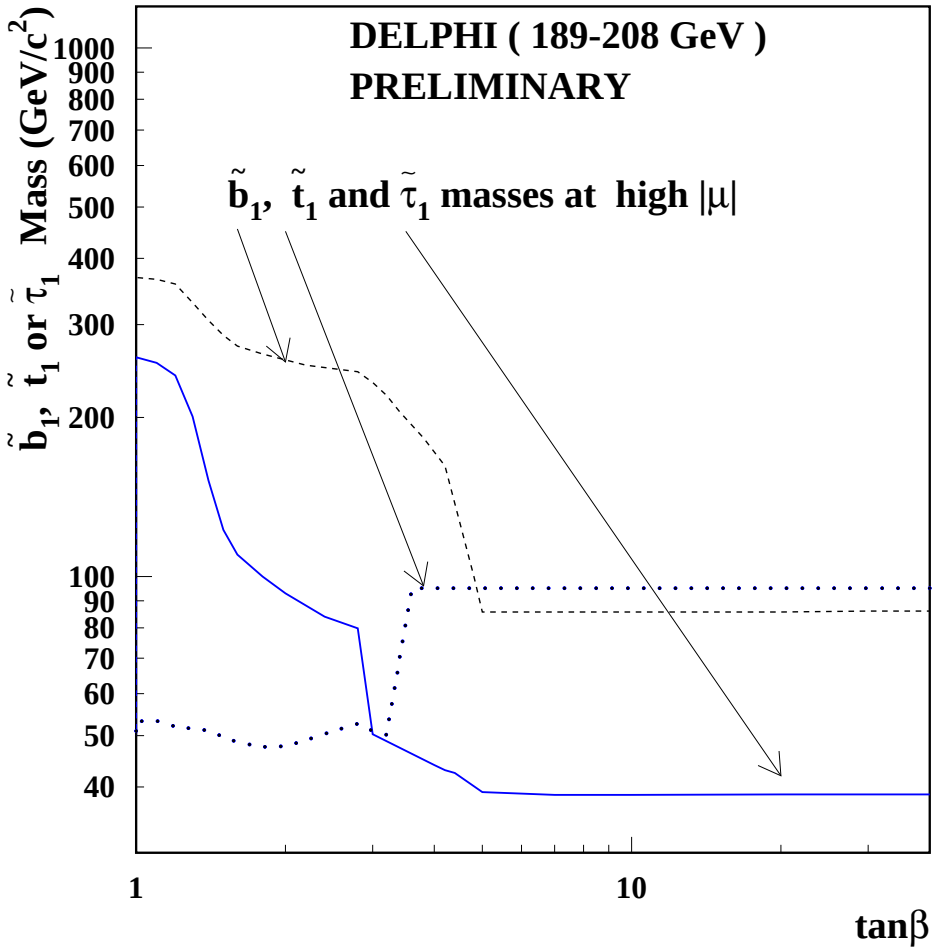

Figure 35: The masses as a function of $\tan\beta$ of the lightest stau (solid curve), stop (dotted curve) and the sbottom (dashed curve), at the highest allowed $|\mu|$ for the lowest non-excluded M_2 value. Mass splitting in the stau (sbottom, stop) sector in the form $A_\tau - \mu\tan\beta$ ($A_b - \mu\tan\beta$, $A_t - \mu/\tan\beta$) was assumed, with $A_\tau = 0$ ($A_b = A_t = 0$).

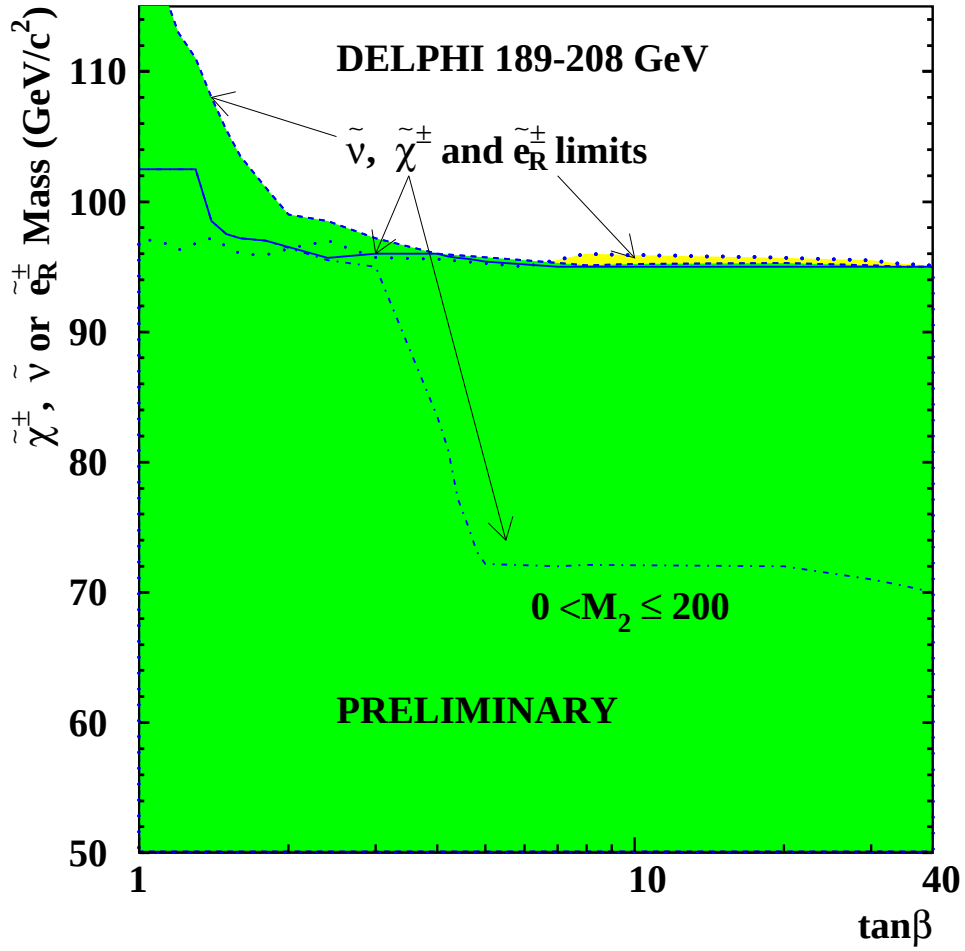

Figure 36: The minimum sneutrino mass (dark shading and the dashed curve) allowed by the slepton and neutralino searches, as a function of $\tan\beta$, together with the limits on the chargino mass (solid curve and dash-dotted curve), and the $\tilde{e}_R$ mass (dotted curve and the light shading). The chargino mass limit indicated by the solid curve and the sneutrino and selectron mass limits were obtained assuming no mass splitting in the third sfermion family ($A_\tau - \mu\tan\beta$=0 in particular). The selectron mass limit is valid for $M_{\tilde{e}_R} - M_{\tilde{\chi}_1^0} > 10$ GeV/c^2. The chargino mass limit indicated with the dash-dotted curve was obtained allowing for mass splitting in the third sfermion family, with $A_\tau = A_b = A_t$=0. This limit would improve to 85 GeV/c^2 if dedicated searches for staus originating from $\tilde{\chi}_2^0\tilde{\chi}_2^0$ production were used.

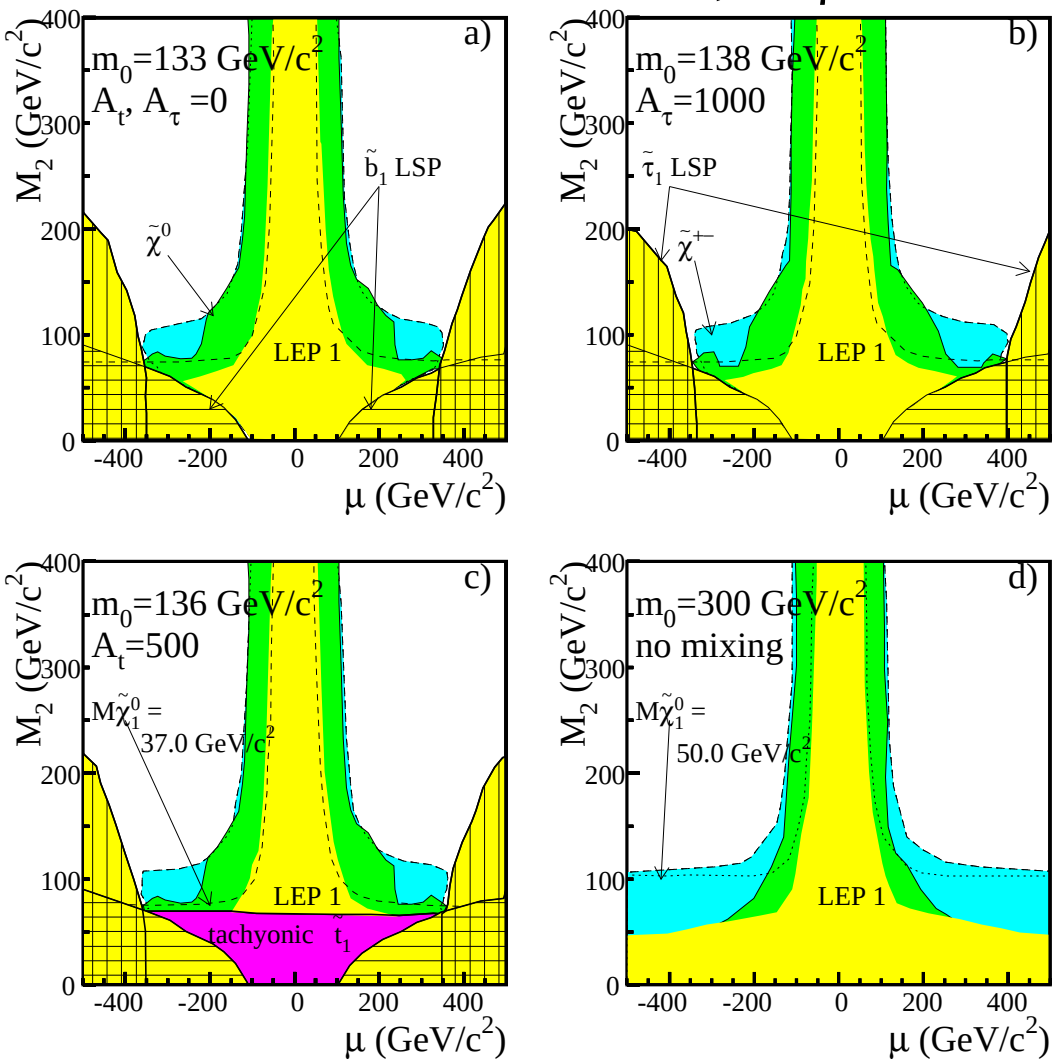

Figure 37: Regions excluded at 95 % confidence level in the (μ, M_2) plane for $\tan\beta = 35$ and different assumptions of mixing in the third family. Light shaded regions are exluded from searches at LEP1 energies, darker shading bounded by the solid line marks regions excluded from neutralino searches, while intermediate shaded regions bounded by the thin dashed line are excluded by chargino searches. For plots a),b),c) $A_b = 0$, and mixing terms in the form $A_\tau - \mu\tan\beta$ ($A_b - \mu\tan\beta$, $A_t - \mu/\tan\beta$) were assumed, with $A_t = 0$ for a),b) and $A_\tau = 0$ for a),c). The no-mixing scenario was used in d) ($A_\tau - \mu\tan\beta$=0, $A_b - \mu\tan\beta$=0 $A_t - \mu/\tan\beta$=0). Plots in a),b),c) are for m_0 values giving the lowest non-excluded LSP mass. In the vertically (horizontally) hatched areas the stau (the sbottom) is the LSP. In the dark shaded region in c) the stop is tachyonic. Relevant isomass contours of the lightest neutralino are also shown (see arrows in c) and d)).